Reduced Order Sparse Modeling for Sensitivity Coefficient Evaluation in Core Analysis

Ryota Katano

Department of Applied Energy

Graduate School of Engineering, Nagoya University

2024

This page is intentionally left blank.

Abstract

The sensitivity analysis (SA) plays a key role in the quantification and the reduction of the nuclear data-induced uncertainty. For easy implementation and efficient SA for various types of neutronics parameters and design systems, the development of a forward-based SA method is strongly desired. Therefore, in this thesis, the two methods for the sensitivity analysis using only forward calculations are newly proposed focusing on the advantages of the forward calculations.

The first one is the adaptive smooth-lasso, which is a lasso-type penalized linear regression. The penalty term of the proposed method is designed to capture the sparsity, the continuity against the induced neutron energy, and the steep changes due to threshold reactions and giant resonances better than the conventional regressions. Through the SA of k_{eff} of an accelerator-driven system (ADS) at the beginning of the cycle (BOC), the better performance of the proposed method is demonstrated in comparison with the conventional regressions.

The second one is the ROM-Lasso, which combines the reduced order modeling and the lasso regression to dramatically improve the calculation cost. In this method, the sensitivity coefficients are expanded by bases of an active subspace obtained in the lower-fidelity model and the expansion coefficients are estimated via the lasso regression. By reducing the effective dimensionality of the nuclear data for the sensitivity analysis, the number of forward calculations can be dramatically reduced by a couple of orders of magnitude. The ROM-Lasso method is verified for several neutronics parameters considering burnup through a one-cycle burnup core calculation of the ADS.

In addition to the development of the methods, the data assimilation (DA) aiming at the reduction of the nuclear-data-induced uncertainty of the design property of the ADS is

investigated as a practice of the application of SA. In this study, the lead-bismuth sample reactivity measurements conducted at the Kyoto University Critical Assembly are employed with the primary aim of examining the uncertainty reduction of the void reactivity of the coolant in the ADS. Through the analysis, the uncertainty is successfully reduced, demonstrating the applicability of forward-based uncertainty quantification (UQ) and DA via SA to the ADS.

The development in this thesis potentially resolves the primary issues in the SA and promotes the application of SA to the various types of neutronics parameters. Furthermore, this thesis demonstrates the forward-based UQ and DA making use of the sensitivity coefficients for neutronics parameters of an innovative system.

Table of Contents

1. Introduction

1.1. Background

Japan's primary energy supply depends on thermal power for about 80% of its demand. Due to its resource-poor situation and its heavy dependence on overseas fossil fuels, Japan's energy has a vulnerability to a stable supply [1]. For example, the energy supply will be potentially threatened by political situations in the Middle East because the Strait of Hormuz is the most important chokepoint of oil transportation. In addition, Russia's aggression against Ukraine took place in 2022 impacted and confused the international and Japanese supply and market price of energy. It is an urgent matter for a sustainable society to establish a well-balanced energy supply with diversified sources.

Nuclear power has great advantages of the capability of producing energy by only the domestic fuel stockpile for several years owing to its massive energy density of nuclear fuels and its lower greenhouse gas emissions. Japan's Strategic Energy Plan recognizes nuclear power as an important baseload energy [2]. However, the Fukushima Dai-ichi nuclear accident caused by the occurrence of the "once in a thousand years" earthquake and subsequent tsunami exposed the problem of the mindset so-called "safety myth" that induced overconfidence in nuclear safety and the lack of countermeasures against severe accidents. Against this background, on the major premise of ensuring safety, Japan plans to restart the nuclear power plants that receive approval under the new safety standards established by the Nuclear Regulatory Association (NRA) and will promote the development of advanced reactors that expectedly enhance safety and technologies for disposal of radioactive waste including transmutations of long-lived nuclides by fast reactors and/or accelerators to reduce the scale of the period during which they show significant levels of radioactivity [1,2].

To design nuclear power systems, it is necessary to perform core analyses that predict

neutronics parameters related to safety and economics by simulating the behavior of the system using computers. Accurate simulations and reliable predictions are important to better understand and optimize the design and safety margins of nuclear systems. The uncertainty quantification (UQ) can help to capture how accurate the simulations are, hence ensuring the credibility of the simulation outcomes and enabling the robust design. In the next section, the overview of the sources of the uncertainty in core analyses is described.

1.2. Overview of uncertainty in core analysis

There are several sources of the uncertainty in the predictions by the core analysis [3]: i) the uncertainty inherent in fundamental formulations that we rely on, ii) the uncertainty of the numerical analysis, iii) the uncertainty of modeling and simplification of the problem, and iv) the uncertainty of the input parameters.

The uncertainty associated with i) is derived from the possibility that the fundamental formulations we believe do not adequately describe the true physics of nature. For example, even in the Boltzmann transport equation, which is considered one of the most exact formulations for the macroscopic neutron transport phenomena, there are several assumptions and approximations to derive it, and the possibility of the gap between the equation and the true physics cannot be completely ruled out [4]. In many cases, especially in the core analysis, this uncertainty is considered negligible.

The uncertainty associated with ii) appears when we numerically solve the equations describing the physics. In general, it is difficult to obtain the analytical solution of the Boltzmann equations except for extremely simplified cases. In deterministic methods, the space, the direction of the flight path, and the energy of neutrons are discretized so that computers can solve the problems in a certain sequential procedure, resulting in discretization errors. Even in the Monte

Carlo method, which employs no discretization and few approximations, the calculation results contain statistical errors because it tracks the neutron trajectory decided by a stochastic procedure and statistically makes guesses for the solutions using estimators.

The uncertainty associated with iii) arises when modeling and/or simplifying a geometry of interest. In critical benchmark problems, sometimes experimenters provide models simplifying and/or neglecting core supporting structure, jigs, and impurity in compositions to make treatments in numerical analysis easier [5]. The geometry is often simplified because there are limitations in the types of meshes that can be handled by the calculation methods.

The nuclear data-induced uncertainty falls into the category of iv). In a core analysis, one uses the nuclear data libraries evaluated in advance as the input parameters of the calculations. Because the macroscopic behavior of the core is dominated by the microscopic neutron-nucleus interactions, the uncertainty of nuclear data propagates to neutronics parameters and ultimately to the design through the core analysis. Recently, the uncertainty in nuclear data has been considered one of the major sources of uncertainty in core analysis, whereas the others can be mitigated by the great improvement of the computers and development of the sophisticated analysis methods [6, 7]. Therefore, this thesis focuses on the nuclear data-induced uncertainty among the above-mentioned sources.

1.3. Nuclear data-induced uncertainty

The core analysis employs the evaluated nuclear data libraries. There is no way to simply describe the underlying physics of neutron-nucleus interactions for all nuclides and all types of reactions through a wide range of incident neutron energy. Thus, the nuclear data are evaluated by the combined use of differential experimental data, nuclear reaction/resonance models, and appropriate approximations, aiming at providing good accuracy in their application

to integral experiments while being faithful to the differential data [8]. Because the differential experimental data are obtained via radiation measurements using neutrons (often generated by an accelerator) and sample materials, there are several sources of uncertainty in the differential experimental data, such as the statistical uncertainty of the radiation measurements, the uncertainty in the determination of the detection efficiency, and the uncertainty of the specification of the samples. Evaluators provide the covariance data of cross sections for various nuclides and types of reactions considering the propagation of the uncertainty and the corresponding correlation (often empirically given) from the differential data through the nuclear model parameters [9].

Sensitivity coefficients of key parameters of the core analysis to the nuclear data are convenient to evaluate the propagation of uncertainties from the nuclear data to these parameters. Sensitivity coefficients are defined as the ratio of small deviations of the neutronics parameters to perturbations for the nuclear data (i.e., the first-order derivative or often given in its dimensionless relative value). The uncertainties of the neutronics parameters can be evaluated by a matrix operation (i.e., the sandwich rule [10]) of a covariance matrix of the nuclear data prepared in advance and a sensitivity matrix made by arranging the sensitivity coefficients. Analyzing some portions of these matrices can help to better understand which nuclides, reactions, and energy regions are major sources of uncertainty. In addition, it is possible to evaluate correlation factors between neutronics parameters via the nuclear data and to quantify the representative factor, which is considered as an index of similarity between a target design and the reactor physics experiments [11, 12]. These analyses will assist in proposing reactor physics experiments for efficient validation of the core analysis.

Data assimilation (DA) is a mathematical methodology to seek the best possible states (e.g., the boundary conditions, input parameters, and calculation control parameters) with the

combined use of the numerical predictions and the actual observations, and then to improve the accuracy of the predictions. In the field of reactor physics, the cross section adjustment is known as a type of DA technique, whose goal is to reduce the uncertainty of the input nuclear data by the adjustment, so that the predictions can well reproduce the integral experiments, and ultimately improve the accuracy of the core analysis for the designed systems. Because such a technique requires knowledge of the relationship between input parameters and predictions, the sensitivity coefficients appear in the formulation of the cross section adjustment [7, 13].

The sensitivity coefficients have another important advantage: once the sensitivity coefficients of the benchmark problems are obtained and provided as a database, analysts can perform UQ and DA without the detailed information of the benchmark problems and without performing the sensitivity analysis (SA) again, even if they prefer to update the covariance data and/or make comparisons between different nuclear data libraries. For such efficient analysis, the Whisper code includes sensitivity profiles for over 1000 criticality benchmarks [14]. Some other activities also provide useful database storing sensitivity profiles for many critical benchmarks [15, 16]. Therefore, the sensitivity coefficients play a key role in the quantification and the reduction of the nuclear data-induced uncertainty.

1.4. Issues in evaluation in sensitivity analysis

To evaluate the sensitivity coefficients, researchers have often employed the adjoint-based method, such as the perturbation theory (PT) for the effective neutron multiplication factor (k_{eff}) [17], the generalized perturbation theory (GPT) expanded to more general responses (e.g., reaction rate ratios) [18, 19], and the depletion perturbation theory (DPT) considering the change of the compositions during burnup [20, 21]. The adjoint-based method can evaluate the change of outputs of core analyses due to the perturbation of the inputs implicitly considering flux changes

by only the inner product operations of the solution of the forward model (i.e., the neutron flux) and the importance functions corresponding to the outputs of interest. By formulating the adjoint models whose solutions are the importance functions, the calculation cost of the adjoint-based method for SA is proportional to the number of the outputs of interest. Hence, the adjoint-based method has a great advantage in terms of the calculation cost when the number of the outputs in interest is much less than that of the inputs (i.e., the number of nuclear data of interest, which corresponds to the product of the number of nuclides, reactions, and energy groups). Because of such an advantage, the adjoint-based method has been used in the analysis of the integral experiments for criticality, control rod worth, reactivity coefficient, and reaction rate ratio measurements. For the wider application of the adjoint-based method, great efforts have been devoted to developing the theory for the different types of neutronics parameters [22, 23] and the adjoint-based capabilities in the continuous energy Monte Carlo codes [24, 25].

Despite the advantage of the adjoint-based method, there are several well-known limitations in practical use: it requires the capability of formulating and solving the adjoint equations for every output of interest. In the case of the PT for the k-eigenvalue problem of the linear neutron transport equation and the neutron diffusion equation, the adjoint equation can be described simply by the transpose of the matrix operators. However, the PT can handle only the effective multiplication factor. The GPT has a wider range of applications than the PT, but it requires the setting of the adjoint sources for each output of interest, careful treatment in the orthogonal conditions of the adjoint fluxes, and a special iterative procedure to calculate the importance functions (so-called the generalized adjoint flux). In addition, because the adjoint sources possibly take positive and negative values simultaneously, it requires a special treatment different from the forward calculations, leading to a single adjoint calculation being more costly than a single forward calculation, depending on the problem settings and solver employed in the

code [26]. Things become complicated when considering multi-physics models. Even for the relatively simple coupling of the neutron transport and burnup, the DPT calculations require special orthogonal conditions for each burnup region and non-intuitive initial conditions, called jumping conditions, for each burnup step. For the coupling with the thermal-hydraulic feedback, which is typically done by 2-step calculations (i.e., assembly-core calculations) considering non-linear effects, the formulation of the adjoint model is expected to be too complicated and is not well established so far. Therefore, because of the difficulty in its formulation and complicated treatment, the use of the adjoint-based method would be impractical for SA for various types of neutronics parameters and design systems. This drawback is expected to be particularly serious for innovative reactors that may not be described by conventional formulations or may require special analyses that differ from existing reactors.

Even if the formulations of the adjoint models are established, the adjoint-based method requires significant modification of the code system, and it requires expensive implementation costs and/or is impractical: the adjoint-based method has to explicitly handle the adjoint model of the entire code system. It makes the implementation of the adjoint-based method difficult in a complicated code system consisting of various kinds of codes developed in various institutes such as the Multi-purpose Advanced Reactor physics analysis system Based on Language of Engineering (MARBLE) [27]. Furthermore, the calculation cost of the adjoint-based method is easily overwhelmed as the number of the outputs in interest surges, e.g., including spatial distribution of power and reaction rate for each time bin and nuclide inventory for each burnup step. This fact diminishes the advantage of the adjoint-based method.

Therefore, an innovative methodology that can perform SA, UQ, and DA without the adjoint calculations is strongly desired.

1.5. Purpose and contents of this study

As highlighted in the previous section, the adjoint-based method has a disadvantage in its implementation for various applications. For this reason, forward calculations attract attention. Recently, some techniques using only forward calculations with reasonably low calculation costs have been proposed for UQ [28, 29] and DA [30, 31]. These methods employ the random sampling and statistically perform UQ and DA. The major drawback of these methods is that they do not explicitly evaluate the sensitivity coefficients.

The most straightforward method for SA using forward calculations is the direct method. In this method, one evaluates sensitivity coefficients of outputs of the core analysis in interest as per their definition by performing perturbed forward calculations for each nuclear data in interest. Although this method suffers from a large number of input parameters of SA, there are a couple of advantages. First, the direct method is easy to perform because it only requires perturbations of input parameters, and no major modification of the code system is needed. Second, the sensitivity coefficients of core parameters that are accessible by analysts are evaluated simultaneously: the calculation cost is independent of the number of outputs of interest as opposed to the number of outputs in the adjoint-based method. Then, if the number of forward calculations in SA is reduced in some manner, such a forward-based method can be a competitive tool for SA of various types of neutronics parameters and design systems. The main objective of this thesis is to develop an efficient method for the SA using only forward calculations focusing on their advantages and to demonstrate UQ and DA using the sensitivity coefficients obtained along with the work in this thesis. More specifically, the objectives are as follows:

(1) Improve the calculation cost of the forward-based SA by employing the random sampling and regression between neutronics parameters and nuclear data based on the sparse modeling technique.

(2) Develop a novel method that dramatically reduces the number of forward calculations based on the combined use of sparse modeling and Reduced Order Modeling (ROM) with the idea of Active Subspace (AS).

(3) Demonstrate UQ and DA with the experiments conducted at a critical assembly for the design property of an innovative system using the sensitivity coefficient obtained along with the work in this thesis.

In Chapter 2, a new method for SA based on the lasso-type penalized linear regression, called the adaptive smooth-lasso, is proposed. As will be described later in Chapter 2, several methods based on the random sampling have been proposed as the forward-based SA method [32, 33]. In this approach using the random sampling, the calculation cost is proportional to the number of samples rather than the number of input parameters. Thus, if better knowledge between the randomly perturbed input parameters and corresponding responses can be acquired with the small number of samples, the calculation cost for SA can be improved. Especially, Reference [33] demonstrated the effectiveness of the L1 norm-constrained regression, which is a technique of the sparse modeling, applied to SA focusing on the sparsity in the sensitivity profiles to cross sections, i.e., most cross sections have a relatively small impact on neutronics parameters. Due to its well-known feature of the L1 norm constraints imposing sparsity in the solution, this approach can accurately estimate the sensitivity coefficients with a smaller number of samples than the traditional L2 norm-constrained regression. However, in the conventional L1 norm approach, cross sections to which the sensitivity coefficient is non-zero (or zero) are assumed to be unknown, leading to poor reproduction of the reference values and large statistical errors as demonstrated later in Section 2.3. In this thesis, to further improve the accuracy of this approach, the additional features of the sensitivity profiles to cross sections are considered, i.e., the continuity of the sensitivity coefficients against the induced neutron energy and the existence of giant resonances

and threshold. Through the estimation of the sensitivity coefficients of k_{eff} of the ADS at the beginning of the cycle (BOC), it is confirmed that the adaptive smooth-lasso method can accurately estimate the sensitivity coefficients with smaller sample sizes than the conventional lasso-type penalized regression methods.

In Chapter 3, the ROM-Lasso method is newly proposed to further reduce the calculation cost of the random-sampling-based method. Through the verification in Chapter 2, the adaptive smooth lasso succeeded in reducing the calculation cost of SA to about one-tenth of the number of input parameters, but the calculation cost is still significant. The proposed method combines the ROM technique and the lasso regression to dramatically reduce the dimensionality of the nuclear data in SA by expanding the sensitivity coefficients with an effective subspace, called Active Subspace (AS), and to determine the important expansion bases, respectively. To obtain AS bases with reasonably lower calculation costs, the idea of the Multi-Level ROM ($\mathrm{M_L}$ROM) [34] was employed. In the proposed method, approximated AS bases are mathematically derived through the Singular Value Decomposition (SVD) [35] of the sensitivity matrices obtained with a lower-fidelity model (e.g., a two-dimensional cylindrical model) for SA of a higher-fidelity model (e.g., a three-dimensional Cartesian model). Owing to the combined use of the lasso regression, AS bases can be optimized for each neutronics parameter. To examine the advantages of the ROM-Lasso method, a one-cycle burnup core calculation of the ADS is performed as a verification. In this verification, SA on multiple parameters after burnup, e.g., the beam current, maximum relative power, and mass of ^{241}Am at the end of the cycle (EOC), is addressed to make use of the advantage of the forward calculations whereas only k_{eff} at BOC is considered in Chapter 2. Through the verification, it is demonstrated that the ROM-Lasso method can successfully reduce the number of sample sizes by a couple of orders of magnitude compared to the adaptive smooth lasso.

In Chapter 4, the DA for lead-bismuth cross sections using sample reactivities obtained at the Kyoto University Critical Assembly (KUCA) is investigated as a practice of the application of the sensitivity coefficients. Though the issue in SA is tackled in Chapters 2 and 3, the final goal of SA is UQ and/or DA as described in Section 1.1–1.3. Japan Atomic Energy Agency (JAEA) has proposed the ADS dedicated to the transmutation of the minor actinides (MAs) produced in high-level radioactive wastes. Because key neutronics parameters of ADS proposed by JAEA have significant uncertainties contributed from lead and bismuth nuclides due to its much amount of inventory of lead-bismuth eutectic (LBE) as the coolant material, JAEA has focused on the lead void reactivity measurements [36, 37] and the lead-bismuth sample reactivity measurements [38] to validate the nuclear data related to those nuclides for application to the design of ADS. In this thesis, the nuclear-data-induced uncertainty is quantified using the sensitivity coefficients obtained in Chapter 3, and the impact on the uncertainty reduction of the coolant void reactivity of the ADS through DA with the sample reactivity experiments [38] is investigated.

Finally, the concluding remarks and future research topics to be tackled are summarized in Chapter 5.

1.6. References for Chapter 1

[1] “Energy White Paper 2023,” Ministry of Economy, Trade and Industry; https://www.enecho.meti.go.jp/about/whitepaper/2023/html/; (current as of Aug. 22, 2023) (in Japanese).

[2] “Strategic Energy Plan,” Ministry of Economy, Trade and Industry; https://www.enecho.meti.go.jp/en/category/others/basic_plan/; (current as of Aug. 22. 2023).

[3] Covariance Data Utilization and Promotion Working Group, JENDL Committee “Final Report of the Covariance Data Utilization and Promotion WG in the JENDL Committee,” JAEA-

Review 2021-014, Japan Atomic Energy Agency (Sep. 2021) (in Japanese); https://doi.org/10.11484/jaea-review-2021-014.

[4] A. K. PRINJA and E. W. LARSEN, "General Principles of Neutron Transport," in Handbook of Nuclear Engineering, D. G. Cacuci, Ed., pp. 427–542, Springer US, Boston, MA (2010); https://doi.org/10.1007/978-0-387-98149-9_5.

[5] "International Handbook of Evaluated Criticality Safety Benchmark Experiments," NEA/NSC/DOC(95)03, T. IVANOVA et al., Eds., Organization for Economic Cooperation and Development, Nuclear Energy Agency (July 2019).

[6] I. KODELI, "Sensitivity Analysis and Uncertainty Propagation from Basic Nuclear Data to Reactor Physics and Safety Relevant Parameters," *Proceedings of Evaluation of Uncertainties in Relation to Severe Accidents and Level-2 Probabilistic Safety Analysis*, Aix-en-Provence, France, (2007).

[7] K. YOKOYAMA, "A Study on Extended Cross section Adjustment Method to Reduce Uncertainty and Improve Reliability of Predicted Neutronics Parameters [Translated from Japanese by the author]," PhD Thesis, Osaka University, (2016) (in Japanese).

[8] P. OBLOŽINSKÝ, M. HERMAN, and S. F. MUGHABGHAB, "Evaluated Nuclear Data," in Handbook of Nuclear Engineering, D. G. Cacuci, Ed., pp. 83–187, Springer US, Boston, MA (2010); https://doi.org/10.1007/978-0-387-98149-9_2.

[9] R. CAPOTE, D. L. SMITH, and A. TRKOV, "Nuclear data evaluation methodology including estimates of covariances," *EPJ Web of Conferences*, **8**, *04001* (2010); https://doi.org/10.1051/epjconf/20100804001.

[10] D. G. CACUCI and M. IONESCU-BUJOR, "Sensitivity and Uncertainty Analysis, Data Assimilation, and Predictive Best-Estimate Model Calibration," in Handbook of Nuclear Engineering, D. G. Cacuci, Ed., pp. 1913–2051, Springer US, Boston, MA (2010);

https://doi.org/10.1007/978-0-387-98149-9_17.

[11] F. BROWN et al., "User Manual for Whisper-1.1," LA-UR-17-20567, Los Alamos National Laboratory (2017).

[12] A. MALDONADO and C. PERFETTI, "Utilizing Sensitivity and Correlation Coefficients from MCNP and Whisper to Guide Microreactor Experiment Design," *Nucl. Sci. Eng.*, **197**, *8*, 2086, (2023); https://doi.org/10.1080/00295639.2022.2162782.

[13] J. B. DRAGT, "Statistical Considerations on Techniques for Adjustment of Differential Cross Sections with Measured Integral Parameters," STEK, The Fast-Thermal Coupled Facility of RCN at Petten, RCN-122, Reactor Centrum Nederland, pp. 85–105 (1970).

[14] B. C. KIEDROWSKI et al., "Whisper: Sensitivity/Uncertainty-Based Computational Methods and Software for Determining Baseline Upper Subcritical Limits," *Nucl. Sci. Eng.*, **181**, *1*, 17 (2015); https://doi.org/10.13182/NSE14-99.

[15] Reactor Integral Test Working Group, JENDL Committee, "Compilation of the Data Book on Light Water Reactor Benchmark to Develop JENDL; Utilization and Extension of 2017 Report (JAEA-Data/Code 2017-006)," JAEA-Data/Code 2023-004, Japan Atomic Energy Agency (Jun. 2023) (in Japanese); https://doi.org/10.11484/jaea-data-code-2023-004.

[16] K. YOKOYAMA et al., "Development of the Unified Cross section Set ADJ2017," JAEA-Research 2018-011, Japan Atomic Energy Agency (Mar. 2019) (in Japanese); https://doi.org/10.11484/jaea-research-2018-011.

[17] B. C. KIEDROWSKI, "MCNP6.1 k-Eigenvalue Sensitivity Capability: A User's Guide," LA-UR-13-22251, Los Alamos National Laboratory (Mar. 2013); https://doi.org/10.2172/1072231

[18] L. N. USACHEV, "Perturbation Theory for the Breeding Ratio and for Other Number Ratios Pertaining to Various Reactor Processes," *J. Nucl. Energy Parts A/B*, **18**, *10*, 571 (1964);

https://doi.org/10.1016/0368-3230(64)90142-9.

[19] A. HARA, T. TAKEDA, and Y. KIKUCHI, "SAGEP: Two Dimensional Sensitivity Analysis Code Based on Generalized Perturbation Theory," JAERI-M 84-027, Japan Atomic Energy Research Institute (Feb. 1984) (in Japanese); https://doi.org/10.11484/jaeri-m-84-027.

[20] M. L. WILLIAMS, "Development of Depletion Perturbation Theory for Coupled Neutron/Nuclide Fields," *Nucl. Sci. Eng.*, **70**, *1*, 20 (1979); https://doi.org/10.13182/NSE79-3.

[21] G. CHIBA, Y. KAWAMOTO, and T. NARABAYASHI, "Development of a fuel depletion sensitivity calculation module for multi-cell problems in a deterministic reactor physics code system CBZ," *Ann. Nucl. Energy*, **96**, 313 (2016); https://doi.org/10.1016/j.anucene.2016.06.013.

[22] I. A. KODELI, "Sensitivity and Uncertainty in the Effective Delayed Neutron Fraction (β_{eff})," *Nucl. Instrum. Meth. Phys. Res. A.*, **715**, 70 (2013); https://doi.org/10.1016/j.nima.2013.03.020.

[23] T. ENDO and A. YAMAMOTO, "Sensitivity Analysis of Prompt Neutron Decay Constant Using Perturbation Theory," *J. Nucl. Sci. Technol*., **55**, *11*, 1245, (2018).

[24] M. AUFIERO et al., "A Collision History-Based Approach to Sensitivity/Perturbation Calculations in the Continuous Energy Monte Carlo Code SERPENT," *Ann. Nucl. Energy*., **85**, 245 (2015); https://doi.org/10.1016/j.anucene.2015.05.008.

[25] C. M. PERFETTI and B. T. REARDEN, "Development of a Generalized Perturbation Theory Method for Sensitivity Analysis Using Continuous-Energy Monte Carlo Methods," *Nucl. Sci. Eng*., **182**, *3*, 354 (2016); https://doi.org/10.13182/NSE15-13.

[26] C. KENNEDY, "GPT-Free Sensitivity Analysis for Reactor Depletion and Analysis," PhD Thesis, North Carolina State University (2015).

[27] K. YOKOYAMA et al., "Development of Comprehensive and Versatile Framework for Reactor Analysis, MARBLE," *Ann. Nucl. Energy*, **66**, 51 (2014); https://doi.org/10.1016/j.anucene.2013.11.047.

[28] M. L. WILLIAMS et al., "A Statistical Sampling Method for Uncertainty Analysis with SCALE and XSUSA," *Nucl. Technol.*, **183**, *3*, 515 (2013); https://doi.org/10.13182/NT12-112.

[29] A. YAMAMOTO et al., "Uncertainty Quantification of LWR Core Characteristics Using Random Sampling Method," *Nucl. Sci. Eng.*, **181**, *2*, 160 (2015); https://doi.org/10.13182/NSE14-152.

[30] T. WATANABE et al., "Cross Section Adjustment Method Based on Random Sampling Technique," *J. Nucl. Sci. Technol.*, **51**, *5*, 590 (2014); https://doi.org/10.1080/00223131.2014.882801.

[31] A. HOEFER et al., "MOCABA: A General Monte Carlo–Bayes Procedure for Improved Predictions of Integral Functions of Nuclear Data," *Ann. Nucl. Energy,* **77**, 514 (2015); https://doi.org/10.1016/j.anucene.2014.11.038.

[32] G. CHIBA et al., "Estimation of Neutronics Parameter Sensitivity to Nuclear Data in Random Sampling-Based Uncertainty Quantification Calculations," *Ann. Nucl. Energy*, **75**, 395 (2015); https://doi.org/10.1016/j.anucene.2014.08.049.

[33] T. WATANABE et al., "Estimation of Sensitivity Coefficient Using Random Sampling and L1-Norm Minimization," *Trans. Am. Nucl. Soc.*, **111**, 1391 (2014).

[34] M. ABDO, "Multi-Level Reduced Order Modeling Equipped with Probabilistic Error Bounds," PhD Thesis, North Carolina State University, (2016).

[35] Z. BAI et al., Eds., Templates for the Solution of Algebraic Eigenvalue Problems: A Practical Guide, Society for Industrial and Applied Mathematics (2000); https://doi.org/10.1137/1.9780898719581.

[36] M. FUKUSHIMA et al., “Lead Void Reactivity Worth in Two Critical Assembly Cores with Differing Uranium Enrichments,” *Nucl. Sci. Eng.,* **189**, *1*, 93 (2018); https://doi.org/10.1080/00295639.2017.1373520.

[37] M. FUKUSHIMA et al., “Systematic Measurements and Analyses for Lead Void Reactivity Worth in a Plutonium Core and Two Uranium Cores with Different Enrichments,” *Nucl. Sci. Eng.,* **194**, *2*, 138 (2020); https://doi.org/10.1080/00295639.2019.1663089.

[38] C. H. PYEON et al., “Void Reactivity in Lead and Bismuth Sample Reactivity Experiments at Kyoto University Critical Assembly,” *Nucl. Sci. Eng.,* published online on Mar. 13 (2023); https://doi.org/10.1080/00295639.2023.2172311.

2. Estimation of sensitivity coefficient based on lasso-type linear regression

2.1. Introduction

The safe and efficient operation of nuclear reactors needs to quantify and reduce the uncertainty of core neutronics parameters predicted by numerical core analysis. In addition, the uncertainties propagated from the nuclear data are still large for a future nuclear system such as the ADS, thus both the differential and integral experiment data for efficient reduction of the uncertainties of the design calculations are desirable. The identification of the dominant nuclear data for uncertainties is important to propose the desired experiment. The sensitivity coefficients of the core neutronics parameter to cross section data are often used for uncertainty quantification based on error propagation, cross section adjustment method, and a method to identify nuclear data for which further improvements are required to reduce uncertainties of target integral neutronics parameters [1–3]. Consequently, the evaluation of the sensitivity coefficients of core neutronics parameters is important in core analysis.

As described in Chapter 1, there are two sensitivity estimation methods, i.e., the direct method, and the adjoint-based method. The direct method estimates the sensitivity coefficients by performing the perturbed calculations for each input parameter. Because the direct method requires only forward calculations and no major modifications of existing codes, the use of the direct method is easy. However, the calculation cost of this method is proportional to the number of input parameters taken into account, thus this method would be impractical due to a large number of input parameters (e.g., fine-group microscopic cross sections). On the other hand, in the adjoint-based method, the adjoint models defined for each interesting neutronics parameter

are evaluated to estimate the sensitivity coefficients [4–6]. The calculation cost of this method depends on the number of output parameters as opposed to the number of input parameters in the direct method. Thus, when the number of the neutronics parameters is less than that of the input parameters, the adjoint-based method is superior to the direct method from the viewpoint of the calculation cost. However, the adjoint-based method generally requires modification of the calculation code system to formulate and solve the adjoint model. It would require a great effort to modify the complicated code system which performs the series of core analyses by combining several codes (e.g., lattice-calculation, core-calculation, and burnup-calculation codes) and the definition of the adjoint model for such a complicated code system will be sometimes difficult. Therefore, the application of the adjoint method would be difficult to perform. Furthermore, the calculation cost of the adjoint-based method is proportional to the number of the neutronics parameters taken into account, thus the adjoint-based method would be also impractical when the number of the neutronics parameters (e.g., power distribution, space/energy flux distribution, and the number density of the nuclides) is large.

As another approach, several methods based on random sampling have been proposed [7, 8]. These methods estimate the sensitivity coefficients by solving the simultaneous linear equations whose solution is the sensitivity coefficients. The calculation cost of these methods is proportional to the number of the random samples, though these methods utilize only forward calculations. Therefore, the calculation cost is less than that of the forward method when the number of samples is smaller than that of nuclear data of interest. However, in such a case, the simultaneous equation for the sensitivity coefficients is an underdetermined system (as described in Section 2.2.1), thus the constraint condition is required. In Reference [8], the sensitivity coefficients are determined based on the L1 norm minimization. Generally, the solution obtained by the L1 norm minimization is sparse, most of the elements of which are zero [9]. In typical

reactor analysis, most of the cross sections have a very small impact on neutronics parameters (i.e., small sensitivity coefficient) and a small part of cross section dominates neutronics parameters (i.e., large sensitivity coefficient). In other words, sensitivity coefficients for cross sections are very "sparse". Consequently, the L1 norm minimization can adequately estimate especially large sensitivity coefficients with a smaller number of the random samples than that of the input parameters [8]. As a similar approach, the penalized linear regression "lasso", in which the L1 norm of the solution vector is considered as the penalized term, is proposed [10]. Lasso can obtain a sparse solution similar to the L1 norm minimization method. However, in the L1 norm minimization and lasso methods, cross sections to which the sensitivity coefficient is non-zero (or zero) are assumed to be unknown. Thus, the non-zero (or zero) sensitivity coefficients are sometimes evaluated as zero (or non-zero).

Now, let us consider the shape of sensitivity coefficients. The energy region of large sensitivity coefficients depends on the type of reactor, e.g., thermal or fast reactor. For instance, in a fast reactor, the sensitivity coefficients have large positive or negative values in the fast energy region and very small values in the thermal energy region. Namely, the non-zero elements of the sensitivity coefficients are not randomly distributed but are clustered in a certain energy region depending on the type of reactor. For this reason, the "smooth-lasso" would be a better choice, whose penalized term consists of not only the L1 norm but also the sum of squares of the difference between adjacent elements [11]. The smooth-lasso can select the sparse solution but the difference between adjacent elements is small. It means that the elements show smooth change for the index of the solution vector. Owing to the smoothness, zero and non-zero elements of a solution vector selected by smooth-lasso would be clustered, respectively. Thus, the smooth-lasso would be more appropriate for the estimation of the sensitivity coefficients than the lasso. However, the sensitivity coefficients would not change smoothly depending on the energy range

due to the threshold reactions and the giant resonance cross sections, although the non-zero elements are distributed in a cluster in certain energy regions. Then, this chapter proposes the weighted penalized linear regression "adaptive smooth-lasso" that would be more appropriate for the estimation of sensitivity coefficients of the neutronics parameters to the microscopic cross sections than the lasso and smooth-lasso. The main objective of this chapter is to confirm the applicability of the adaptive smooth-lasso compared to the two conventional methods, i.e., the lasso and the smooth-lasso. In this chapter, the applicability of the adaptive smooth-lasso is demonstrated through the estimation of SA of the effective multiplication factor k_{eff} of an ADS.

The remainder of this chapter is organized as follows. In Section 2.2, the estimation of the sensitivity coefficients based on the random sampling and the penalized linear regression is described. In Section 2.3, the numerical results of the proposed method are shown in comparison with the conventional and the direct methods. Finally, concluding remarks are summarized in Section 2.4.

2.2. Method

2.2.1. Penalized regression in random sampling of cross section

Firstly, let us consider that the numbers of the cross sections, the neutronics parameters, and the samples are N, one, and M, respectively. Using the first-order approximation of the Taylor expansion, the relative variation of the neutronics parameter obtained with small relative variations of the cross sections is approximately expressed as follows:

$$\Delta R_i = \sum_{j=1}^{N} \Delta T_{ij} g_j, \tag{2.1}$$

where i is the index of the sample, j is the index of the cross sections, ΔR_i is a relative variation of the neutronics parameter in the i-th sample, ΔT_{ij} is a relative variation of the j-th cross section in the i-th sample, and g_j is the relative sensitivity coefficient of the neutronics parameter to the j-th cross section [$g_j \equiv (dR/R)/(dT_j/T_j)$]. Equation (2.1) can be represented in a matrix-vector form as follows:

$$\Delta\vec{R} = \Delta\mathbf{T}\vec{g}, \tag{2.2}$$

where, $\Delta\vec{R}$, $\Delta\mathbf{T}$, and $\vec{g}$ can be written as follows:

$$\Delta\vec{R} = (\Delta R_1, \Delta R_2, \dots, \Delta R_M)^T, \tag{2.3}$$

$$\Delta\boldsymbol{T} = \begin{pmatrix} \Delta T_{11} & \Delta T_{12} & \dots & \Delta T_{1N} \\ \Delta T_{21} & \Delta T_{22} & \dots & \Delta T_{2N} \\ \vdots & \vdots & \ddots & \vdots \\ \Delta T_{M1} & \Delta T_{M2} & \dots & \Delta T_{MN} \end{pmatrix}, \tag{2.4}$$

$$\vec{g} = (g_1, g_2, \dots, g_N)^T. \tag{2.5}$$

$\Delta\vec{R}$, $\Delta\mathbf{T}$, and $\vec{g}$ are M-dimensional column vector, M-by-N matrix, and N-dimensional column vector, respectively. In the estimation of the sensitivity coefficients, Equation (2.2) is a simultaneous linear equation whose solution is the vector $\vec{g}$. When $M < N$, the number of equations is fewer than that of unknowns (i.e., elements of $\vec{g}$) so the solution of Equation (2.2) cannot be uniquely determined. For such an underdetermined system, the solution $\vec{g}$ can be determined by the penalized linear regression as follows [12]:

$$\vec{g} = \text{argmin}\left\{\frac{1}{2}\sum_{i=1}^{M}\left(\Delta R_i - \sum_{j=1}^{N}\Delta T_{ij} g_j\right)^2 + p(\vec{g})\right\}, \tag{2.6}$$

where, $p(\vec{g})$ is the penalty term and the argmin of a function is the values of the arguments at which the function is minimized. The various types of the penalty term are proposed as follows [12]:

$$p(\vec{g}) = \frac{\lambda}{2}\sum_{j=1}^{N} g_j^2, \tag{2.7}$$

$$p(\vec{g}) = \lambda \sum_{j=1}^{N} |g_j|, \tag{2.8}$$

$$p(\vec{g}) = \lambda_1 \sum_{j=1}^{N} |g_j| + \frac{\lambda_2}{2}\sum_{j=2}^{N}\left(g_j - g_{j-1}\right)^2, \tag{2.9}$$

where the regressions by Equation (2.7) through Equation (2.9) are called the ridge, lasso, and smooth-lasso, respectively. The parameters λ, λ_1 and λ_2 in Equation (2.7) through Equation (2.9) are user-defined hyperparameters. Equation (2.6) determines $\vec{g}$ which minimizes the summation of the residual sum of squares between $\Delta\vec{R}$ and $\Delta\mathbf{T}\vec{g}$, and the penalty term $p(\vec{g})$ depending on $\vec{g}$. The penalty term prohibits a solution whose elements are inappropriately large (e.g., point at infinity).

Figure 2.1 illustrates a difference between a solution by the ridge and the lasso. Figure 2.1 is a two-dimensional figure; however, each axis corresponds to $g_1, g_2, \ldots, g_N$. The ellipses in

Figure 2.1 represent contours that have the same residual sum of squares term, and the inner lines correspond to the smaller residual. Furthermore, the circle and the square centered at the origin represent the contour of the penalty term for the ridge and the lasso ($p(\vec{g})$ = const), respectively. The contact point of the ellipse and contour of the penalty term is the solution that reduces both the residual sum of squares and the penalty term. As shown in Figure 2.1, the lasso solution tends to be located at a corner, which contains a zero coefficient. On the other hand, no corner exists in the ridge penalty term thus the sparse solutions are rarely selected. The sensitivity coefficients of the neutronics parameters to the multi-group microscopic cross sections are generally sparse, hence the lasso will be appropriate for the estimation of the sensitivity coefficients.

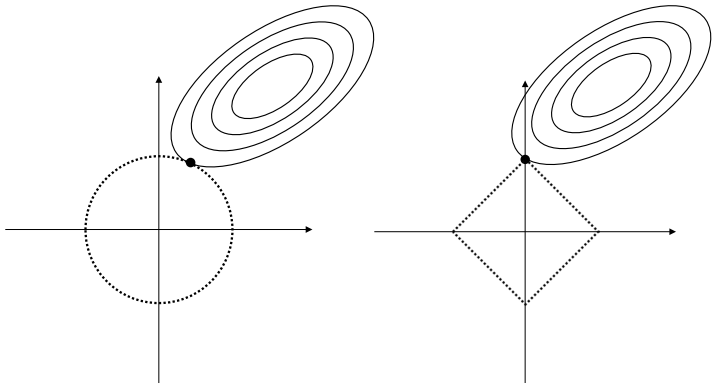

(a) ridge (b) lasso

Figure 2.1 Illustration of (a) the ridge and (b) lasso regressions.

The penalty term of the smooth-lasso is defined as the sum of squares of the difference between adjacent elements. Therefore, the smooth-lasso selects the solution whose adjacent elements have close values while keeping the sparsity. Namely, the zero and non-zero elements of the solution obtained by smooth-lasso would be distributed in a cluster while the lasso does not consider the structure of the non-zero elements. The large sensitivity coefficients of the neutronics parameters to the microscopic cross sections are distributed in certain energy regions depending

on the type of reactor, thus the smooth-lasso is expected more appropriate for the estimation of the sensitivity coefficients than the lasso. However, the elements of the solution obtained by smooth-lasso change smoothly depending on the energy index. Thus, the solution obtained by smooth-lasso would fail to reproduce the rapid changes of sensitivity coefficient due to threshold reactions or giant resonance cross sections.

2.2.2. Adaptive smooth-lasso

As mentioned in the previous section, the solution obtained by the smooth-lasso would not sufficiently reproduce the steep energy dependence of the sensitivity coefficients. Then, the weighted penalized regression "adaptive smooth-lasso" is newly proposed. The penalty term of the adaptive smooth-lasso is defined as follows:

$$p(\vec{g}) = \lambda_1 \sum_{j=1}^{N} v_j |g_j| + \frac{\lambda_2}{2} \sum_{j=2}^{N} w_j \left(g_j - g_{j-1}\right)^2. \tag{2.10}$$

Equation (2.10) represents the penalty term of smooth-lasso multiplied by the weight v_j and w_j. Here the weight v_j and w_j are defined as follows.

$$v_j = \frac{1}{1 + c\left|\tilde{g}_j\right|^{\gamma}}, \tag{2.11}$$

$$w_j = \frac{1}{1 + c\left(\frac{\left|\tilde{g}_j\right| + \left|\tilde{g}_{j-1}\right|}{2}\right)^{\gamma}}. \tag{2.12}$$

The element $\tilde{g}$ is the sensitivity coefficient estimated by the smooth-lasso, and the constants c

and γ are user-defined hyperparameters ($c > 0$ and $\gamma > 0$). As can be seen in Equation (2.11) and (2.12), the range of weight v_j and w_j is [0, 1]. These weights (i.e., v_j and w_j) take small values for the large absolute values of the non-zero elements of the sensitivity coefficients obtained by smooth-lasso (i.e., $\tilde{g}_j$ or $\tilde{g}_{j-1}$). As the smaller values of the weight v_j, the L1 norm penalty term gets smaller. Thus the j-th sensitivity coefficient g_j tends to take a larger absolute value. Furthermore, as the smaller values of the weight w_j, the penalty term of the sum of squares of the difference between adjacent elements gets smaller. Thus, the large difference between the adjacent elements (i.e., steep changes between $\tilde{g}_{j-1}$ and $\tilde{g}_j$) is allowed. Namely, it is expected that the adaptive smooth-lasso can emphasize the non-zero elements and allow steep changes between the adjacent elements than the smooth-lasso. For zero elements, the weight remains one, thus zero element distribution would be similar between the smooth-lasso and adaptive smooth-lasso. For the larger value of c, the weights v_j and w_j take smaller values. For the smaller value of γ, the weights v_j and w_j take smaller values for smaller absolute values of non-zero elements, i.e., larger absolute values and steep changes are allowed even for small absolute values of non-zero elements estimated by the smooth-lasso.

The adaptive smooth-lasso requires four user-defined hyperparameters, i.e., λ_1, λ_2, c, and γ. For example, when c is zero, the adaptive smooth-lasso is equivalent to the smooth-lasso. When λ_2 is also zero, the adaptive smooth-lasso is equivalent to the lasso. Namely, the sensitivity coefficients estimated by the adaptive smooth-lasso depend on the hyperparameters. In this chapter, as mentioned later in Section 2.3, the hyperparameters in the adaptive smooth lasso (i.e., λ_1, λ_2, c, and γ) are determined by preliminary calculations so that the estimated sensitivity coefficients can reproduce the reference values.

2.3. Numerical verification

2.3.1. Verification conditions

To verify the proposed method, SA of the effective neutron multiplication factor k_{eff} of an ADS is performed. As the ADS core, the basic concept investigated in JAEA was adopted [13]. **Figure 2.2** shows the two-dimensional R-Z geometry of the ADS. The MA core region in the ADS is composed of fuel, cladding tubes, and LBE coolant. The volume ratio of these component materials is 0.27:0.10:0.63. The k_{eff} of the ADS initial core was set to 0.97 by adjusting the weight ratio of zirconium nitride (ZrN) and plutonium (Pu) + MA nitride [(Pu+MA)-N]. The isotopic compositions of the actinides are listed in **Table 2.1**.

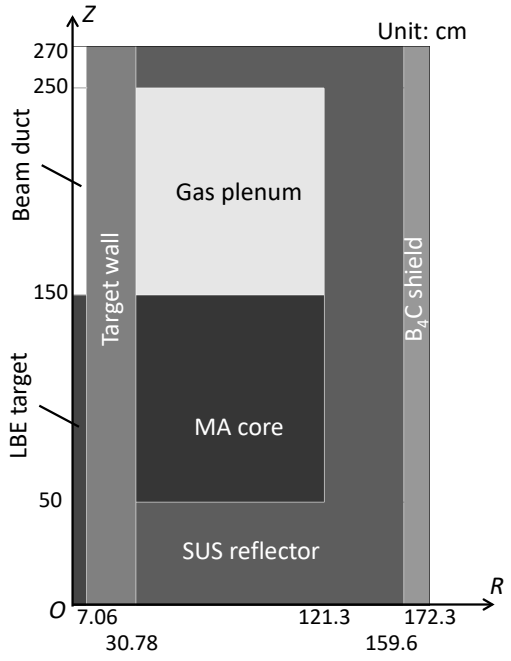

Figure 2.2 Two-dimensional R-Z geometry for ADS initial core.

Table 2.1. Isotopic composition of actinides in the MA core region.

Nuclide	Composition [wt%]	Nuclide	Composition [wt%]
^{234}U	0.01	^{241}Am	23.19
^{237}Np	34.21	^{242m}Am	0.04
^{238}Pu	0.71	^{243}Am	9.68
^{239}Pu	16.17	^{243}Cm	0.02
^{240}Pu	7.41	^{244}Cm	2.95
^{241}Pu	3.22	^{245}Cm	0.29
^{242}Pu	2.07	^{246}Cm	0.03

The ADS3D code was used to perform the core calculation [14]. The criterion of outer iteration for k_{eff} was set to 1.0×10^{-7}. The energy-group structure was the 73-energy-group from 0.1 eV to 20 MeV employed in the fast group constant sets (UFLIB.J40 [15]) based on JENDL-4.0. As the input parameters, a total of 13286 multi-group microscopic cross sections are taken into account: there are 73 group cross sections for seven reactions (capture, fission, the average number of neutrons per fission $\bar{\nu}$, (n,2n), inelastic scattering, elastic scattering, and average scattering cosine $\bar{\mu}$) of 26 nuclides, i.e. 13268 = $73 \times 7 \times 26$. The indices of a microscopic cross section of the first energy group are listed in **Table 2.2**. The index of the G-th group microscopic cross section for the n-th row nuclide and the r-th column reaction is defined as:

$$j = G + 73 \times (r - 1) + 73 \times 7 \times (n - 1). \tag{2.13}$$

By defining the index as Equation (2.13), the adjacent elements are arranged in the order of energy, thus the non-zero values cluster within a particular energy range can be considered by the smooth-lasso.

Table 2.2. Index of the microscopic cross section of the first energy group.

Nuclide	Capture	Fission	$\bar{\nu}$	(n,2n)	Inelastic scattering	Elastic scattering	$\bar{\mu}$
^{54}Fe	1	74	147	220	293	366	439
^{56}Fe	512	585	658	731	804	877	950
^{57}Fe	1023	1096	1169	1242	1315	1388	1461
^{90}Zr	1534	1607	1680	1753	1826	1899	1972
^{91}Zr	2045	2118	2191	2264	2337	2410	2483
^{92}Zr	2556	2629	2702	2775	2848	2921	2994
^{94}Zr	3067	3140	3213	3286	3359	3432	3505
^{96}Zr	3578	3651	3724	3797	3870	3943	4016
^{204}Pb	4089	4162	4235	4308	4381	4454	4527
^{206}Pb	4600	4673	4746	4819	4892	4965	5038
^{207}Pb	5111	5184	5257	5330	5403	5476	5549
^{208}Pb	5622	5695	5768	5841	5914	5987	6060
^{209}Bi	6133	6206	6279	6352	6425	6498	6571
^{237}Np	6644	6717	6790	6863	6936	7009	7082
^{241}Am	7155	7228	7301	7374	7447	7520	7593
^{242m}Am	7666	7739	7812	7885	7958	8031	8104
^{243}Am	8177	8250	8323	8396	8469	8542	8615
^{243}Cm	8688	8761	8834	8907	8980	9053	9126
^{244}Cm	9199	9272	9345	9418	9491	9564	9637
^{245}Cm	9710	9783	9856	9929	10002	10075	10148
^{246}Cm	10221	10294	10367	10440	10513	10586	10659
^{238}Pu	10732	10805	10878	10951	11024	11097	11170
^{239}Pu	11243	11316	11389	11462	11535	11608	11681
^{240}Pu	11754	11827	11900	11973	12046	12119	12192
^{241}Pu	12265	12338	12411	12484	12557	12630	12703
^{242}Pu	12776	12849	12922	12995	13068	13141	13214

Each microscopic cross section was uniformly sampled in the range of ±5 % (this range was empirically determined). It is worth noting that SA based on the random sampling does not require correlations between cross sections as opposed to UQ based on the random sampling, and the sampling was done independently for each cross section. The relative sensitivity coefficients of k_{eff} to the 13268 microscopic cross sections are estimated with 100, 200, 500, 750, 1000, 1500, 2000, and 4000 samples by the lasso, the smooth-lasso, and the adaptive smooth-lasso. **Table 2.3** lists the user-defined tuning parameters used in this verification calculation. These values in Table 2.3 were determined based on preliminary calculations so that the estimated sensitivity coefficients can well reproduce the reference values obtained by the direct method. For lasso, we utilize λ_1 in Table 2.3 as λ in Equation (2.8).

Table 2.3. The values of tuning parameters used for sensitivity coefficient estimation.

parameter	value
λ_1	1.0×10^{-4}
λ_2	0.10
c	30.0
γ	0.50

The reference values of the relative sensitivity coefficients are evaluated with the direct method with the central difference approximation using 5% perturbation (i.e., one non-perturbed forward calculation and 13286×2 times perturbed forward calculations are additionally performed). The difference between the estimated and reference values of the sensitivity coefficients are quantified by relative difference norm defined as:

$$e = \frac{\|\vec{g}_{\mathrm{est}} - \vec{g}_{\mathrm{ref}}\|_2}{\|\vec{g}_{\mathrm{ref}}\|_2}, \tag{2.14}$$

where, $\vec{g}_{\mathrm{est}}$ and $\vec{g}_{\mathrm{ref}}$ are the sensitivity coefficients obtained by three penalized linear regression and by the direct method, respectively and $\|\vec{x}\|_2$ represents the L2 norm of a vector $\|\vec{x}\|_2$. When the estimated values are equal to the reference values, the relative difference norm defined by Equation (2.14) is zero.

The statistical errors of the sensitivity coefficients and the difference norm of Equation (2.14) with the lasso, the smooth-lasso, and the adaptive smooth-lasso are evaluated by the resampling technique so-called Jackknife technique [16].

2.3.2. Results

Figures 2.3 (a)–(d) show the sensitivity coefficients obtained by the direct method, lasso, smooth-lasso, and adaptive smooth-lasso with 750 samples. As shown in the result by the direct method, most of the sensitivity coefficients are zero, i.e., sparse. The result by the lasso shows that the many sensitivity coefficients are miss-predicted as non-zero values for the cross sections whose reference value of sensitivity coefficient is zero. As can be seen from the result of the smooth-lasso and the adaptive smooth-lasso in Figure 2.3, some sensitivity coefficients cannot completely reproduce the reference values although the tuning parameters are optimized. This is because the sample number of 750 is significantly smaller than the number of input parameters (i.e., 13286 in this chapter) and the information about the relation between the input parameters and the response is not enough to completely reproduce the sensitivity coefficients. However, we can observe that the smooth-lasso and the adaptive smooth-lasso can reproduce the structure of the non-zero values of the sensitivity coefficients better than the lasso.

Figures 2.4 (a)–(c) compare the sensitivity coefficients to the fission cross sections of ^{239}Pu obtained by lasso, smooth-lasso, and adaptive smooth-lasso with 750 samples with the reference values obtained by the direct method. Figure 2.4 (a) shows that some relative sensitivity

coefficients obtained by lasso take zero or small values for the indexes where the reference values are not negligible. Figure 2.4 (b) shows that the relative sensitivity coefficients obtained by smooth-lasso are smaller than those of reference and fail to reproduce the steep change of the sensitivity coefficients for the index. Figure 2.4 (c) shows that the relative sensitivity coefficients obtained by adaptive smooth-lasso are emphasized to reproduce the reference values and capture the steep change tendency of the reference values compared to smooth-lasso.

Figure 2.5 shows the relative difference norm for each method versus the number of samples. As shown in Figure 2.5, the difference norms are decreased as the number of samples increases. The relative difference norms by the lasso are the largest and those by the adaptive smooth lasso are the smallest among the three penalized linear regressions.

Figure 2.6 shows the comparison of the relative sensitivity coefficients obtained by each method with 750 samples and those obtained by the direct method. In Figure 2.6, the horizontal and vertical axes represent the relative sensitivity coefficients of the k_{eff} obtained by the direct method and each method, respectively. The error bars in Figure 2.6 are the standard deviations estimated by the Jackknife technique. As shown in Figure 2.6 (a), we observe the "cross" plots centered at the origin in the lasso result. This result indicates that the sensitivity coefficients are miss-predicted as non-zero (or zero) values for the cross sections whose sensitivity coefficients are zero (or non-zero). This is because the lasso does not consider the structure of the non-zero elements for energy. In addition, the error bars of the lasso result are larger than those of the smooth-lasso and the adaptive smooth-lasso results. This is also because the structure of the non-zero elements is not considered, i.e., the indexes for non-zero sensitivity coefficients are frequently changed according to the Jackknife resample of cross sections. In Figure 2.5, due to the cross plots, the error norm by the lasso is the largest among the three estimation methods. In Figures 2.6 (b) and (c), we cannot observe the cross plots and the error bars are smaller than those

of the lasso result. These results indicate that the smooth-lasso and adaptive smooth-lasso well reproduce the structure of the non-zero elements of sensitivity coefficients compared to the lasso. As shown in Figure 2.6 (b), most of the absolute values of sensitivity coefficients obtained by the smooth-lasso are smaller than those of reference. The sensitivity coefficients whose neighbor sensitivity coefficient is zero or small are underestimated since the smooth-lasso selects the solution whose adjacent elements take close values. Consequently, the smooth-lasso fails to accurately reproduce the steep changes of the sensitivity coefficients for the energy and underestimates the absolute values of sensitivity coefficients.

The adaptive smooth-lasso reduces the underestimation tendency compared to the smooth-lasso as shown in Figure 2.6 (c). This is because the large absolute values of sensitivity coefficients are emphasized, and the steep changes of the sensitivity coefficients are allowed by the weighted penalty term of the adaptive smooth-lasso. Because the cross plots and underestimation tendencies are mitigated, the relative difference norm by the adaptive smooth-lasso is the smallest among the three penalized linear regressions as shown in Figure 2.5: compared to 2000 samples in the conventional lasso regression, 20% of the relative difference norm was achieved with 1000 samples in the adaptive smooth lasso. In conclusion, the adaptive smooth-lasso newly proposed in this study can be a better candidate for SA without adjoint calculations than the other two conventional regressions.

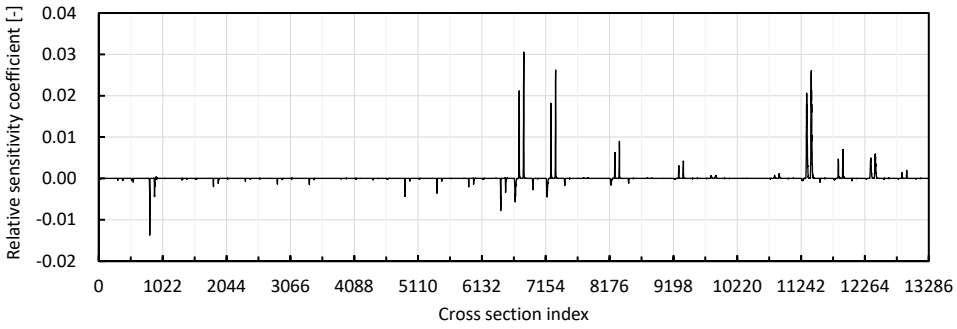

(a) direct method

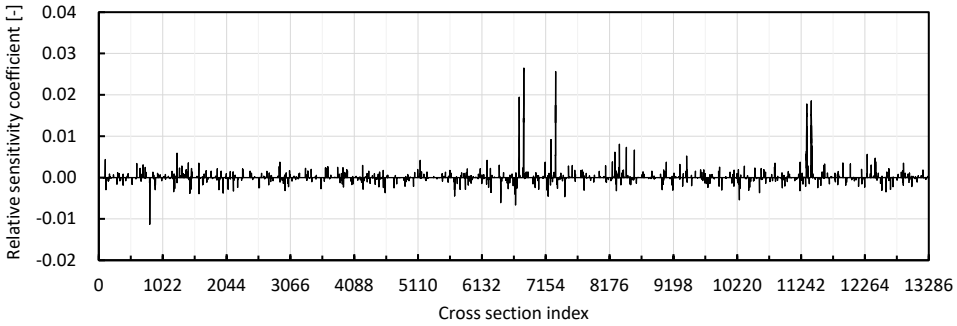

(b) lasso

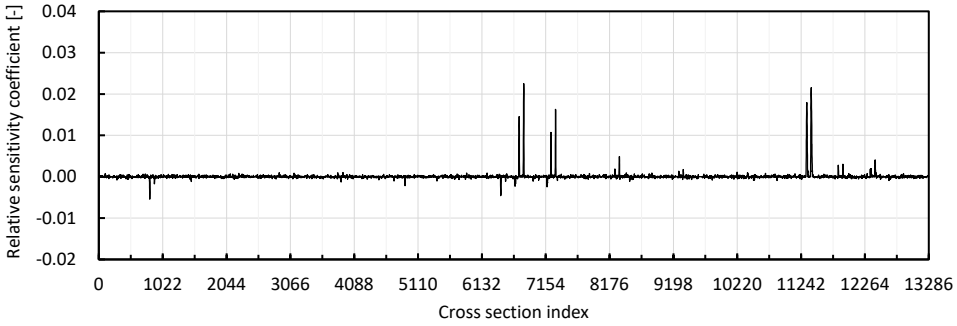

(c) smooth-lasso

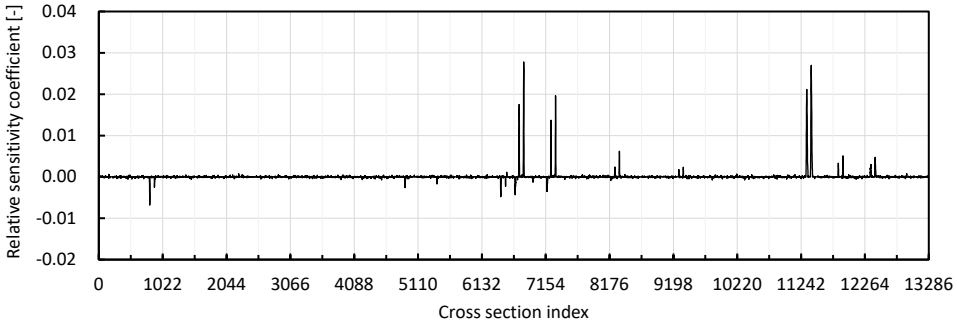

(d) adaptive smooth-lasso

Figure 2.3 Relative sensitivity coefficients of k_{eff} of ADS initial core with 750 samples.

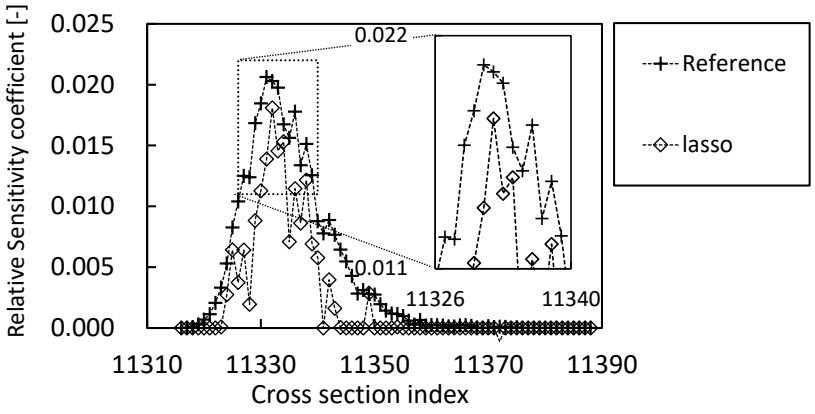

(a) lasso

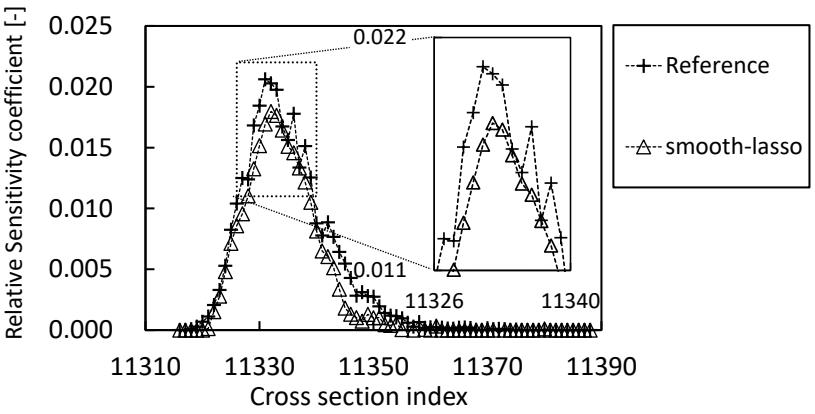

(b) smooth-lasso

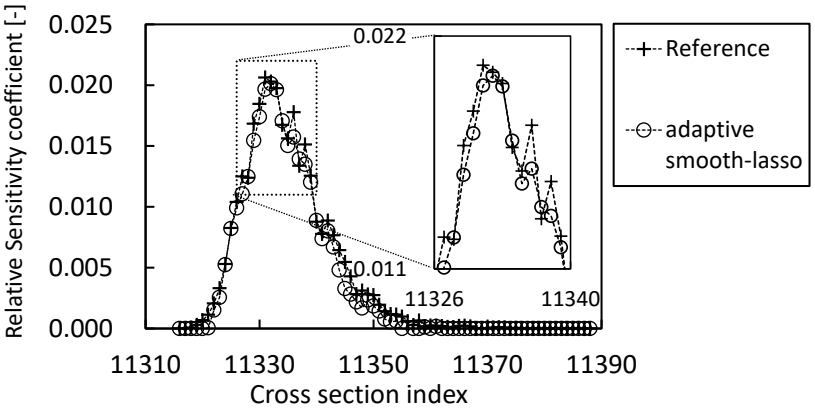

(c) adaptive smooth-lasso

Figure 2.4 Relative sensitivity coefficients of k_{eff} to the fission cross section of ^{239}Pu with 750 samples.

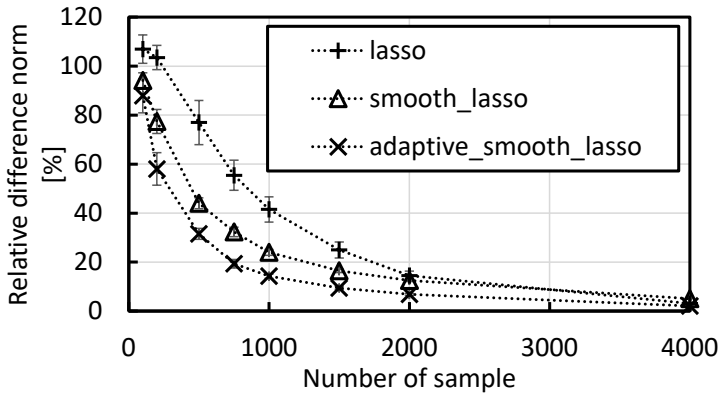

Figure 2.5 The number of samples versus relative difference norm of relative sensitivity of k_{eff} of ADS initial core.

2.3.3. Issue in adaptive smooth lasso

As shown in Figure 2.6 (c), the sensitivity coefficients with large absolute values were reproduced by the adaptive smooth-lasso with a sample size of the order of 1000. However, in other words, it still requires about 1000 forward calculations of SA of about 10000 nuclear data, indicating that a dramatic improvement in the calculation cost has not been achieved. The adaptive smooth-lasso aimed at capturing the feature of the sensitivity coefficients for the incident neutron energy by introducing the additional penalty term and weights. In the next chapter, as another approach to capture the feature of the sensitivity coefficients, the ROM-Lasso method is proposed focusing on the ROM technique based on the AS.

The other open issue is the determination of four hyperparameters. Because the estimated results are sensitive to these hyperparameters, they should be optimized to accurately estimate the sensitivity coefficients. However, in this work, they were determined manually so that the estimated sensitivity coefficients well reproduced the reference values by the direct method. The optimization method without reference values of the direct method is desirable for the practical application.

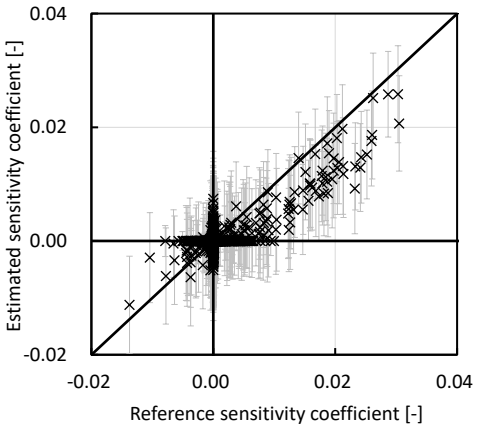

(a) lasso

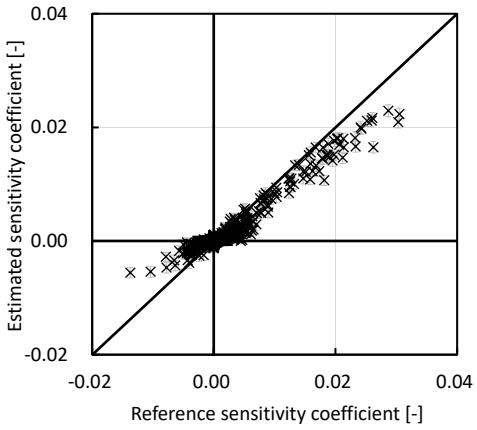

(b) smooth-lasso

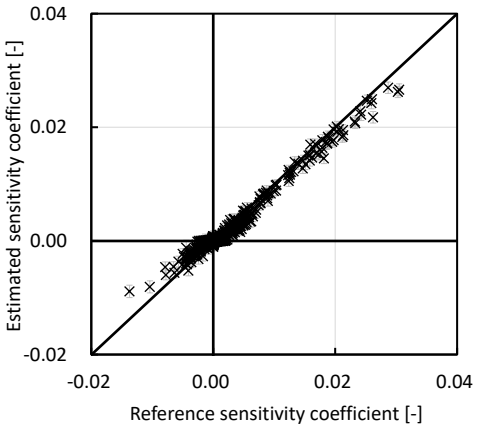

(c) adaptive smooth-lasso

Figure 2.6 Comparison of relative sensitivity coefficients of k_{eff} of ADS initial core. The number of samples is 750.

2.4. Conclusions

The adaptive smooth-lasso is newly proposed as an estimation method of the sensitivity coefficients of the neutronics parameters using the random sampling. The proposed method is based on a lasso-type penalized linear regression. The proposed method utilizes the weighted penalty term aiming to reproduce the sensitivity coefficients having steep energy dependence with a small number of samples. The proposed method utilizes only forward calculations.

To verify the proposed method, three lasso-type penalized regressions including the proposed method were applied for the estimation of the relative sensitivity coefficients of k_{eff} of an ADS. A total of 13286 cross sections, i.e., 73-group microscopic cross sections of 26 nuclides are considered. Through the verification calculation, it is confirmed that sensitivity coefficients obtained by the proposed method can accurately reproduce those of the direct method with smaller samples compared to the other two conventional methods, i.e., the lasso and smooth-lasso.

Even though the better performance of the adaptive smooth-lasso was demonstrated in comparison with the conventional regressions, the dramatic reduction in the number of forward calculations was not achieved from the direct method. In addition, the proposed method has a disadvantage in the optimization of four user-defined hyperparameters. Such an optimization of multiple hyperparameters is an open issue.

To achieve future reduction of the calculation cost, the ROM-Lasso method is proposed focusing on the ROM technique based on the AS in the next chapter. Since the ROM-Lasso method considers only one hyperparameter, a conventional method for the parameter optimization is applied as discussed later in Section 3.2.2. Therefore, the issue of the multiple-hyperparameter optimization can be avoided.

2.5. References for Chapter 2

[1] H. IWAMOTO et al., "Sensitivity and Uncertainty Analysis for an Accelerator-Driven System with JENDL-4.0," *J. Nucl. Sci. Technol.,* **50**, *8*, 856 (2013); https://doi.org/10.1080/00223131.2013.811954.

[2] T. TAKEDA et al., "Prediction Uncertainty Evaluation Methods of Core Performance Parameters in Large Liquid-Metal Fast Breeder Reactors," *Nucl. Sci. Eng.,* **103**, *2*, 157 (1989); https://doi.org/10.13182/NSE89-1.

[3] G. CHIBA, M. TSUJI, and T. NARABAYASHI, "Variance Reduction Factor of Nuclear Data for Integral Neutronics Parameters," *Nuclear Data Sheets*, **123**, 62 (2015); https://doi.org/10.1016/j.nds.2014.12.011.

[4] L. N. USACHEV, "Perturbation Theory for the Breeding Ratio and for Other Number Ratios Pertaining to Various Reactor Processes," *J. Nucl. Energy Parts A/B*, **18**, *10*, 571 (1964); https://doi.org/10.1016/0368-3230(64)90142-9.

[5] M. L. WILLIAMS, "Development of Depletion Perturbation Theory for Coupled Neutron/Nuclide Fields," *Nucl. Sci. Eng.*, **70**, *1*, 20 (1979); https://doi.org/10.13182/NSE79-3.

[6] G. CHIBA et al., "Nuclear Data-Induced Uncertainty Quantification of Neutronics Parameters of Accelerator-Driven System," *J. Nucl. Sci. Technol.*, **53**, *10*, 1653 (2016); https://doi.org/10.1080/00223131.2015.1127185.

[7] G. CHIBA et al., "Estimation of Neutronics Parameter Sensitivity to Nuclear Data in Random Sampling-Based Uncertainty Quantification Calculations," *Ann. Nucl. Energy*, **75**, 395 (2015); https://doi.org/10.1016/j.anucene.2014.08.049.

[8] T. WATANABE et al., "Estimation of Sensitivity Coefficient Using Random Sampling and L1-Norm Minimization," *Trans. Am. Nucl. Soc.*, **111**, 1391 (2014).

[9] E. J. CANDES and M. B. WAKIN, "An Introduction to Compressive Sampling," *IEEE Signal Process. Mag*., **25**, *2*, 21 (2008); https://doi.org/10.1109/MSP.2007.914731.

[10] R. TIBSHIRANI, "Regression Shrinkage and Selection via the Lasso," *J. R. Stat. Soc. B*, **58**, *1*, 267 (1996); https://doi.org/10.1111/j.2517-6161.1996.tb02080.x.

[11] D. M. HAWKINS and E. M. MABOUDOU-TCHAO, "Smoothed Linear Modeling for Smooth Spectral Data," *International Journal of Spectroscopy*, **2013**, 8 pages (2013); https://doi.org/10.1155/2013/604548.

[12] N. MAHMOOD, "Sparse Ridge Fusion for Linear Regression," Master's Thesis, University of Central Florida (2013).

[13] K. TSUJIMOTO et al., "Neutronics Design for Lead-Bismuth Cooled Accelerator-Driven System for Transmutation of Minor Actinide," *J. Nucl. Sci. Technol.*, **41**, *1*, 21 (2004); https://doi.org/10.1080/18811248.2004.9715454.

[14] T. SUGAWARA et al., "Development of Three-Dimensional Reactor Analysis Code System for Accelerator-Driven System, ADS3D and Its Application with Subcriticality Adjustment Mechanism," *J. Nucl. Sci. Technol.*, **53**, *12*, 2018 (2016); https://doi.org/10.1080/00223131.2016.1179600.

[15] K. SUGINO et al., "Preparation of Fast Reactor Group Constant Sets UFLIB.J40 and JFS-3-J4.0 Based on the JENDL-4.0 Data," JAEA-Data/Code 2011-017, Japan Atomic Energy Agency (Jan. 2012) (in Japanese); https://doi.org/10.11484/jaea-data-code-2011-017

[16] B. EFRON, "The Jackknife, the Bootstrap and Other Resampling Plans," Society for Industrial and Applied Mathematics (1982); https://doi.org/10.1137/1.9781611970319

3. Development of ROM-Lasso method for sensitivity coefficient evaluation

3.1. Introduction

In the previous chapter, the adaptive smooth lasso method has been proposed to address the challenges of the forward-based SA. However, it has been clarified that the adaptive smooth lasso still requires ~1000 forward calculations for SA of ~10000 cross sections, and a dramatic improvement has not been achieved.

In this chapter, by focusing on the ROM technique [1], further reduction of the calculation cost of the forward-based SA is tackled. In the ROM technique, input parameters (and/or output parameters) are expanded by AS, and unimportant parameter sets (i.e., orthogonal components to AS) are identified through a mathematical method such as SVD [2], thereby reducing the effective number of parameters, which is a couple of orders of magnitude smaller than the original number of parameters. Abdo et al. proposed M_LROM to attain an approximated AS using a lower-fidelity model, whose dimensionality is less than that of the target model with higher dimensionality and complexity [3]. Based on this idea, a sensitivity coefficient evaluation method for core analyses of light water reactors has been proposed, in which the assembly calculation performed in advance of the core calculation is regarded as a lower-fidelity model [4].

The main objective of this chapter is to improve the lasso regression method applied to the sensitivity coefficient evaluation via ROM. It is important to determine the optimal AS for the sensitivity coefficient evaluation with reasonably lower calculation costs. In this chapter, the use of approximated AS bases obtained with a lower-fidelity model (e.g., a two-dimensional cylindrical ADS model) is proposed for the lasso regression-based SA of a higher-fidelity model

(e.g., a three-dimensional (3-D) Cartesian ADS model). Through a one-cycle burnup core calculation, the applicability of the proposed method is verified. In this chapter, the proposed method is referred to as the ROM-Lasso method. As a first step, it is examined that the lasso procedure with the ROM expectedly works in the case where the lower-fidelity model well reproduces the higher-fidelity model (i.e., the ADS model that has high axial symmetry and can be well approximated with the 2-D cylindrical model). In the verification, SA on multiple parameters after burnup, e.g., the coolant void reactivity at the BOC, the beam current, maximum relative power, and mass of ^{241}Am at the end of the cycle (EOC), is addressed to make use of the advantage of the forward calculations whereas only k_{eff} at BOC is considered in Chapter 2.

The remainder of this chapter is organized as follows. Section 3.2 presents the theoretical descriptions of the ROM-Lasso method. Section 3.3 describes the basic specifications of the 2-D and 3-D ADS models employed in this study and the calculation conditions. Section 3.4 presents the results and a discussion of the verification calculation. Section 3.5 provides concluding remarks and future research directions.

3.2. Method

3.2.1. Regression-based sensitivity analysis

In this subsection, the regression-based SA is briefly reminded. As described in the previous chapter, the penalized linear regression determines the solution as follows:

$$\begin{aligned} \vec{g} &= \mathrm{argmin}\left\{\frac{1}{2M}\left\|\Delta\vec{R}-\Delta\mathbf{T}\vec{g}\right\|_2^2 + p(\vec{g})\right\}, \\ \left\|\Delta\vec{R}-\Delta\mathbf{T}\vec{g}\right\|_2^2 &= \sum_{i=1}^{M}\left(\Delta R_i - \sum_{j=1}^{N}\Delta T_{ij}g_j\right)^2. \end{aligned} \tag{3.1}$$

Note that Equation (3.1) is a repeat of Equation (2.6), but the matrix-vector representation is used for the residual sum of squares term for readability in the next subsection and it is divided by the number of samples (i.e., *M*). In the lasso method, $p(\vec{g})$ is expressed as follows:

$$p(\vec{g}) = \lambda \sum_{j=1}^{N} |g_j|, \tag{3.2}$$

where λ is a user-determined hyperparameter, and the penalty term is proportional to the sum of the absolute values (i.e., L1-norm) of the solutions. For a better choice, the adaptive smooth-lasso imposes an additional term and weights on the penalty term defined as follows:

$$p(\vec{g}) = \lambda_1 \sum_{j=1}^{N} v_j |g_j| + \frac{\lambda_2}{2} \sum_{j=2}^{N} w_j (g_j - g_{j-1})^2, \tag{3.3}$$

where λ_1 and λ_2 are the user-determined hyperparameters, and the weights v_j and w_j are

$$v_j = \frac{1}{1 + c|\tilde{g}_j|^{\gamma}}, \tag{3.4}$$

$$w_j = \frac{1}{1 + c\left(\frac{\left||\tilde{g}_j| + |\tilde{g}_{j-1}|\right|}{2}\right)^{\gamma}}. \tag{3.5}$$

Here, $\tilde{g}_j$ is an element of the solution that is pre-estimated by regression with the setting of $v_j = w_j = 1$. c and γ are also user-determined hyperparameters ($c > 0$ and $\gamma > 0$).

In the previous chapter, it was demonstrated that the adaptive smooth lasso can successfully reduce the number of core analyses to approximately a tenth of the direct method for SA of k_{eff} of the two-dimensional (2-D) ADS model at the beginning of the cycle (BOC). However, this number is still large for a precise model, such as the 3-D ADS model with multi-cycle analyses. In addition, the adaptive lasso method is disadvantageous in that it requires four hyperparameters. Because the prediction accuracy is sensitive to these hyperparameters, the hyperparameters must be chosen carefully. In the previous chapter, these hyperparameters were adjusted so that the estimated sensitivity coefficients better reproduced those of the direct method.

3.2.2. ROM-Lasso method

In this subsection, the theory of the novel ROM-Lasso method is described. In the ROM approach, the vector of sensitivity coefficients is expanded by AS bases, and the orthogonal components to AS are ignored.

When there are L vectors of sensitivity coefficients of the lower-fidelity model (e.g., 2-D cylindrical model), they can be arranged to form a sensitivity matrix of the lower-fidelity model as follows:

$$\mathbf{G}_{\text{lower}} = \left(\vec{g}_{\text{lower}}^{(1)}, \cdots, \vec{g}_{\text{lower}}^{(L)}\right), \tag{3.6}$$

where L is the number of neutronics parameters of interest, $\mathbf{G}_{\text{lower}}$ is an $N \times L$ matrix, and N is the number of cross sections of interest. SVD can be used to mathematically derive the effective subspace that well represents the original space. $\mathbf{G}_{\text{lower}}$ can be decomposed using SVD as follows:

$$\mathbf{G}_{\text{lower}} = \mathbf{U}\mathbf{D}\mathbf{V}^{\text{T}}, \tag{3.7}$$

where **U** is an $N \times N$ unitary matrix, **V** is an $L \times L$ unitary matrix, and **D** is an $N \times L$ diagonal matrix with singular values ($d_1 \geq d_2 \geq \cdots \geq d_L \geq 0$). When singular values less than the r-th largest singular value are neglected (i.e., $d_1 \geq \cdots \geq d_r > d_{r+1} \approx \cdots \approx d_L \approx 0$), the sensitivity matrix of the lower-fidelity model can be approximated as follows:

$$\mathbf{G}_{\text{lower}} \approx \mathbf{U}_r \mathbf{D}_r \mathbf{V}_r^{\text{T}}, \tag{3.8}$$

where $\mathbf{U}_r$ is the $N \times r$ matrix, $\mathbf{V}_r$ is the $L \times r$ matrix, and $\mathbf{D}_r$ is the $r \times r$ diagonal matrix which has $d_1 \geq \cdots \geq d_r > 0$ for its diagonal elements. Because the r+1-th and subsequent column vectors of **U** are negligible to represent $\mathbf{G}_{\text{lower}}$, the column vector of $\mathbf{G}_{\text{lower}}$ can be expanded by the orthogonal bases of $\mathbf{U}_r$ as follows:

$$\vec{g}_{\text{lower}}^{(l)} \approx \mathbf{U}_r \vec{f}^{(l)}, \tag{3.9}$$

where $\vec{g}_{\text{lower}}^{(l)}$ is the l-th column vector of $\mathbf{G}_{\text{lower}}$ and $\vec{f}^{(l)}$ is the expansion coefficient vector of $\vec{g}^{(l)}$. When r is significantly smaller than N, the effective number of input parameters can be significantly reduced from the original number of cross sections. That is, the number of unknowns in Equation (3.1) will be significantly reduced by $\mathbf{U}_r$ ($\mathbf{U}_r$ is the AS bases). In the M_LROM approach, it is assumed that when the lower-fidelity model adequately approximates the higher-fidelity model (e.g., 3-D Cartesian model), the AS bases $\mathbf{U}_r$ obtained with the lower-fidelity model can be used to expand the vectors of sensitivity coefficients of the higher-fidelity model.

By expanding the vector of sensitivity coefficients of the higher-fidelity model via $\mathbf{U}_r$,

the variation of the neutronics parameter for the higher-fidelity model can be rewritten as follows:

$$\Delta\vec{R}_{\text{higher}} = \mathbf{\Delta T U}_r\vec{f}_{\text{higher}}. \tag{3.10}$$

Equation (3.1) is also rewritten as follows:

$$\vec{f} = \text{argmin}\left\{\frac{1}{2M}\left\|\Delta\vec{R} - \Delta\mathbf{T}\mathbf{U}_r\vec{f}\right\|_2^2 + p(\vec{f})\right\}. \tag{3.11}$$

The subscript of "higher" is omitted for readability. In this chapter, the use of the penalty term defined in Equation (3.12) is proposed, as in the case of the conventional lasso method:

$$p(\vec{f}) = \lambda\sum_{j=1}^{r}|f_j|. \tag{3.12}$$

Thus, the sensitivity coefficient vector of the higher-fidelity model can be obtained by $\vec{g} \approx \mathbf{U}_r\vec{f}$. If the sensitivity vector of the higher-fidelity model can be well reconstructed with the linear combination of $\mathbf{G_{lower}}$ (or, the corresponding bases $\mathbf{U}_r$), one of the reasonable options to reduce the dimensional complexity is to truncate the bases with the significantly small singular values. However, the absolute values of the expansion coefficients do not necessarily correspond to the order of the expansion bases (or, to the magnitude of the corresponding singular values in the estimation of $\mathbf{U}_r$**)**. In other words, it is not obvious whether the truncation approach is always effective in expanding any type of target sensitivity coefficient. For this reason, this study used sparse modeling for the expansion coefficients $\vec{f}$ rather than the truncation approach. Owing to the auto-selectivity of the lasso method, the expansion coefficients of the primary bases among

the AS bases can be automatically obtained.

It is worth noting that the continuity versus energy and steep changes due to threshold and resonance cross sections of the neutron-induced reactions are already considered in the AS bases because they are obtained from the sensitivity coefficients of the lower-fidelity model. Because the proposed method has only one hyperparameter, the cross-validation (CV) technique [5] can be easily applied to the optimization of the hyperparameter as opposed to four hyperparameters in the adaptive smooth-lasso.

The ROM-Lasso method has an intriguing feature in that the AS bases can be assumed based on the neutronics parameters. That is, the AS basis sets can be optimized for each neutronics parameter. Let us suppose that there are two neutronics parameters $R^{(1)}$ and $R^{(2)}$ and we want to obtain the corresponding sensitivity coefficient vectors $\vec{g}^{(1)}$ and $\vec{g}^{(2)}$. The corresponding expansion coefficients $\vec{f}^{(1)}$ and $\vec{f}^{(2)}$ can be determined by the ROM-Lasso method using two different AS bases, as follows:

$$\begin{aligned}\vec{f}^{(1)} &= \mathrm{argmin}\left\{\frac{1}{2M}\left\|\Delta\vec{R}^{(1)} - \Delta\mathbf{T}\mathbf{U}^{(1)}_{r^{(1)}}\vec{f}^{(1)}\right\|_2^2 + \lambda^{(1)}\sum_{j=1}^{r^{(1)}}\left|f_j^{(1)}\right|\right\},\\ \vec{f}^{(2)} &= \mathrm{argmin}\left\{\frac{1}{2M}\left\|\Delta\vec{R}^{(2)} - \Delta\mathbf{T}\mathbf{U}^{(2)}_{r^{(2)}}\vec{f}^{(2)}\right\|_2^2 + \lambda^{(2)}\sum_{j=1}^{r^{(2)}}\left|f_j^{(2)}\right|\right\},\end{aligned} \tag{3.13}$$

where $\mathbf{U}^{(1)}_{r^{(1)}}$ and $\mathbf{U}^{(2)}_{r^{(2)}}$ are AS bases that are optimized for each neutronics parameter. r and λ are also different for each neutronics parameter; however, $\Delta\mathbf{T}$ in Equation (3.13) is common in the two equations. Because $\mathbf{U}^{(1)}_{r^{(1)}}$ is optimized for $R^{(1)}$ by ignoring the components orthogonal to $\mathbf{U}^{(1)}_{r^{(1)}}$, reconstruction of $\vec{g}^{(2)}$ by $\mathbf{U}^{(1)}_{r^{(1)}}$ will be difficult, especially when $\vec{g}^{(2)}$ is almost

orthogonal to $\vec{g}^{(1)}$. However, Equation (3.13) indicates that AS bases can be chosen according to the neutronics parameters independently of random sampling. That is, we can evaluate these two sensitivity coefficient vectors simultaneously using two different AS bases, even if these vectors are orthogonal to each other. In addition, $\mathbf{\Delta T}$ can be an arbitrary perturbed cross section set, and $\Delta\vec{R}^{(1)}$ and $\Delta\vec{R}^{(2)}$ are relative deviations evaluated in the higher-fidelity model using $\mathbf{\Delta T}$. The AS bases are used only in the lasso regression process performed after the random sampling process for the higher-fidelity model. In other words, the AS bases are not used in the random sampling process for the higher-fidelity model. Therefore, if more appropriate AS bases are found after random sampling, they can be used for a more accurate evaluation. In this work, neutronics parameters are divided into some groups (referred to as AS-groups in this thesis) according to their properties (e.g., core integral parameters, mass of heavy nuclides, and mass of rare earth elements in fission product), and the AS bases are obtained for each AS-group so that each AS is optimized for each AS-group.

The most straightforward method to obtain the optimal AS bases is the use of the sensitivity coefficients of the neutronics parameters of interest. However, this method is irrelevant because it requires a sensitivity matrix that is yet to be obtained. Therefore, an M_LROM approach was used to obtain the approximated AS bases. In this chapter, the use of the sensitivity coefficients of the multiple neutronics parameters of the 2-D cylindrical model is proposed to evaluate the sensitivity coefficients of the 3-D Cartesian model. If the calculation cost of the 2-D model is much smaller than that of the 3-D model, we can reduce the total calculation cost, including finding AS bases when we evaluate the sensitivity coefficients of the 2-D model via the direct method.

Figure 3.1 shows a schematic view of the ROM-Lasso method. The ROM-Lasso method can be summarized as follows.

a. Perform the direct method in the lower-fidelity model (e.g., 2-D cylindrical model) to evaluate the sensitivity vectors.
b. Divide sensitivity vectors into AS-groups according to neutronics parameters and perform SVD to obtain AS bases according to the AS-groups.
c. Perform random sampling in the higher-fidelity model (e.g., 3-D Cartesian model) to evaluate the deviations of target neutronics parameters.
d. Evaluate the sensitivity vectors of the target neutronics parameters in the higher-fidelity model using Equation (3.13).

Steps a–b and Step c are interchangeable when all cross sections of interest in the higher-fidelity model are considered in the lower-fidelity model.

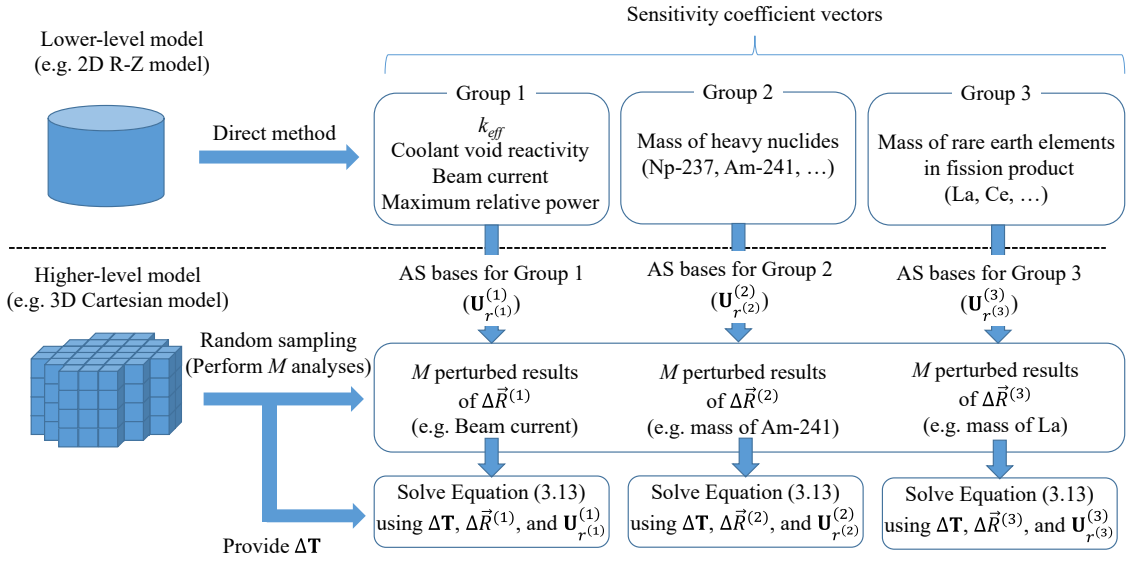

Figure 3.1 Schematic view of the ROM-Lasso method.

3.3. Verification calculation condition

3.3.1. Basic specification of ADS

In this subsection, the basic specifications of the ADS proposed by JAEA [6] are described. The ADS model was updated from [7], whereas the ADS model used in the previous chapter was based on [7]. The ADS is composed of a subcritical core loaded with MA nitride fuels

and operated by spallation neutrons generated by a proton beam accelerator and an LBE target. The basic specifications of the fuel assemblies and pins are summarized in **Table 3.1**, and **Figure 3.2** shows the arrangement of the fuel assemblies used in this study.

The beam duct is inserted from the upper part to the center of the core, and a 1.5 GeV proton beam is injected into the LBE target through the beam duct to produce spallation neutrons. The inside of the beam duct must be a vacuum to transport the proton beam.

The isotopic composition of MA and Pu for MA nitrides was based on a previous study [7]. The fuel region of the subcritical core has two MA fuel regions (the inner and outer cores). The MA fuel consists of trans-uranium (TRU) nitride ((MA + Pu) N) and ZrN. **Table 3.2** lists the weight ratios of PuN to TRU nitride and those of ZrN to MA fuel for the two fuel regions. **Table 3.3** lists the weight ratios of TRU in the MA core regions. Detailed specifications of the dimension of the beam duct and the composition of reflectors and shielding are provided in Reference [6].

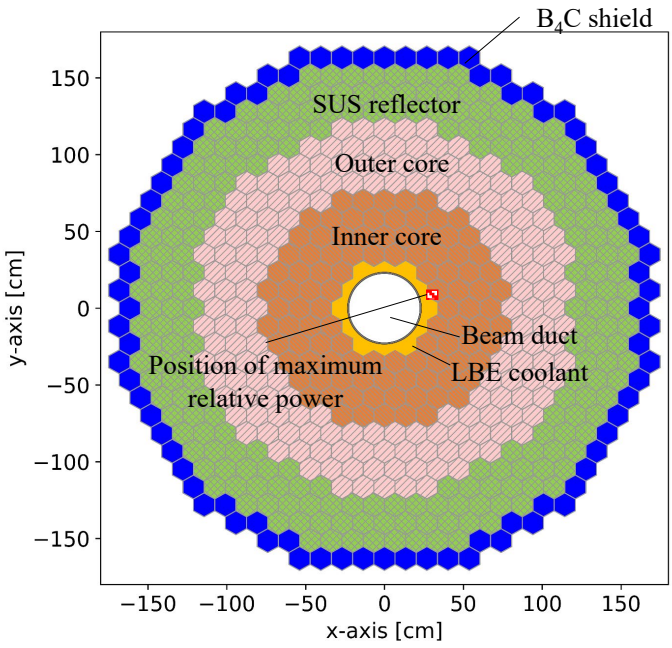

Figure 3.2 The arrangement of fuel assemblies.

Table 3.1. Basic specification of fuel assemblies and pins.

Fuel Assembly (FA)		Fuel Pin	
Type	Hexagonal duct-less	Composition	(MA + Pu)N + ZrN
	Number of FAs	Cladding tube material	T91 steel
Inner core	102	Pellet smear density [%]	85
Outer core	174	Cladding outer diameter [mm]	7.65
Total	276	Cladding inner diameter [mm]	6.65
Number of fuel pins per FA	121	Pellet outer diameter [mm]	6.49
Pitch of FA [mm]	134.5	Pin pitch [mm]	11.48
Width of FA [mm]	133.5	Active height [mm]	1000
Number of fuel pins per FA	121		
Number of tie rods per FA	6		

Table 3.2. Weight ratio of nitrides at BOC

ZrN / (MA + Pu + Zr)N [wt%]	
Inner core	38.9
Outer core	28.9
PuN / (MA + Pu)N [wt%]	
Inner core	27.3
Outer core	27.3

Table 3.3. Isotopic composition of actinides in the MA core region.

Slightly modified from Table 2.1.

Nuclide	(wt%)	Nuclide	(wt%)
^{234}U	0.01	^{241}Am	23.94
^{237}Np	35.36	^{242m}Am	0.04
^{238}Pu	0.65	^{243}Am	10.01
^{239}Pu	14.88	^{243}Cm	0.02
^{240}Pu	6.84	^{244}Cm	3.05
^{241}Pu	2.96	^{245}Cm	0.3
^{242}Pu	1.9	^{246}Cm	0.03

3.3.2. Calculation Conditions

To investigate whether the lasso procedure with the ROM expectedly works for a highly symmetric system, the ADS model with high axial symmetry is considered. For this purpose, ADS3D [8] was used for both 2-D cylindrical and 3-D Cartesian models of the ADS. ADS3D uses SLAROM-UF [9] to generate effective multigroup microscopic cross sections, PARTISN [10] for neutron transport calculations for both the eigenvalue problem and the fixed source problem, and BURNUP solver in MARBLE [11], which is implemented by NumPy [12] and SciPy [13] libraries, for burnup calculations. Because ADS3D consists of multiple calculation codes developed in different institutes, the implementation and application of the adjoint-based method are difficult.

In this work, sensitivity coefficients of neutronics parameters to self-shielded effective multigroup microscopic cross sections were evaluated. A couple of previous studies have shown the importance of obtaining sensitivity coefficients to infinite diluted cross sections for rigorous uncertainty evaluation in light water reactors [14, 15]. Correction methods have been also proposed under the assumption of the Bondarenko-type self-shielding factor model [14–16]. Note, however, that Chiba et al. pointed out that the self-shielding effect does not significantly impact

the uncertainty evaluation of fast reactors [16]. As an example, the uncertainty of k_{eff} for a typical fresh fuel pin cell used in the ADS [6] has been evaluated using the TSUNAMI-1D module of SCALE-6.2 [17]. SCALE-6.2 has the capability of evaluating the so-called "implicit sensitivity", which is a portion of the sensitivity coefficients of the self-shielded cross sections to the infinite diluted cross sections, with the aid of the BONAMIST module. It has been confirmed that the impact of the self-shielding effects on the sensitivity coefficients and nuclear data-induced uncertainty of k_{eff} was negligibly small, e.g., the uncertainties evaluated with and without the implicit effect were 1.5054 and 1.5058 (%dk/k), respectively. Therefore, the impact on ADSs is also expected to be small in this study, though the rigorous evaluation of the sensitivity coefficients of the other neutronics parameters considering the self-shielding effect could be a future research topic.

Figure 3.3 shows the 2-D cylindrical model used for the lower-fidelity model to obtain the AS bases. Because PARTISN can handle only structured meshes, each region was homogenized by volume ratios such that the volume and mass of nuclides were preserved. The vacuum boundary conditions were considered for the upper, lower, and outer boundaries. The burnup regions of both the inner and outer fuel regions were divided into four radial and ten axial regions. The total number of burnup regions was 80 (i.e., $(4 + 4) \times 10 = 80$).

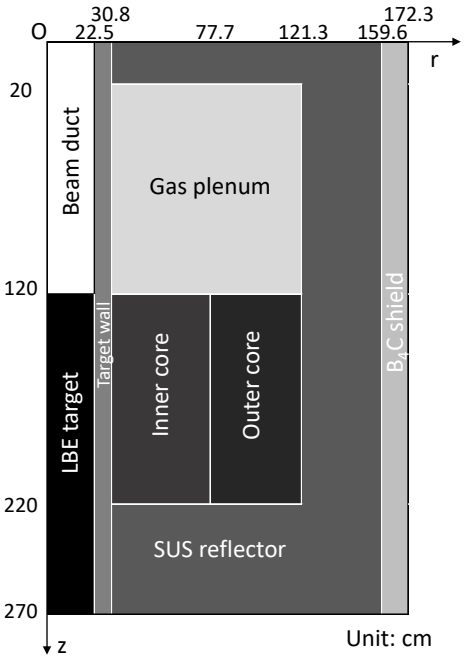

Figure 3.3 Geometry of the two-dimensional cylindrical model.

In the 3-D Cartesian model, each mesh in the x-y direction was made to preserve the area of a quarter of the cross section of the hexagonal assembly and the mass of nuclides. **Figure 3.4** shows the conversion of the hexagonal grid to the Cartesian mesh. For the higher-fidelity model, the reflective boundary conditions are considered on the x = 0 and y = 0 axes. Assemblies located in hexagonal symmetry around the origin and mirror symmetry with respect to a plane 30° from the x-axis are treated as one burnup region, thereby reducing the number of burnup regions in the radial direction from 74 (i.e., the number of assemblies in the quadrant of the core) to 28. The number of axial divisions on the z-axis in the fuel region was 10, as in the case of the cylindrical model. Because there are 28 burnup regions in the radial direction, the total number of burnup regions was 280. Then, the calculation time of the 3-D model was approximately 10 times longer than that of the 2-D model. As described later in Section 3.3.3, the AS bases were obtained by the direct method in the 2-D model, i.e., the total reduction of the calculation time including the

construction of the AS was about one-tenth of the direct method. The efficient construction of the AS is a future topic.

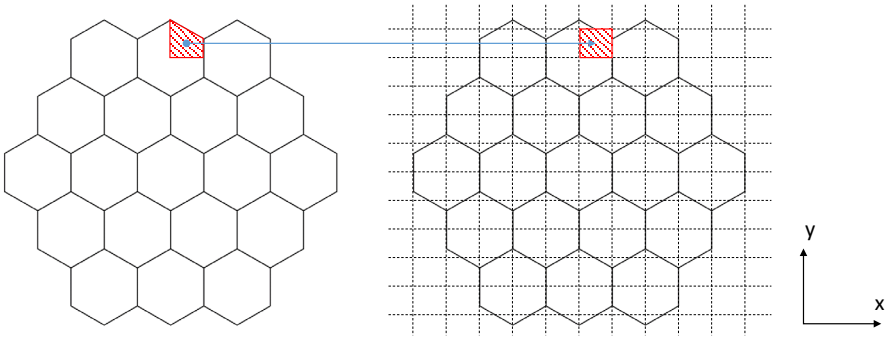

Figure 3.4 Illustration of mesh conversion from hexagonal grid to Cartesian mesh.

The 70-group-energy-structured UFLIB.J40 library [18] based on JENDL-4.0 [19] was used to generate the multigroup microscopic cross sections in SLAROM-UF. The neutron energy ranged from 10^{-5} eV to 20 MeV.

The burnup calculations were performed assuming 800 MWt and 600-day operations. The duration of each burnup step was 200 d. Because BURNUP performs burnup calculations using microscopic cross sections and neutron flux calculated by PARTISN, the contributions of number density change due to the cross section perturbations were directly included.

The effective multiplication factor (k_{eff}) was 0.98089 at the BOC, and the burnup reactivity between BOC and the end of the cycle (EOC) was approximately 0.813% dk/k/k' in the 3-D Cartesian model. Fixed source calculations in this chapter used the external neutron source generated by protons of 1.5 GeV and the LBE target using PHITS [20]

3.3.3. Neutronics parameters for AS and sensitivity coefficient evaluation

As input parameters, 193 microscopic reactions and 13510 cross sections (i.e., 193

microscopic reactions and 70 energy groups = 13510) were considered. **Table 3.4** lists the nuclides and reactions for the input parameters used in this study.

To construct the AS, the sensitivity coefficients of the neutronics parameters were evaluated for the three AS-groups in the 2-D ADS model as shown in **Table 3.5**. These sensitivity coefficients were evaluated using the direct method with a 5% one-sided difference approximation, i.e., perturbed calculations were repeatedly performed by increasing each cross section by 5%, and sensitivity coefficients were evaluated using the relative changes from the non-perturbed calculation. That is, the perturbed burnup calculations of the 2-D ADS model were performed 13510 times. The parameters in Table 3.5 were divided into three AS-groups and constructed three different ASs corresponding to these AS-groups. As described in Section 3.2.2, the truncation approach was not considered in this study, and the number of the dimensions of AS-group 1, 2, and 3 were 16, 42, and 24, respectively.

To demonstrate the advantage of the forward-based method, SA on several different types of neutronics parameters after burnup were taken into account: the beam current of the proton beam accelerator, the mass of ^{241}Am, and the maximum relative power at the EOC, and the coolant void reactivity at the BOC of the 3-D ADS model were considered as the target neutronics parameters that were simultaneously reproduced by the ROM-Lasso method in Section 3.4. The external neutron source intensity is proportional to the beam current of the proton beam accelerator and the beam current is adjusted to keep the core power of 800 MWt and varies from about 10 mA to 15 mA with the burnup. Evaluation of the beam current is important for the design of a feasible beam window that forms the boundary between the core and accelerator. Evaluation of the mass of ^{241}Am is also important because the ADS aims to transmute MA nuclides, including ^{241}Am. To examine the applicability of the proposed method to the local neutronics parameter, the evaluation of the sensitivity coefficients of the maximum relative power at EOC was tackled. The

position of the maximum relative power at EOC is shown in Figure 3.2 (i.e., the mesh of the inner fuel region closest to the beam duct) and its axial position was the center of the fuel region. In addition to the above parameters, the evaluation of the sensitivity coefficients of the coolant void reactivity at the BOC is also addressed to demonstrate that the forward-based method can simultaneously perform SA for various properties at different time steps, though the sensitivity coefficients of a reactivity without burnup can be relatively easily evaluated by PT.

Table 3.4. Nuclide and reactions for input parameters.

Material	Nuclide	Reaction	Number of microscopic reactions[*a]
Fuel	$^{235, 238}$U; ^{237}Np; $^{238, 239, 240, 241, 242}$Pu; $^{241, 242m, 243,}$Am; $^{243, 244, 245, 246}$Cm;	capture, fission, $\bar{\nu}$, $\bar{\mu}$, (n,2n), elastic scattering, inelastic scattering, fission spectrum	120 (15 nuclides × 8 reactions)
	^{15}N	elastic scattering	1 (1 nuclide × 1 reaction)
Coolant and spallation target	$^{204, 206, 207, 208}$Pb; ^{209}Bi	capture, $\bar{\mu}$, (n,2n), elastic scattering, inelastic scattering	25 (5 nuclides × 5 reactions)
Shielding	$^{10, 11}$B	capture, elastic scattering	4 (2 nuclides × 2 reactions)
Cladding and reflector	^{16}O; ^{23}Na; $^{52, 53}$Cr; ^{55}Mn; ^{56}Fe; $^{58, 60}$Ni	capture, $\bar{\mu}$, (n,2n), elastic scattering, inelastic scattering	40 (8 nuclides × 5 reactions)
	^{90}Zr	capture, (n,2n), inelastic scattering	3 (1 nuclide × 3 reactions)

[a] In total: 193 microscopic reactions.

Table 3.5. Neutronics parameters for sensitivity coefficient evaluation.

AS group	Parameters	The number of parameters
1	k_{eff} Coolant void reactivity Beam current Maximum relative power	16 (4 parameters × 4[a] burnup steps)
2	Mass of 14 heavy nuclides (^{237}Np; $^{238, 239, 240, 241, 242}$Pu; $^{241, 242m, 243,}$Am; $^{242, 243, 244, 245, 246}$Cm;)	42 (14 nuclides × 3 burnup steps)
3	Mass of eight rare earth elements in fission product (La, Ce, Pr, Nd, Sm, Eu, Gd, Tb)	24 (8 nuclides × 3 burnup steps)

[a] BOC + three burnup steps.

Based on Equation (3.13) of the ROM-Lasso method shown in Figure 3.1, the sensitivity coefficients of the beam current and mass of ^{241}Am were reproduced using the AS constructed with AS-group 1 and AS-group 2, respectively. Using the AS constructed with AS-group 3, the results of the sensitivity coefficients of the mass of lanthanum (La) are also provided in Appendix A as an example of rare earth elements, which accompany MAs in the partitioning process and can impact the neutronics parameters of subsequent cycles [6]. The sensitivity coefficients of the maximum relative power at the EOC and the coolant void reactivity at the BOC were also reproduced using AS-group 1.

The number of random samples for the 3-D model was 30, which is a couple of orders of magnitude less than the number of input parameters. The input parameters were uniformly sampled within the range of ±5%. The perturbation range was empirically given based on Reference [21]. In the lasso procedure of the ROM-Lasso, the leave-one-out CV (LOOCV) was

used to optimize λ in Equation (3.12). The statistical errors of the estimated sensitivity coefficients were evaluated using the jackknife method [22]. Note that the lasso regression of Equation (3.13) was also applied for the target neutronics parameters corresponding to AS-group1 as well as the other target neutronics parameters even though the sample size (i.e., 30) is larger than the dimension of AS-group 1 (i.e., 16). The direct method was used to evaluate the reference values, that is, the perturbed burnup calculations of the 3-D ADS model were performed 13510 times.

For a better comparison, the sensitivity coefficients were estimated using the conventional lasso method and the adaptive smooth lasso with 30 and 300 samples. The hyperparameter of λ in the lasso method was optimized using the LOOCV. Four hyperparameters of the adaptive smooth lasso were manually optimized so that the estimated sensitivity coefficients agreed with reference values.

3.4. Results and discussion

Figures 3.5 (a)–(c) show a comparison of the results of the sensitivity coefficients of the beam current at EOC to the $\bar{\nu}$ of ^{237}Np, where the largest absolute value of the sensitivity coefficients was observed, using the ROM-Lasso, the lasso, and adaptive smooth-lasso methods. The AS constructed by AS-group 1 was used for the ROM-Lasso method. **Table 3.6** lists the comparison of the user-defined parameters for the ROM-Lasso, lasso, and adaptive smooth lasso methods for the evaluation of the sensitivity coefficients of the beam current at EOC. As shown in Figure 3.5, the sensitivity coefficients obtained using the ROM-Lasso method were in good agreement with the reference values within the standard deviation (1σ). Conversely, the lasso and adaptive smooth lasso methods with 30 samples failed to reproduce the sensitivity coefficients. When the number of random samples to 300 increased, sensitivity coefficients were estimated as

non-zero values, and the signs were consistent. However, the discrepancy and the standard deviation were significantly large, unlike in the case of the proposed method. As an example of the application of the ROM-Lasso to a threshold reaction, to which the sensitivity coefficients are not smooth versus the energy, **Figure 3.6** shows a comparison of the results of the sensitivity coefficients of the beam current at EOC to the inelastic scattering cross section of ^{56}Fe. The threshold energy of this reaction is 862.07 KeV. As shown in Figure 3.6, the results of the proposed method with only 30 samples can successfully capture the steep change of the sensitivity coefficients at the threshold energy, whereas the adaptive smooth lasso with 300 samples evaluated the sensitivity coefficients below the threshold energy as non-zero values. These results indicate that the proposed method can successfully reduce the computational burden using the ROM technique. Other sensitivity coefficients to the top 20 cross sections with the largest absolute values are shown in Appendix A (Figure A.1, A.2, and A.3).

Table 3.6. Parameters for the penalty term for sensitivity coefficients of beam current.

Parameter	ROM-Lasso[a]	Lasso[a]	Adaptive smooth lasso[b]
λ_1	7.9×10^{-6}	4.0×10^{-7}	1.0×10^{-5}
λ_2			5.0×10^{-4}
c			50
γ			0.8

[a] λ_1 was determined by the LOOCV.

[b] Parameters for the adaptive smooth lasso were manually determined so that the estimated sensitivity coefficients reproduced the reference values.

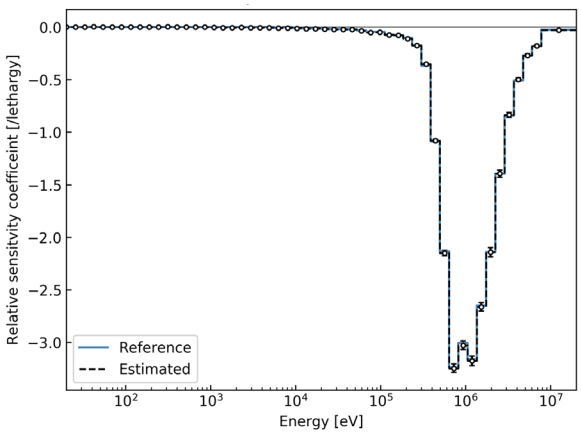

(a) ROM-Lasso with 30 samples

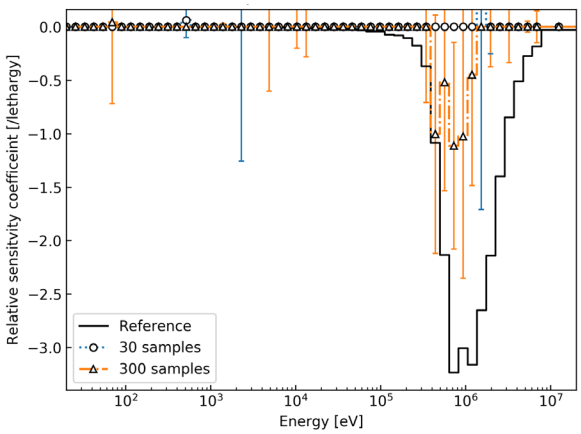

(b) lasso with 30 and 300 samples

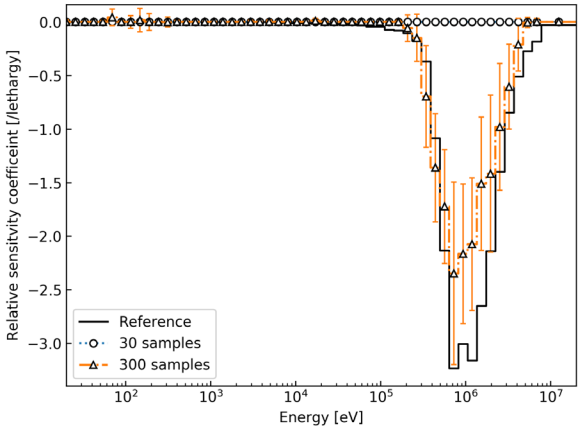

(c) adaptive smooth lasso with 30 and 300 samples

Figure 3.5 Sensitivity coefficients of beam current at EOC to $\bar{\nu}$ of ^{237}Np estimated by each method.

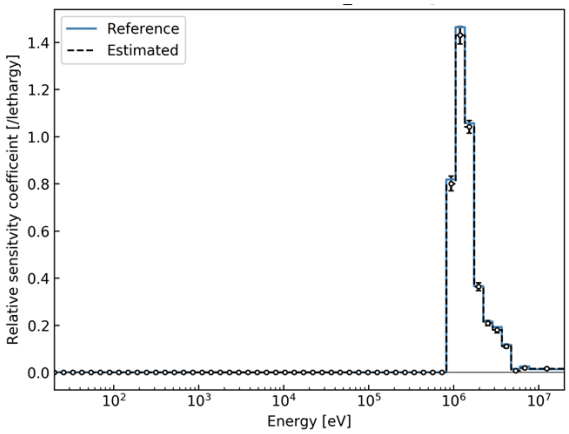

(a) ROM-Lasso with 30 samples

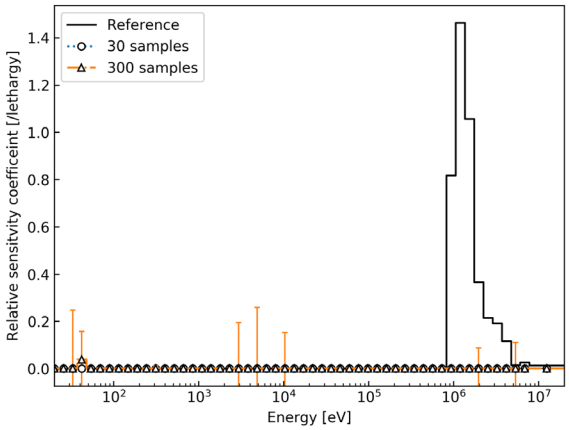

(b) lasso with 30 and 300 samples

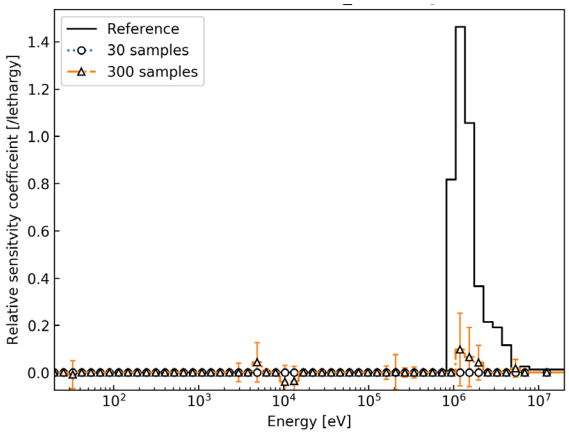

(c) adaptive smooth lasso with 30 and 300 samples

Figure 3.6 Sensitivity coefficients of beam current at EOC to inelastic scattering cross section of ^{56}Fe estimated by each method.

To demonstrate the validity of Equation (3.13), **Figure 3.7** shows the result of the sensitivity coefficients of the mass of ^{241}Am at EOC to the capture cross section of ^{241}Am, where the largest absolute value of the sensitivity coefficients was observed, estimated by the ROM-Lasso method. λ_1 was 8.7×10^{-8} for the mass of ^{241}Am. Again, it is emphasized that the AS constructed by AS-group 2 was used, unlike in the case of the beam current using AS-group 1, whereas the perturbed responses were simultaneously evaluated by random sampling. As shown in Figure 3.7, the estimated sensitivity coefficients were also in good agreement with the reference values within the standard deviation. For supplemental information, the sensitivity coefficients of mass of ^{241}Am and La at EOC to the top 20 cross sections with the largest absolute values are also shown in Appendix A (Figure A.4 and A.5).

To demonstrate the applicability of the proposed method to a local neutronics parameter, **Figure 3.8** shows the result of the sensitivity coefficients of the maximum relative power at EOC to the $\bar{\nu}$ of ^{237}Np, where the largest absolute value of the sensitivity coefficients was observed, estimated by the ROM-Lasso method. λ_1 was 4.7×10^{-6} for the maximum relative power. Discrepancies from the reference values exceeded slightly 1σ in the energy range over 1 MeV. However, the estimated sensitivity coefficients of the local neutronics parameter (i.e., the maximum relative power) were in good agreement with the reference values despite using AS-group1 that consisted of integrated parameters (i.e., k_{eff}, the coolant void reactivity, and the beam current which is proportional to the core power) and the maximum relative power of the 2-D cylindrical model. The ROM-Lasso method aims to reconstruct the sensitivity coefficients by the linear combination of the orthogonal bases. Therefore, if the reference sensitivity coefficients of the maximum relative power in the higher-fidelity model can be well approximated by the linear combination of AS bases estimated by the lower-fidelity model, the ROM-Lasso method can reproduce the sensitivity coefficients even when using the integrated parameters of the lower-

fidelity model. Choice of the optimal neutronics parameters of the lower-fidelity model is not trivial and should be addressed in the future.

For supplemental information, the sensitivity coefficients of the relative maximum power at EOC to the top 20 cross sections with the largest absolute values are shown in Appendix A (Figure A.6). The sensitivity coefficients of the coolant void reactivity at the BOC were also successfully reproduced by the proposed method as shown in Appendix A (Figure A.7). The obtained sensitivity coefficients of the coolant void reactivity will be used for DA tackled in the next chapter.

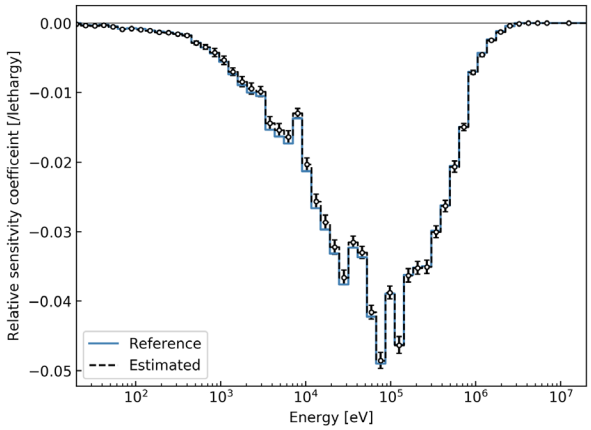

Figure 3.7 Sensitivity coefficients of mass of ^{241}Am- at EOC to capture cross section of ^{241}Am estimated by the ROM-Lasso method.

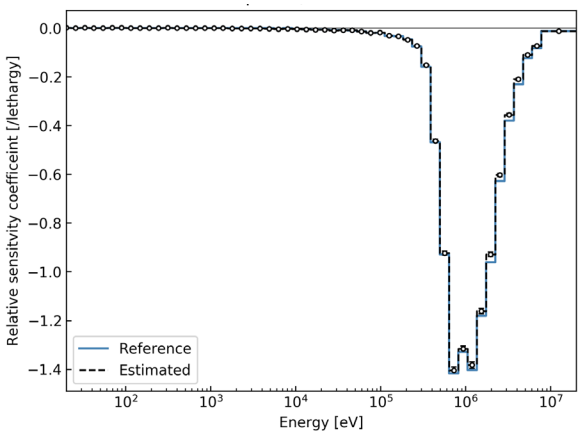

Figure 3.8 Sensitivity coefficients of maximum relative power to $\bar{\nu}$ of ^{237}Np estimated by the ROM-Lasso method.

Owing to the ROM-Lasso method, the number of random samplings can be dramatically reduced by a couple of orders of magnitude (i.e., from about 1000 to 30 in this thesis). However, as mentioned in Section 3.3.2, the calculation time of the 2-D model was approximately one-tenth that of the 3-D model, that is, the total reduction of the calculation time including the construction of the AS was only about one-tenth of the direct method used to evaluate the reference values. Therefore, the reduction in the calculation cost of the construction of the AS will be addressed in the future. A possible remedy to address this challenge could be the employment of a model with coarser mesh and/or looser convergence tolerances for the AS construction in the lower-fidelity model, as proposed in reference [4].

In this thesis, transport calculations on both the lower- and higher-fidelity models were based on the deterministic method, i.e., the evaluated sensitivity coefficients could have uncertainty due to discretization. For more accurate SA, the application of the continuous energy Monte Carlo calculations would be a future topic of interest. Recently, a useful tool [23] has been available to perturb cross section libraries for the continuous energy Monte Carlo codes. Provided

the AS obtained by the 2-D model is applied to the continuous energy Monte Carlo calculations, this approach would be efficient because the calculation cost of the Monte Carlo calculations is generally larger than that of the deterministic method, and the relative calculation cost of the AS construction becomes smaller when the Monte Carlo calculations are considered as the higher-fidelity model.

In this chapter, the feasibility of the ROM-Lasso method for the highly symmetrical system is demonstrated where the 2-D cylindrical model may adequately reproduce the 3-D Cartesian model. However, more general systems do not necessarily have geometric symmetry, and it is not obvious how to construct the lower-fidelity model. Therefore, the choice of an appropriate lower-fidelity model would be another challenge that has to be addressed in the future.

Furthermore, the reproducibility of the sensitivity coefficients by the ROM-Lasso was confirmed by directly comparing the estimated values and the reference values obtained by the direct method. However, in more general cases, it is important to estimate the error bounds by the orthogonal components to the AS without the direct method to check whether the sensitivity vector of the higher-fidelity model is well included in a subspace spanned by the sensitivity vectors of the lower-fidelity model. Estimation of such an error bound should be addressed in the future.

In this chapter, the range of the uniform sampling of the cross sections was empirically chosen as ± 5%. When the perturbation of the cross sections is too small, the perturbation of the neutronics parameters will be affected by the round-off errors. For the too-large perturbation, the higher-order derivatives degrade the accuracy of the sensitivity coefficients (i.e., the first-order derivative). Determination of the optimal range of the perturbation of the cross sections is also a future task.

3.5. Conclusions

The sensitivity coefficients of the target neutronics parameters to the cross sections are important for uncertainty evaluation and reduction. In this chapter, the ROM-Lasso method is newly proposed, which is enhanced by the ROM technique for further reduction of the calculation cost to evaluate the sensitivity coefficient that uses only forward calculations. The ROM-Lasso method can flexibly choose AS bases according to neutronics parameters. In this chapter, AS bases were constructed using the sensitivity coefficient matrix of the lower-fidelity model (i.e., the 2-D ADS model), and random sampling was performed for the higher-fidelity model (i.e., the 3-D ADS model). The numerical verification has clarified that the ROM-Lasso method can successfully reduce the number of samplings by a couple of orders of magnitude and simultaneously evaluate the sensitivity coefficients of the several neutronics parameters after burnup.

Through Chapter 2 and Chapter 3, the development of the practical methodology for the forward-based SA has been addressed. Especially, Chapter 3 has demonstrated the applicability of the ROM-Lasso method through the verification calculation considering multiple neutronics parameters after burnup. However, as discussed in Chapter 1, the final goal of SA is performing UQ and/or DA, aiming at reliable core analyses. In the next chapter, as an example of the application of the sensitivity coefficients for a design property of a future system, UQ and DA are performed for the coolant void reactivity of the ADS using the sample reactivity measurements conducted at KUCA.

There are still open technical issues in the ROM-Lasso method that should be addressed in the future. First, in this chapter, the sensitivity coefficients to the effective self-shielded microscopic cross sections were evaluated. To evaluate those to the infinite diluted cross sections, one should use the correction methods proposed in References [14] and [17]. Second, in this

chapter, AS bases were constructed using 2-D ADS sensitivity coefficients. Although the number of calculations in the higher-fidelity model is dramatically reduced using the ROM-Lasso method, additional calculations in the lower-fidelity model are required to construct AS bases. The reduction in the calculation cost of the construction of the AS will be addressed in the future. Third, application to SA on Monte Carlo transport calculations will be also a future topic in terms of improving the accuracy of sensitivity coefficients and relative calculation cost of the AS construction. Fourth, the choice of an appropriate lower-fidelity model and identification of neutronics parameters of the lower-fidelity model will be also addressed in the future. Fifth, the estimation of error bounds by the orthogonal components to the AS will be also tackled in the future. Finally, the determination of an optimal range of the perturbation of the cross sections will be also a future task.

3.6. References for Chapter 3

[1] Y. BANG et al., "Hybrid reduced order modeling for assembly calculations," *Nucl. Eng. Des*., **295**, 661 (2015); https://doi.org/10.1016/j.nucengdes.2015.07.020.

[2] Z. BAI et al., Eds., Templates for the Solution of Algebraic Eigenvalue Problems: A Practical Guide, Society for Industrial and Applied Mathematics (2000); https://doi.org/10.1137/1.9780898719581.

[3] M. ABDO, "Multi-Level Reduced Order Modeling Equipped with Probabilistic Error Bounds," PhD Thesis, North Carolina State University, (2016).

[4] R. KATANO et al., "Estimation of Sensitivity Coefficients of Core Characteristics based on Reduced-Order Modeling using Sensitivity Matrix of Assembly Characteristics," *J. Nucl. Sci. Technol*., **54**, *6*, 637 (2017); https://doi.org/10.1080/00223131.2017.1299052.

[5] K. V. LUND, "The Instability of Cross-Validated Lasso," Master's thesis, University of Oslo,

(2013).

[6] T. SUGAWARA, R. KATANO, and K. TSUJIMOTO, “Impact of Impurity in Transmutation Cycle on Neutronics Design of Revised Accelerator-Driven System,” *Ann. Nucl. Energy*., **111**, 449 (2018); https://doi.org/10.1016/j.anucene.2017.09.017.

[7] K. TSUJIMOTO et al., “Neutronics Design for Lead-Bismuth Cooled Accelerator-Driven System for Transmutation of Minor Actinide,” *J. Nucl. Sci. Technol*., **41**, *1*, 21 (2004); https://doi.org/10.1080/18811248.2004.9715454.

[8] T. SUGAWARA et al., “Development of Three-Dimensional Reactor Analysis Code System for Accelerator-Driven System, ADS3D and its Application with Subcriticality Adjustment Mechanism,” *J. Nucl. Sci. Technol*., **53**, *12*, 2018 (2016); https://doi.org/10.1080/00223131.2016.1179600.

[9] T. HAZAMA, G. CHIBA, and K. SUGINO, “Development of a Fine and Ultra-Fine Group Cell Calculation Code SLAROM-UF for Fast Reactor Analyses,” *J. Nucl. Sci. Technol*., **43** *8*, 908 (2006); https://doi.org/10.1080/18811248.2006.9711176.

[10] R. E. ALCOUFFE et al., “PARTISN: A Time-Dependent, Parallel Neutral Particle Transport Code System,” LA-UR-05-3925, Los Alamos National Laboratory (2005).

[11] K. YOKOYAMA et al., “Development of Comprehensive and Versatile Framework for Reactor Analysis, MARBLE,” *Ann. Nucl. Energy*, **66**, *51* (2014); https://doi.org/10.1016/j.anucene.2013.11.047.

[12] S. VAN DER WALT, S. C. COLBERT, and G. VAROQUAUX, “The NumPy Array: A Structure for Efficient Numerical Computation,” *Comput. Sci. Eng*., **13**, *2*, 22 (2011); https://doi.org/10.1109/MCSE.2011.37.

[13] P. VIRTANEN et al., “SciPy 1.0: Fundamental Algorithms for Scientific Computing in Python,” *Nat. Methods*, **17**, *3*, 261 (2020); https://doi.org/10.1038/s41592-019-0686-2.

[14] M. L. WILLIAMS, B. L. BROADHEAD, and C. V. PARKS, “Eigenvalue Sensitivity Theory for Resonance-Shielded Cross Sections,” *Nucl. Sci. Eng.*, **138**, *2*, 177 (2001); https://doi.org/10.13182/NSE00-56.

[15] B. FOAD and T. TAKEDA, “Importance of self-shielding for improving sensitivity coefficients in light water nuclear reactors,” *Ann. Nucl. Energy*, **63**, 417 (2014); https://doi.org/10.1016/j.anucene.2013.07.037.

[16] G. CHIBA, A. TSUJI, and T. NARABAYASHI, “Resonance Self-Shielding Effect in Uncertainty Quantification of Fission Reactor Neutronics Parameters,” *Nucl. Eng. Technol.*, **46**, *3*, 281 (2014); https://doi.org/10.5516/NET.01.2014.707

[17] B. T. REARDEN et al., “TSUNAMI-1D: Control Module for One-Dimensional Cross section Sensitivity and Uncertainty,” in “SCALE Code System,” ORNL/TM-2005/39, Version 6.2, p. 6-5, B. T. REARDEN and M. A. JESSEE, Eds, Oak Ridge National Laboratory, Oak Ridge, Tennessee (2016).

[18] K. SUGINO et al., “Preparation of Fast Reactor Group Constant Sets UFLIB.J40 and JFS-3-J4.0 based on the JENDL-4.0 Data,” JAEA-Data/Code 2011-017, Japan Atomic Energy Agency (Jan. 2012) (in Japanese); https://doi.org/10.11484/jaea-data-code-2011-017.

[19] K. SHIBATA et al., “JENDL-4.0: A New Library for Nuclear Science and Engineering,” *J. Nucl. Sci. Technol.*, **48**, *1*, 1 (2011); https://doi.org/10.1080/18811248.2011.9711675.

[20] T. SATO et al., “Features of Particle and Heavy Ion Transport code System (PHITS) version 3.02,” *J. Nucl. Sci. Technol.*, **55**, *6*, 684 (2018); https://doi.org/10.1080/00223131.2017.1419890.

[21] T. WATANABE, et al., “Estimation of Sensitivity Coefficient using Random Sampling and L1-Norm Minimization,” *Trans. Am. Nucl. Soc.*, **111**, 1391 (2014).

[22] B. EFRON, “The Jackknife, the Bootstrap and Other Resampling Plans,“ Society for

Industrial and Applied Mathematics (1982); https://doi.org/10.1137/1.9781611970319.

[23] K. TADA et al., “Development of Ace File Perturbation Tool Using FRENDY,” *J. Nucl. Sci. Technol.*, **60**, *6*, 624 (2023); https://doi.org/10.1080/00223131.2022.2130463.

4. Data assimilation for lead-bismuth cross sections using sample reactivity experiments

4.1. Introduction

In this chapter, as a demonstration of the application of the sensitivity coefficients, UQ and DA of the coolant void reactivity of the ADS are performed using the sensitivity coefficients obtained in the previous chapter together with the lead (Pb) and bismuth (Bi) sample reactivity measurement data obtained at KUCA A-core.

Pb and LBE are considered to be candidates of coolant and reflector materials for the lead-cooled fast reactor (LFR) of Generation IV and the ADS as nuclear transmutation systems for high-level radioactive waste because of their attractive properties including inertness against water and air, low melting points, high boiling points, good retention capability for fission products, good shielding capability for gamma radiation, and low-absorption cross sections. However, the impact of uncertainty induced by inelastic scattering cross sections of Pb and Bi is significant on the neutronics parameters, especially on the coolant void reactivity of the ADS [1]. A target accuracy ranging between 5% and 7% for the coolant reactivity has also been proposed and discussed in the OECD/NEA WPEC subgroups [2, 3]. As shown later in Section 4.4, the model of the ADS in this chapter based on Reference [4], which is a revised version from Reference [1], has an uncertainty of 6.3% in the coolant void reactivity, which slightly exceeds the lower value of the target accuracy discussed so far (i.e., 5%).

For improvement requirements on the nuclear data to achieve a target accuracy of design properties of advanced systems, the use of integral experiments and DA is considered important [5]. Several experiments have provided integral data for the validation of Pb cross sections, such

as a series of experiments conducted in a Pb-reflected, water-moderated, uranium-fuel rod array of the experimental criticality facility at SRSC Valduc (CEA, France), known as LEU-COMP-THERM-027 in the International Criticality Safety Benchmark Evaluation Project (ICSBEP) [6]. Measurements of neutron multiplication factors and spectral indices in plutonium fuel with Pb coolant in the critical assembly BFS-61, known as BFS1-LMFR-EXP-002 in the International Reactor Physics Experiment Evaluation (IRPhE) [7], have also been conducted. To further expand the integral data for Pb and Bi cross sections, JAEA has focused on analyzing the reactivity worths relevant to nuclear characteristics that are highly sensitive to Pb and Bi nuclear cross sections: The JAEA has conducted the sample reactivity measurements in a solid-moderated and solid-reflected core (A-core) at the KUCA [8, 9]. In a previous study [8], the C/E values of these sample reactivities of the KUCA A-core were successfully improved by the DA analyses. However, the impact of DA on the uncertainty reduction in the coolant void reactivity of the ADS has not been evaluated.

The main objective of this chapter is to perform DA using the sensitivity coefficients obtained in the previous chapter and the sample reactivity measurement data obtained at the KUCA with the primary aim of examining the uncertainty reduction of the void reactivity of the LBE coolant in the ADS as an example of DA for a future system using the sensitivity coefficients. Experiment analyses of the KUCA including SA were performed with MCNP-6.2 [10] together with JENDL-4.0 nuclear data library [11]. The impact of DA on the uncertainty reduction in the coolant void reactivity of the ADS is investigated using the sensitivity coefficients obtained in Chapter 3. For better practice than the previous DA analysis of Reference [8], the experimental uncertainties and the corresponding correlations are re-evaluated and highlighted as will be discussed later in Section 4.2. Using the sensitivity coefficients and the experimental uncertainties, the DA analysis is performed by the MARBLE code system [12]. Through the DA analyses using

the sample reactivities obtained at KUCA, it is demonstrated that the uncertainty in the coolant void reactivity of the ADS is successfully reduced, achieving the provisional target accuracy in this chapter discussed later in Sec. 4.3. In addition to the KUCA data, the DA analysis with the integral experimental data set including sensitivity database used for the ADJ2017 [13] is performed to further reduce the uncertainty in the coolant void reactivity of the ADS.

The remainder of this chapter is organized as follows. Section 4.2 provides a brief description of the sample reactivity experiments conducted at KUCA. Section 4.3 describes the formulation of DA and gives a brief description of ADJ2017. The results of DA with KUCA experiments and discussions are presented in Section 4.4, while Section 4.5 presents the conclusions and remarks.

4.2. Reactivity experiments at KUCA

4.2.1 Brief description of experiment

Detailed information about the KUCA experiments, including core configurations and fuel rod composition, is given in Reference [9]. Sample reactivity experiments were carried out in the A-core at KUCA. The KUCA A-core is a solid-moderated and solid-reflected thermal core consisting of highly enriched uranium (HEU) fuel and polyethylene plates. Two core configurations were used to vary the neutron energy spectra: an HEU core and a low-enriched uranium (LEU) core, presenting core configurations shown in **Figures 4.1(a) and 4.1(b)**, respectively. These cores contained five sample fuel rods surrounded by normal fuel rods. **Figures 4.2(a), 4.2(b), and 4.2(c)** show the configurations of the fuel rods for these cores as follows: the normal fuel rod termed “F” was identical for both the HEU and LEU cores and contained 60 unit cells at the axial center sandwiched by polyethylene moderators and reflectors. The unit cell consisted of two HEU fuel plates (2×2×1/16-inch) and one polyethylene plate (2×2×1/8-inch) as

shown in Figure 4.2(a). Here, the HEU fuel plate was made of uranium-aluminum (U-Al) alloy. The partial fuel rods ("40" and "14" for the HEU core and "16" for the LEU core) shown in Figure 4.2(a) were equipped to adjust the excess reactivity. For instance, the fuel rod termed "16" had only 16 unit cells at the axial center and 44 dummy cells constituting two 1/16-inch Al plates and 1/8-inch polyethylene plates to maintain the height of the fuel region at the axial center. The sample fuel rod in the HEU core was similar to the normal fuel rods, but the polyethylene plates of 40 cells at the axial center were replaced by 1/8-inch thick plates of sample materials, i.e., Pb, Bi, Al plates, and an Al spacer (whose specification is given in Reference [9]), as shown in Figure 4.2(b). The ^{235}U enrichment of the HEU core was 93 wt%. In the LEU core, 1/24-inch (1.05 mm) natural uranium (NU) metal plates were inserted into the 20 cells at the axial center, as shown in Figure 4.2(c). The number of enriched uranium plates for the LEU core sample rod was the same as that for the HEU core sample rod, and the average ^{235}U enrichment of the test region was reduced to 17 wt% because of the additional usage of the NU metal plates. The test region of the sample fuel rods was axially divided into three parts. For the HEU sample fuel rods, the test region was divided into 10, 20, and 10 cells of 40 unit cells each in the lower, central, and upper regions, respectively. For the LEU sample fuel rods, the test region was divided into 5, 10, and 5 cells of 20 unit cells each, respectively. The core patterns were designated "Al/Al/Al" when the sample materials for all three parts were Al plates, and "Pb/Al/Pb" if the upper and lower parts were substituted with Pb plates. The Al spacers were termed "Vd" in this chapter.

The excess reactivities for certain sample patterns were measured by inserting a B_2O_3 control rod from the top into the core. The worth of the control rods was calibrated by the rod drop method. The control rods designated "C3" and "C2" were used for the HEU and LEU cores, respectively. **Tables 4.1(a) and 4.1(b)** give the sample loading patterns and corresponding measured excess reactivity for the HEU core and the LEU core, respectively. Table 4.1 also lists

the sample substitution patterns and corresponding sample reactivities. The experimental uncertainties listed in Table 4.1 have been re-evaluated in this chapter, as discussed later in Section 4.2.3, and differ from the values reported in Reference [9].

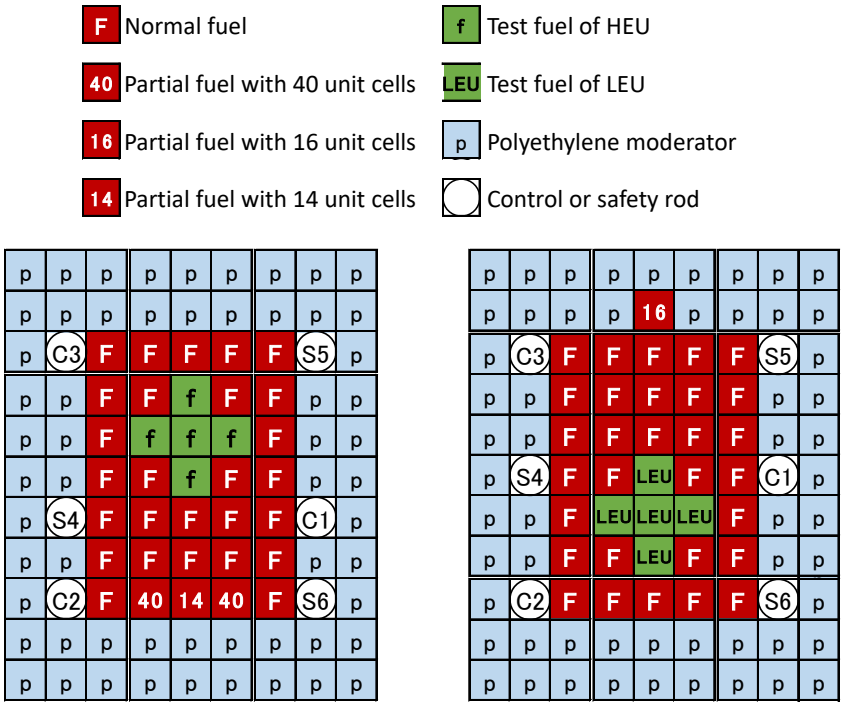

(a) HEU core (b) LEU core

Figure 4.1 Top view of the area around the fuel region of experimental cores.

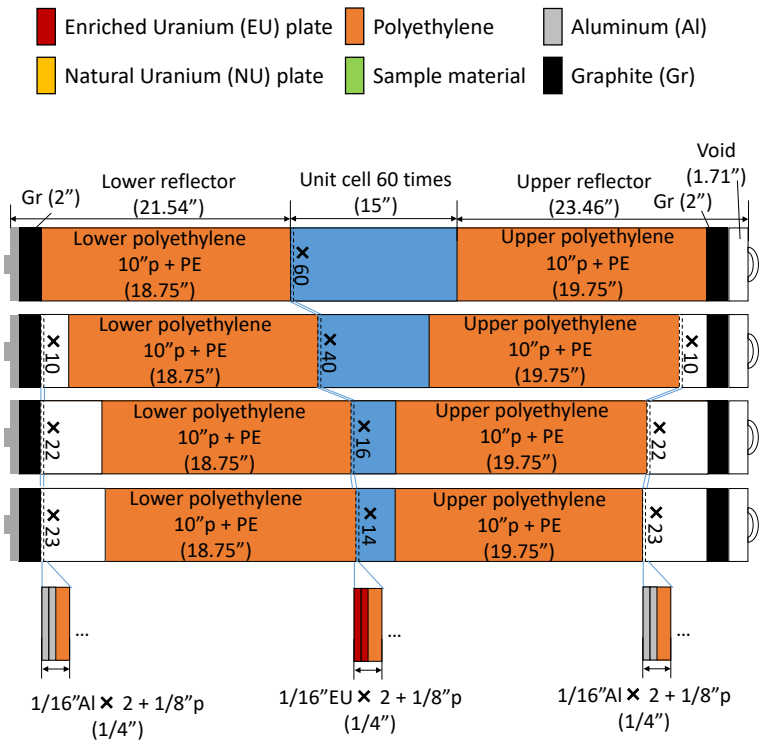

(a) Fuel rods termed “F”, “40”, “16”, and “14” ordered from top to bottom.

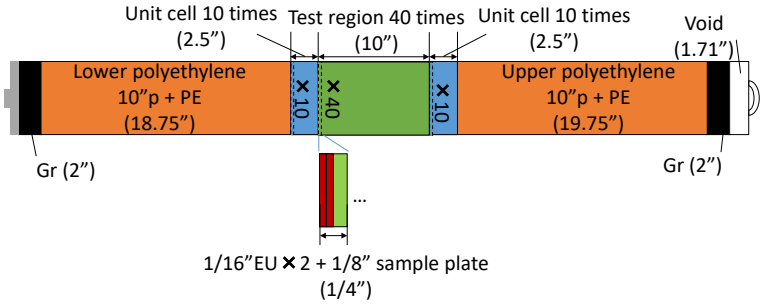

(b) Test fuel rod of HEU core termed “f”.

Figure 4.2 Side view of fuel rods.

“Gr”, “EU”, “NU”, “PE”, and “p” represent graphite block, HEU fuel plates, natural uranium plates, polyethylene reflector, and polyethylene moderator, respectively.

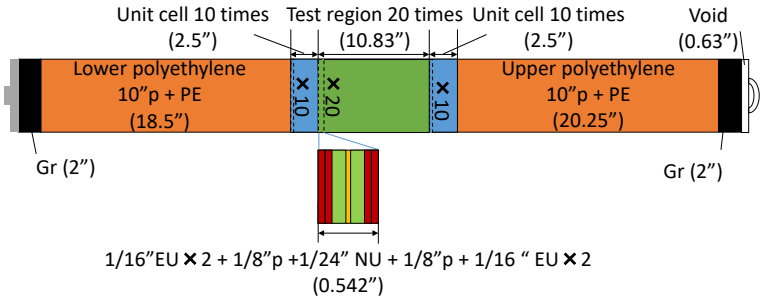

(c) Test fuel rod of LEU core termed "LEU".

Figure 4.2 (continued) Side view of fuel rods.

"Gr", "EU", "NU", "PE", and "p" represent graphite block, HEU fuel plates, natural uranium plates, polyethylene reflector, and polyethylene moderator, respectively.

Table 4.1 Measured excess and sample reactivities and corresponding uncertainties (1σ).

(a) HEU core

Case	Pattern (U/C/L)	Excess reactivity [pcm][a]			Sample Case	Sample worth [pcm]		
A	Al/Al/Al	72.0	±	4.9	-	-	-	-
B	Pb/Pb/Pb	241.9	±	6.1	Al → Pb (B − A)	169.8	±	7.6
C	Pb/Vd/Pb	38.7	±	3.6	Pb sample (B − C)	203.2	±	6.9
D	Bi/Bi/Bi	166.5	±	6.5	Al → Bi (D − A)	94.5	±	8.0
E	Bi/Vd/Bi	0.0	±	0.1	Bi sample (D − E)	166.5	±	6.5

(b) LEU core

Case	Pattern (U/C/L)	Excess reactivity [pcm][b]			Sample Case	Sample worth [pcm]		
A	Al/Al/Al	152.4	±	7.5	-	-	-	-
B	Pb/Pb/Pb	280.3	±	7.8	Al → Pb (B − A)	127.9	±	10.4
C	Pb/Vd/Pb	116.1	±	6.8	Pb sample (B − C)	164.2	±	10.0
D	Bi/Bi/Bi	228.8	±	8	Al → Bi (D − A)	76.4	±	10.6
E	Bi/Vd/Bi	75.6	±	5.6	Bi sample (D − E)	153.2	±	9.6

[a] Measured with C3 control rod and the other rods were fully withdrawn.

[b] Measured with C3 control rod and the other rods were fully withdrawn.

4.2.2. Eigenvalues and uncertainty

The MCNP6.2 code, together with the JENDL-4.0 nuclear data library, was used to perform eigenvalue calculations of clean core models (i.e., fully withdrawn control rods). Sensitivity coefficients of the effective multiplication factor (k_{eff}) to 84 microscopic reactions, including capture, fission, (n,2n), and elastic/inelastic-scattering cross sections of nuclides for uranium, polyethylene, control rods, and air, as well as $\bar{\nu}$ values and fission spectra of uranium nuclides, were evaluated by the ksen card, which is a perturbation capability based on the adjoint weighted tally [14]. The energy group structure was taken from the SCALE 56-group structure [15]. A sample reactivity from a loading pattern "A" to "B" $\Delta\rho_{\text{A}\to\text{B}}$ is defined by subtracting the excess reactivities of these patterns ρ_{A} and ρ_{B} as follows:

$$\begin{aligned} \Delta\rho_{\text{A}\to\text{B}} \equiv \rho_{\text{B}} - \rho_{\text{A}} &= \left(1 - \frac{1}{k_{\text{eff,B}}}\right) - \left(1 - \frac{1}{k_{\text{eff,A}}}\right), \\ \therefore \Delta\rho_{A\to B} &= \frac{1}{k_{\text{eff,A}}} - \frac{1}{k_{\text{eff,B}}}. \end{aligned} \tag{4.1}$$

Then, the sensitivity coefficients of the sample reactivity were evaluated by the chain rule of the differential, which is adopted in the TSAR module of the SCALE code system [15]. In this method, the relative sensitivity coefficient of the sample reactivity to an arbitrary parameter α can be evaluated as follows:

$$\frac{\alpha}{\Delta\rho_{\text{A}\to\text{B}}}\frac{d(\Delta\rho_{\text{A}\to\text{B}})}{d\alpha} = \frac{\frac{1}{k_{\text{eff,B}}}\left(\frac{\alpha}{k_{\text{eff,B}}}\frac{dk_{\text{eff,B}}}{d\alpha}\right) - \frac{1}{k_{\text{eff,A}}}\left(\frac{\alpha}{k_{\text{eff,A}}}\frac{dk_{\text{eff,A}}}{d\alpha}\right)}{\Delta\rho_{\text{A}\to\text{B}}}. \tag{4.2}$$

In the sample reactivity measurements, only the sample materials in the test region change before

and after substitution. Therefore, it is expected that the sensitivity coefficients to factors that are invariant before and after the substitution, such as uranium and polyethylene, will be canceled by the subtraction of Equations (4.1) and (4.2), and the high sensitivity coefficients to the sample material will be extracted. We will see such a subtraction effect later in Sec. 4.2.2.2. The number of histories was 6.14×10^9 (128,000 histories per batch, 48,000 active batches with 100 skip batches) for all configurations, resulting in a standard deviation of approximately 1 pcm in the MCNP eigenvalue calculations. The cross section-induced uncertainty was also evaluated based on the covariance data of JENDL-4.0. The covariance data were processed using NJOY99 [16].

4.2.2.1. Eigenvalues

Tables 4.2(a) and 4.2(b) present the calculated excess and sample reactivities corresponding to the measurements for the HEU and LEU cores, respectively. Table 4.2 gives the C/E (calculation/experiment) values for the sample reactivities and the corresponding uncertainties. The uncertainties for the sample reactivities listed in Table 4.2 are the Monte Carlo uncertainties and the total calculation uncertainties, which are the square root of the sum squares of the Monte Carlo and cross section-induced uncertainties discussed later in Section 4.2.2.2. As shown in Table 4.2, large discrepancies of C/E beyond the total uncertainties were found in the "Bi sample" for the HEU core. As discussed later in Section 4.3.1, this sample reactivity was determined to be an outlier and was excluded from the DA analysis performed in Section 4.4.

Table 4.2 Calculated excess and sample reactivities.

(a) HEU core

Case	Pattern (U/C/L)	Excess reactivity [pcm]	Sample Case	Sample worth [pcm]	Monte Carlo uncertainty (1σ) [pcm]	Total calculation uncertainty (1σ) [pcm][a]	C/E [-]	Exp. + Monte Carlo uncertainty (1σ) [-][b]	Exp. + total calculation uncertainty (1σ) [-][b]
A	Al/Al/Al	112.4 ± 1.3	-	-	-	-	-	-	-
B	Pb/Pb/Pb	283.7 ± 1.3	Al → Pb (B − A)	171.3	1.6	16.7	1.0	0.05	0.11
C	Pb/Vd/Pb	61.0 ± 1.3	Pb sample (B − C)	222.7	1.6	11.3	1.1	0.04	0.07
D	Bi/Bi/Bi	221.5 ± 1.3	Al → Bi (D − A)	109.1	1.6	8.8	1.2	0.10	0.14
E	Bi/Vd/Bi	28.5 ± 1.3	Bi sample (D − E)	193.0	1.6	8.2	1.2	0.05	0.07

(b) LEU core

Case	Pattern (U/C/L)	Excess reactivity [pcm]	Sample Case	Sample worth [pcm]	Monte Carlo uncertainty (1σ) [pcm]	Total calculation uncertainty (1σ) [pcm][a]	C/E [-]	Exp. + Monte Carlo uncertainty (1σ) [-][b]	Exp. + total calculation uncertainty (1σ) [-][b]
A	Al/Al/Al	73.9 ± 1.3	-	-	-	-	-	-	-
B	Pb/Pb/Pb	201.6 ± 1.3	Al → Pb (B − A)	127.6	1.6	12.3	1.00	0.08	0.13
C	Pb/Vd/Pb	19.0 ± 1.3	Pb sample (B − C)	182.6	1.6	8.7	1.11	0.07	0.09
D	Bi/Bi/Bi	146.8 ± 1.3	Al → Bi (D − A)	72.8	1.6	6.2	0.95	0.13	0.16
E	Bi/Vd/Bi	-7.0 ± 1.3	Bi sample (D − E)	153.8	1.6	5.2	1.00	0.06	0.07

[a] the square root of sum squares of Monte Carlo and cross-section-induced uncertainties.

[b] Including experimental uncertainties.

4.2.2.2. Cross section-induced uncertainty

As an example, **Table 4.3** lists the breakdown of the cross section-induced uncertainties for the k_{eff} of the "Bi/Bi/Bi" pattern and the sample reactivity of the "Bi sample" of the HEU core for representative microscopic reactions. The uncertainty values in Table 4.3 are relative to the mean values. The most significant contributor was the fission spectrum of ^{235}U for both k_{eff} and the sample reactivity. However, the relative contributions of uranium-related reactions in the sample reactivity were significantly reduced by the subtraction. The magnitude of the contribution from ^{209}Bi (i.e., an inelastic-scattering cross section of 1.94%) was comparable to that of uranium reactions (i.e., the fission spectrum of 3.52%), indicating that high sensitivity to ^{209}Bi was successfully attained. Due to the absence of Al-related covariance data in JENDL-4.0, the contributions from ^{27}Al are zero in Table 4.3. **Table 4.4** lists the cross section-induced uncertainties and the correlation matrix of the sample reactivity experiments used to perform the DA analyses in this chapter. The covariance matrix of the sample reactivity experiments was evaluated based on the sandwich formula [17]: Using the variables described later in Section 4.3.1, the covariance matrix is given by $\mathbf{GMG^T}$, which is a square matrix whose order is the number of experiments considered (i.e., 8×8 matrix in Table 4.4). Correlation coefficients will be calculated by dividing each element of the covariance matrix by standard deviations (i.e., the square root of the diagonal components of the covariance matrix). Here the relative uncertainty of the Bi sample of the HEU core (i.e., 4.17%) was nearly the same as the sum of squares for the breakdowns listed in Table 4.3.

Table 4.3 Breakdown of cross-section-induced uncertainty of k_{eff} in the HEU core related to Bi.

Component	Reaction-Reaction		k_{eff} of Bi/Bi/Bi [pcm]	Bi sample [%]
Fuel plate and Al plate	^{235}U fission spectrum	^{235}U fission spectrum	643.2	3.52
	^{235}U	^{235}U	278.5	0.34
	^{235}U capture	^{235}U capture	201.0	0.22
	^{235}U fission	^{235}U fission	88.0	0.29
	^{27}Al elastic scattering	^{27}Al elastic scattering	0.0	0.00
	^{27}Al inelastic scattering	^{27}Al inelastic scattering	0.0	0.00
	^{27}Al capture	^{27}Al capture	0.0	0.00
Polyethylene	^{1}H elastic scattering	^{1}H elastic scattering	228.1	0.28
	^{1}H capture	^{1}H capture	254.9	0.89
	C elastic scattering	C elastic scattering	0.0	0.00
	C inelastic scattering	C inelastic scattering	0.0	0.00
Bi sample	^{209}Bi elastic scattering	^{209}Bi elastic scattering	0.0	0.00
	^{209}Bi (n, $2n$)	^{209}Bi (n, $2n$)	0.0	0.00
	^{209}Bi capture	^{209}Bi capture	0.0	0.00
	^{209}Bi inelastic scattering	^{209}Bi inelastic scattering	7.4	1.94

Table 4.4 Cross section-induced uncertainty and correlation matrix of calculated sample reactivity experiments for the different experiments.

Core	Case	Uncertainty [%]	Correlation matrix [-] HEU Al → Pb	HEU Pb sample	HEU Al → Bi	HEU Bi sample	LEU Al → Pb	LEU Pb sample	LEU Al → Bi	LEU Bi sample
HEU	Al → Pb	9.73	1.00	0.90	0.21	0.31	0.98	0.88	0.04	0.28
	Pb sample	5.04	0.90	1.00	0.34	0.63	0.89	0.99	0.13	0.57
	Al → Bi	7.94	0.21	0.34	1.00	0.80	0.17	0.32	0.86	0.84
	Bi sample	4.17	0.31	0.63	0.80	1.00	0.30	0.62	0.59	0.96
LEU	Al → Pb	9.67	0.98	0.89	0.17	0.30	1.00	0.90	0.08	0.26
	Pb sample	4.78	0.88	0.99	0.32	0.62	0.90	1.00	0.13	0.57
	Al → Bi	8.57	0.04	0.13	0.86	0.59	0.08	0.13	1.00	0.67
	Bi sample	3.39	0.28	0.57	0.84	0.96	0.26	0.57	0.67	1.00

4.2.3. Covariance matrices of experiments and calculations

Covariance matrices of experiments and calculations were evaluated by considering: i) aleatoric errors in the control rod position, ii) the control rod worth, iii) the mass of sample materials, and iv) calculation uncertainties and correlations from MCNP-6.2. Using the notations as will be defined later in Section 4.3.1, the experimental covariance matrix $\mathbf{V}_e$ corresponds to the sum of matrices of i), ii), and iii), and the calculation model covariance matrix $\mathbf{V}_m$ corresponds to the matrix of iv).

4.2.3.1. Control rod position

The acquired control rod positions were deviated for each measurement, hence, the excess reactivities contain aleatoric uncertainty. Although the measurement uncertainties are shown in Reference [9], the number of measurements for each loading pattern was small. In

particular, only two measurements were performed for each HEU core loading pattern. The aleatoric uncertainties of the control rod position were then re-evaluated by modeling the deviations as a normal distribution with a mean value taken as zero for each loading pattern. Then, the aleatoric uncertainties of the sample reactivities derived from the control rod position were evaluated by error propagation. A detailed description is given in Appendix B. **Table 4.5** lists these aleatoric uncertainties and the corresponding correlations among the sample reactivities. Although no correlation is assumed for each control rod position measurement, some correlations appeared among the sample reactivities because they shared loading patterns before or after replacement. For example, a non-zero correlation was found between "Al → Pb" and "Al → Bi" because these sample cases shared the reference loading pattern "Al/Al/Al". The HEU and LEU cores were taken to critical by different control rods, and it was assumed that there was no correlation between the HEU and LEU cores.

Table 4.5 Uncertainty and correlation of sample reactivities induced by control rod position

			Correlation matrix [-]							
			HEU				LEU			
Core	Case	Uncertainty [%]	Al → Pb	Pb sample	Al → Bi	Bi sample	Al → Pb	Pb sample	Al → Bi	Bi sample
HEU	Al → Pb	4.33	1.00	0.63	0.40	0.00	0.00	0.00	0.00	0.00
	Pb sample	3.22	0.63	1.00	0.00	0.00	0.00	0.00	0.00	0.00
	Al → Bi	8.41	0.40	0.00	1.00	0.79	0.00	0.00	0.00	0.00
	Bi sample	3.77	0.00	0.00	0.79	1.00	0.00	0.00	0.00	0.00
LEU	Al → Pb	8.04	0.00	0.00	0.00	0.00	1.00	0.52	0.49	0.00
	Pb sample	5.99	0.00	0.00	0.00	0.00	0.52	1.00	0.00	0.00
	Al → Bi	13.88	0.00	0.00	0.00	0.00	0.49	0.00	1.00	0.59
	Bi sample	6.17	0.00	0.00	0.00	0.00	0.00	0.00	0.59	1.00

4.2.3.2. Control rod worth

The control rod worths for the C3 rod of the HEU cores and the C2 rod of the LEU cores were measured using the rod drop method. Neutron counts were measured before and after the rod drop using two fission chambers. The uncertainty of the control rod worth was estimated to be 1% based on the statistical uncertainty of the neutron counts and assuming a Poisson process. **Table 4.6** lists the uncertainties induced by the control rod worths and the corresponding correlations among the sample reactivities. Since the control rod worth determines the absolute values of the excess and the sample reactivities, all correlations must be one. The correlations between the HEU core and the LEU core were neglected because different control rods were used for these cores.

Table 4.6 Uncertainty and correlations of sample reactivities induced by control rod worth

			Correlation matrix [-]							
			HEU				LEU			
Core	Case	Uncertainty [%]	Al → Pb	Pb sample	Al → Bi	Bi sample	Al → Pb	Pb sample	Al → Bi	Bi sample
HEU	Al → Pb	1.00	1.00	1.00	1.00	1.00	0.00	0.00	0.00	0.00
	Pb sample	1.00	1.00	1.00	1.00	1.00	0.00	0.00	0.00	0.00
	Al → Bi	1.00	1.00	1.00	1.00	1.00	0.00	0.00	0.00	0.00
	Bi sample	1.00	1.00	1.00	1.00	1.00	0.00	0.00	0.00	0.00
LEU	Al → Pb	1.00	0.00	0.00	0.00	0.00	1.00	1.00	1.00	1.00
	Pb sample	1.00	0.00	0.00	0.00	0.00	1.00	1.00	1.00	1.00
	Al → Bi	1.00	0.00	0.00	0.00	0.00	1.00	1.00	1.00	1.00
	Bi sample	1.00	0.00	0.00	0.00	0.00	1.00	1.00	1.00	1.00

4.2.3.3. Mass of sample plates

Table 4.7 lists the mass and the uncertainty per plate for Pb, Bi, and Al plates, and the Al spacer due to manufacturing tolerance measured on several dozen plates with an electric scale. The relative uncertainties of the total mass were estimated by assuming no correlation for each plate. For example, there were 200 plates in the test region (i.e., 40 plates per fuel rod and 5 fuel rods) in the Pb/Pb/Pb pattern for both the HEU and LEU cores; thus, the relative uncertainty of the total mass was calculated by dividing the square root of 200, resulting in a relative uncertainty of 0.12%. The error propagation from the sample mass to k_{eff} was estimated using the kpert option of MCNP-6.2, which is a capability based on the first-order perturbation theory [10]. **Table 4.8** lists the uncertainties induced by the mass of the sample materials and corresponding correlations among the sample reactivities. Small correlations were found between the Pb sample and the Bi sample, which shared the Al spacers in the center of the test region. However, these correlations were negligibly small (i.e., $<10^{-4}$) due to the small relative uncertainty of the Al spacer mass. Because the series of experiments on the HEU core was conducted in different years than those on the LEU core, and because the positions of the sample material plates were considered to be sufficiently shuffled, the correlation between the HEU and LEU cores was expected to be negligible.

Table 4.7 Mass of sample plate[a] and corresponding relative uncertainty (1σ)

Material	Mass [g]			Relative uncertainty [%]
Pb plate	86.171	±	1.501	1.74
Bi plate	71.353	±	0.439	0.62
Al plate	22.046	±	0.068	0.30
Al spacer	2.404	±	0.002	0.07

a The size of plates was 2 × 2 × 1/8 in.

Table 4.8 Uncertainty and correlations of sample reactivities induced by sample mass

Core	Case	Uncertainty [%]	Correlation matrix [-] HEU Al → Pb	HEU Pb sample	HEU Al → Bi	HEU Bi sample	LEU Al → Pb	LEU Pb sample	LEU Al → Bi	LEU Bi sample
HEU	Al → Pb	0.34	1.00	0.69	0.09	0.00	0.00	0.00	0.00	0.00
	Pb sample	0.16	0.69	1.00	0.00	0.00	0.00	0.00	0.00	0.00
	Al → Bi	0.19	0.09	0.00	1.00	0.64	0.00	0.00	0.00	0.00
	Bi sample	0.06	0.00	0.00	0.64	1.00	0.00	0.00	0.00	0.00
LEU	Al → Pb	0.38	0.00	0.00	0.00	0.00	1.00	0.66	0.07	0.00
	Pb sample	0.14	0.00	0.00	0.00	0.00	0.66	1.00	0.00	0.00
	Al → Bi	0.24	0.00	0.00	0.00	0.00	0.07	0.00	1.00	0.69
	Bi sample	0.06	0.00	0.00	0.00	0.00	0.00	0.00	0.69	1.00

4.2.3.4. Calculation uncertainty

Reference [8] indicates a difference of approximately 100 pcm in the k_{eff} of the KUCA A-core between two continuous energy Monte Carlo codes (i.e., MCNP and SCALE6.2/KENO-VI [15]), despite using an identical nuclear data library and using the as-built modeled geometry for both codes. Based on this knowledge, the numerical bias of k_{eff} is roughly estimated to be 100 pcm. However, due to the subtraction, the numerical bias seen in k_{eff} could be canceled in the evaluation of sample reactivities when using the same Monte Carlo codes for both before and after sample substitution. Therefore, only the Monte Carlo statistical errors are considered for the calculation uncertainties of the sample reactivities. **Table 4.9** lists the uncertainties calculated from Table 4.2 and the corresponding correlations. Due to subtracting values with similar magnitudes of statistical errors, correlation factors of 0.5 appeared among the experiments sharing identical loading patterns before or after replacement.

Table 4.9 Calculation uncertainty and correlations of sample reactivities.

Core	Case	Uncertainty [%]	Correlation matrix [-] HEU Al → Pb	HEU Pb sample	HEU Al → Bi	HEU Bi sample	LEU Al → Pb	LEU Pb sample	LEU Al → Bi	LEU Bi sample
HEU	Al → Pb	0.89	1.00	0.50	0.50	0.00	0.00	0.00	0.00	0.00
	Pb sample	0.68	0.50	1.00	0.00	0.00	0.00	0.00	0.00	0.00
	Al → Bi	1.39	0.50	0.00	1.00	0.50	0.00	0.00	0.00	0.00
	Bi sample	0.79	0.00	0.00	0.50	1.00	0.00	0.00	0.00	0.00
LEU	Al → Pb	1.19	0.00	0.00	0.00	0.00	1.00	0.50	0.50	0.00
	Pb sample	0.83	0.00	0.00	0.00	0.00	0.50	1.00	0.00	0.00
	Al → Bi	2.08	0.00	0.00	0.00	0.00	0.50	0.00	1.00	0.50
	Bi sample	0.99	0.00	0.00	0.00	0.00	0.00	0.00	0.50	1.00

4.3. Data assimilation

4.3.1. Methodology

In this chapter, the methodology in the development of ADJ2017 is used [13]. The formulation of the cross section adjustment is:

$$\vec{T}_{\mathrm{adj}} = \vec{T}_0 + \mathbf{M}\mathbf{G}^{\mathrm{T}}\left(\mathbf{G}\mathbf{M}\mathbf{G}^{\mathrm{T}} + \mathbf{V}_{\mathrm{e}} + \mathbf{V}_{\mathrm{m}}\right)^{-1}\left(\vec{R}_{\mathrm{e}} - \vec{R}_{\mathrm{c}}(\vec{T}_0)\right), \tag{4.3}$$

$$\mathbf{M}_{\mathrm{adj}} = \mathbf{M} - \mathbf{M}\mathbf{G}^{\mathrm{T}}\left(\mathbf{G}\mathbf{M}\mathbf{G}^{\mathrm{T}} + \mathbf{V}_{\mathrm{e}} + \mathbf{V}_{\mathrm{m}}\right)^{-1}\mathbf{G}\mathbf{M}, \tag{4.4}$$

where $\vec{T}_0$ and $\vec{T}_{\mathrm{adj}}$ are the cross sections in vector form before and after adjustment; $\vec{R}_{\mathrm{e}}$ and $\vec{R}_{\mathrm{c}}$ are vectors of experimental parameters and corresponding values calculated with $\vec{T}_0$, $\mathbf{M}$ and $\mathbf{M}_{\mathrm{adj}}$ are the covariance matrices of cross sections before and after adjustment, $\mathbf{G}$ is the

sensitivity matrix of experimental parameters to cross sections, $\mathbf{V}_\mathrm{e}$ is the covariance matrix of the experimental parameters, and $\mathbf{V}_\mathrm{m}$ is the covariance matrix of the calculation model.

Outliers and/or underestimation of uncertainties can result in inappropriate adjustment. To mitigate the effect of outliers, they were detected in the sample reactivity experiments using the following criterion adopted in ADJ2017:

$$\chi = \frac{|C/E - 1|}{\sqrt{v}} > 2, \tag{4.5}$$

where v is the diagonal component of $\mathbf{GMG}^\mathrm{T} + \mathbf{V}_\mathrm{e} + \mathbf{V}_\mathrm{m}$, i.e., the variance of the experiment. Assuming a normal distribution, the likelihood of Equation (4.5) being realized is less than 5%, which means that the measured values may be outliers and/or that experimental uncertainties may be underestimated. **Figure 4.3** shows the chi values evaluated by Equation (4.5). Only the Bi sample of the HEU core exceeded this criterion, and so it was excluded from DA in Section 4.4.

If adjustments were made using only the sample reactivities, which are the differences between the excess reactivities, the results of the criticality calculations using the adjusted cross sections could deviate significantly from the critical state. Therefore, the k_eff of the "Al/Al/Al" pattern for the HEU core is included in the DA analysis as a reference core to maintain the critical state after the adjustment. A total of eight experiments (i.e., seven sample reactivities and one k_eff) were used.

Cross section alterations occur in the adjustment for high-sensitivity coefficients and/or large uncertainties so as to reduce the trace of the posterior covariance matrix [18]. If covariance data are absent for such nuclides, the cross sections of the other nuclides compensate for the adjustment. Here, ^{27}Al was used in the experiments, but the corresponding covariance data is not available in JENDL-4.0. The adjustment in this chapter aimed to evaluate the impact of the sample

reactivity experiment on the uncertainty reduction, and the absence corresponds to the effectiveness of Equation (4.4) with the assumption of no uncertainty in the ^{27}Al cross sections.

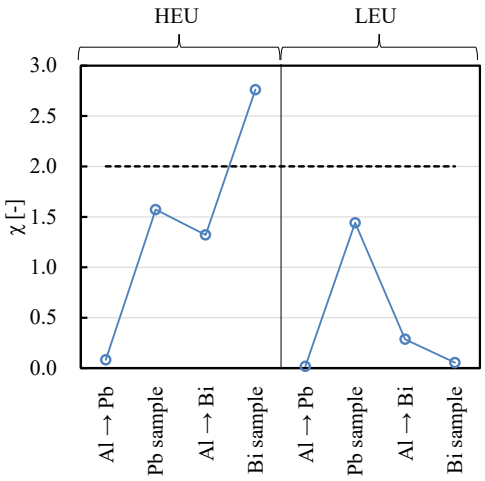

Figure 4.3 Chi values of sample reactivity by Eq. (4.3).

(Dashed line represents the criterion.)

4.3.2. Brief description of ADS

Reference [4] provides a detailed specification of the ADS used in this chapter. The MA-nitride fuel consists of transuranium [i.e., MAs and plutonium (Pu) nuclides] nitride and the inert material of zirconium nitride. The beginning-of-cycle (BOC) k_{eff} value was adjusted to 0.98 by the volume ratio of Pu-nitride to (MA + Pu)-nitride for the first cycle.

In this chapter, the prior and posterior cross section-induced uncertainties of the void reactivity at the BOC of the first cycle were evaluated using the sensitivity coefficients obtained in the previous chapter. For the sensitivity coefficient evaluation, 157 microscopic reactions were considered, including capture, fission, (n,2n), and elastic/inelastic-scattering cross sections for MA fuels, structure materials, and LBE nuclides, and $\bar{\nu}$ values and fission spectra for heavy nuclides. Because the fuel is composed of Pu-nitride, and uranium nuclides accompany the fuel fabrication process, the microscopic cross sections of plutonium and uranium nuclides were

considered [4]. Note that Al is not contained in the ADS, and the coefficients for sensitivity to ^{27}Al were zero. Of the microscopic reactions to which sensitivity coefficients were evaluated for the KUCA and the ADS, 174 reactions were practically considered in the DA analysis for which covariance data were provided. **Table 4.10** lists the microscopic reactions considered in the DA analysis. Here, $\bar{\mu}$ values were excluded to be consistent with the work of Reference [8, 9]. The sensitivity coefficients of the ADS and the ADJ2017 were given in the 70-energy-group structure of UFLIB [19]. This structure is typically used for the analysis of fast systems in Japan. The sensitivity coefficients of the sample reactivities at the KUCA and covariance matrices were re-evaluated in the 70-energy-group structure, and then the DA analysis discussed later in Section 4.4.2 was performed with this structure.

As described in Section 4.1, the target accuracy ranging between 5% and 7% for the coolant reactivity has been proposed and discussed in the OECD/NEA WPEC subgroups [2, 3]. Regarding the target accuracy, the report of the WPEC subgroup [2] describes as follows: *"These target accuracies reflect the perceived state of the art from an R&D point of view, even if they are not the result of a systematic analysis, which should necessarily involve industrial partners."* Although the target accuracy of the coolant void reactivity of the ADS should be determined considering many factors, such as the voiding scenario and the subcriticality required to keep the ADS safe, a provisional criterion of 5% (i.e., the lower value of the range) was used for the coolant void reactivity in this chapter.

4.3.3. Integral data for ADJ2017

The ADJ2017 is a cross section set based on JENDL-4.0, aimed at improving the accuracy of fast reactors through DA by adopting 620 integral experiments. These experiments include data sets that are highly sensitive to MAs, such as a series of experiments with neptunium

dioxide at the BFS in Russia, measurements of fission reaction rates of MAs at the FCA-IX core in Japan, and MA irradiation tests at the JOYO reactor in Japan. Considerable effort has been devoted to the evaluation of these experiments, including sensitivity coefficient evaluation, experimental uncertainty evaluation, correlation evaluation, and calculation uncertainty estimation. The data sets for the ADJ2017 including sensitivity coefficients, C/E values, experimental and calculation uncertainties, and the corresponding correlations are accessible and available in YAML format on the webpage of the ADJ2017 report [13] (see the link in the reference list), which can be interpreted by MARBLE, and on which DA can be easily performed. In this chapter, the combined impact of DA on uncertainty reduction was also demonstrated using previously available and accessible data.

Table 4.10 Microscopic reactions considered in DA analysis.

Only reactions termed “yes” were considered.

Nuclide	capture	fission	elastic scattering	inelastic scattering	(n,2n)	$\bar{\nu}$	fission spectrum
^{234}U	yes	yes	yes	yes	yes	yes	yes
^{235}U	yes	yes	yes	yes	yes	yes	yes
^{236}U	yes	yes	yes	yes	yes	yes	yes
^{238}U	yes	yes	yes	yes	yes	yes	yes
^{237}Np	yes	yes	yes	yes	yes	yes	yes
^{238}Pu	yes	yes	yes	yes	yes	yes	yes
^{239}Pu	yes	yes	yes	yes	yes	yes	yes
^{240}Pu	yes	yes	yes	yes	yes	yes	yes
^{241}Pu	yes	yes	yes	yes	yes	yes	yes
^{242}Pu	yes	yes	yes	yes	yes	yes	yes
^{241}Am	yes	yes	yes	yes	yes	yes	yes
^{242m}Am	yes	yes	yes	yes	yes	yes	yes
^{243}Am	yes	yes	yes	yes	yes	yes	yes
^{243}Cm	yes	yes	yes	yes	yes	yes	yes
^{244}Cm	yes	yes	yes	yes	yes	yes	yes
^{245}Cm	yes	yes	yes	yes	yes	yes	yes
^{246}Cm	yes	yes	yes	yes	yes	yes	yes

Table 4.10 (continued) Microscopic reactions considered in DA analysis.

Only reactions termed “yes” were considered.

Nuclide	capture	fission	elastic scattering	inelastic scattering	(n,2n)	$\bar{\nu}$	fission spectrum
^{1}H	yes	no	yes	no	no	no	no
^{10}B	yes	no	yes	no	no	no	no
^{11}B	yes	no	yes	no	no	no	no
^{15}N	no	no	yes	no	no	no	no
^{16}O	yes	no	yes	yes	yes	no	no
^{52}Cr	yes	no	yes	yes	yes	no	no
^{53}Cr	yes	no	yes	yes	yes	no	no
^{55}Mn	yes	no	yes	yes	yes	no	no
^{56}Fe	yes	no	yes	yes	yes	no	no
^{58}Ni	yes	no	yes	yes	yes	no	no
^{60}Ni	yes	no	yes	yes	yes	no	no
^{90}Zr	yes	no	no	yes	yes	no	no
^{204}Pb	yes	no	yes	yes	yes	no	no
^{206}Pb	yes	no	yes	yes	yes	no	no
^{207}Pb	yes	no	yes	yes	yes	no	no
^{208}Pb	yes	no	yes	yes	yes	no	no
^{209}Bi	no	no	no	yes	no	no	no
$^{nat.}$C	no	no	no	no	no	no	no
^{14}N	no	no	no	no	no	no	no
^{27}Al	no	no	no	no	no	no	no
^{40}Ar	no	no	no	no	no	no	no

4.4. Results

4.4.1. Adjustment

DA based on Equation (4.3) was performed using the experimental data of the sample reactivity from KUCA discussed in Section 4.2 with the SCALE 56-group structure. **Figure 4.4** shows prior and posterior C/E values of the sample reactivities. The posterior sample reactivities

were predicted based on the alterations (i.e., $\vec{T}_{adj} - \vec{T}_0$) and sensitivity coefficients. The error bars represent the square root of the sum of squares of calculation uncertainties and cross section-induced uncertainties (1σ). The prior and posterior k_{eff} and the corresponding cross section-induced uncertainties (1σ) were 1.00112 ± 0.00820 and 1.00110 ± 0.00099, respectively, indicating that criticality was maintained before and after the adjustment. The prior and posterior C/E values of k_{eff} were not changed significantly (1.000 ± 0.008 and 1.000 ± 0.002, respectively) but the uncertainty was reduced. As shown in Figure 4.4, the posterior C/E values of the HEU core were closer to unity. Interestingly, the "Bi sample" of the HEU core also approached unity, although it was excluded from the DA analysis. For the "Al → Bi" of the LEU core, the posterior C/E value worsened, but the movement was limited within the range of experimental uncertainty. **Table 4.11** lists the posterior cross section-induced uncertainties and the correlation matrix of the sample reactivity experiments. The posterior uncertainties were reduced by approximately half, except for the "Al → Bi" of the HEU and LEU cores, whose experimental uncertainties were relatively larger than the other measurements.

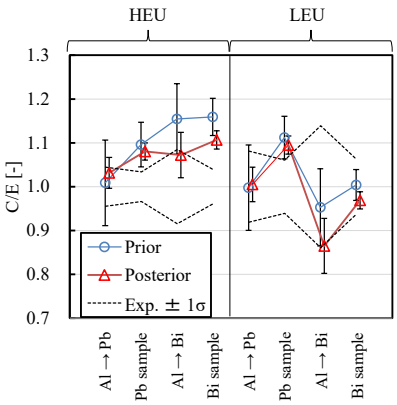

Figure 4.4 Prior and posterior C/E value.

The error bars represent the square root of the sum of squares of calculation and cross-section-induced uncertainties (1σ).

Table 4.11 Posterior cross-section-induced uncertainty and correlation matrix of sample reactivities

Core	Case	Uncertainty [%]	Correlation matrix [-] HEU Al → Pb	HEU Pb sample	HEU Al → Bi	HEU Bi sample	LEU Al → Pb	LEU Pb sample	LEU Al → Bi	LEU Bi sample
HEU	Al → Pb	3.42	1.00	0.77	0.40	0.33	0.87	0.68	0.32	0.32
	Pb sample	1.84	0.77	1.00	0.27	0.63	0.83	0.91	0.33	0.51
	Al → Bi	4.99	0.40	0.27	1.00	0.72	0.28	0.23	0.82	0.75
	Bi sample	1.93	0.33	0.63	0.72	1.00	0.41	0.62	0.68	0.86
LEU	Al → Pb	3.76	0.87	0.83	0.28	0.41	1.00	0.85	0.43	0.37
	Pb sample	1.88	0.68	0.91	0.23	0.62	0.85	1.00	0.33	0.54
	Al → Bi	5.92	0.32	0.33	0.82	0.68	0.43	0.33	1.00	0.78
	Bi sample	1.69	0.32	0.51	0.75	0.86	0.37	0.54	0.78	1.00

Figure 4.5 shows the cross section alterations and 1σ of the prior and posterior standard deviations for the inelastic-scattering cross sections of ^{206}Pb and ^{209}Bi. As shown in Figures 4.5 (a) and (b), the alteration of the inelastic-scattering cross sections of ^{206}Pb and ^{209}Bi was within 1σ of the posterior standard deviation. As discussed in Reference [9], the inelastic-scattering cross sections of ^{27}Al have a comparable impact to those of Pb and Bi on sample reactivities, such as "Al → Bi". However, the covariance data of ^{27}Al are not given in JENDL-4.0 (nor in the latest version of JENDL-5 [20]). To evaluate the more practical effectiveness of the KUCA data on uncertainty reduction, it is desirable to evaluate and verify the ^{27}Al cross sections and covariance data in the future. To validate the alterations obtained in this chapter, it is also desirable to further expand and evaluate integral experimental data (e.g., void reactivity measurements in a fast system [21]) related to Pb and Bi cross sections. The C/E values, experimental and calculated uncertainties and correlations, and sensitivity coefficients used in this chapter are provided as

supplemental material in a YAML format readable by MARBLE (see Appendix C).

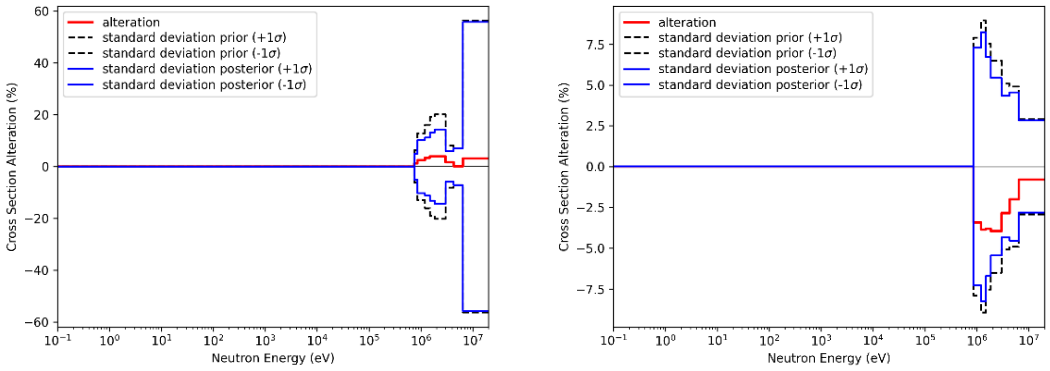

(a) ^{206}Pb / inelastic scattering (b) ^{209}Bi / inelastic scattering

Figure 4.5 Cross section alterations by DA.

4.4.2. Impact on ADS

Table 4.12 lists cross section-induced uncertainties of the coolant void reactivity at the BOC of the ADS without DA, with DA using KUCA data, with DA using ADJ2017 data, and with DA using KUCA and ADJ2017 data. The 70-energy-group structure of UFLIB was used. The DA with KUCA data shown in Table 4.12 successfully reduced the uncertainty of the void reactivity from 6.3% to 4.8%, despite KUCA being a solid-reflected, solid-moderated, uranium-fuel thermal reactor while the ADS is an LBE-cooled, MA-nitride-fuel fast reactor. Here, the DA with only KUCA data readily met the uncertainty criterion set (i.e., 5% in this chapter).

Table 4.12. Prior and posterior cross-section-induced uncertainty of coolant void reactivity of JAEA-ADS

Parameter	Prior	Posterior		
		KUCA	ADJ2017	KUCA+ADJ2017
Void reactivity [%]	6.3	4.8	5.5	3.6

However, considering the incompleteness of the covariance data in JENDL-4.0, further reduction in the uncertainty is desirable. The integral data for ADJ2017 include measurements that are highly sensitive to the cross sections of MA nuclides; thus, the combined use of KUCA data and ADJ2017 data reduced the uncertainty to 3.6%, while DA with only ADJ2017 still exceeded the criterion (i.e., 5.5%). To efficiently reduce the total uncertainty, it is important to reduce the major contributions, because the total uncertainty is approximated by the square root of the sum of the squares of each contribution. **Figures 4.6(a)** through **4.6(c)** illustrate the uncertainty breakdowns of the coolant void reactivity at the BOC of the ADS without DA, with DA using KUCA data, and with DA using KUCA and ADJ2017 data, respectively. The contributions of the (n,2n) reactions were negligibly small [the maximum value was 0.02% of (n,2n) of ^{208}Pb]. A comparison of Figures 4.6(a) and 4.6(b) indicates that the uncertainties induced by the inelastic-scattering cross sections of ^{206}Pb and ^{209}Bi were effectively reduced for the coolant void reactivity and that the major source of the uncertainty changed to ^{237}Np and ^{56}Fe. Figure 4.6(c) shows that the uncertainties induced by the MA nuclides and ^{56}Fe were remarkably reduced by the integral data of ADJ2017 for the fast reactor. As calculated from the breakdowns in Figure 4.6, even if we were able to completely eliminate the contributions from Pb and Bi nuclides, the total uncertainty would only be reduced to approximately 3.6%, which is comparable to that obtained with the combined KUCA and ADJ2017 data.

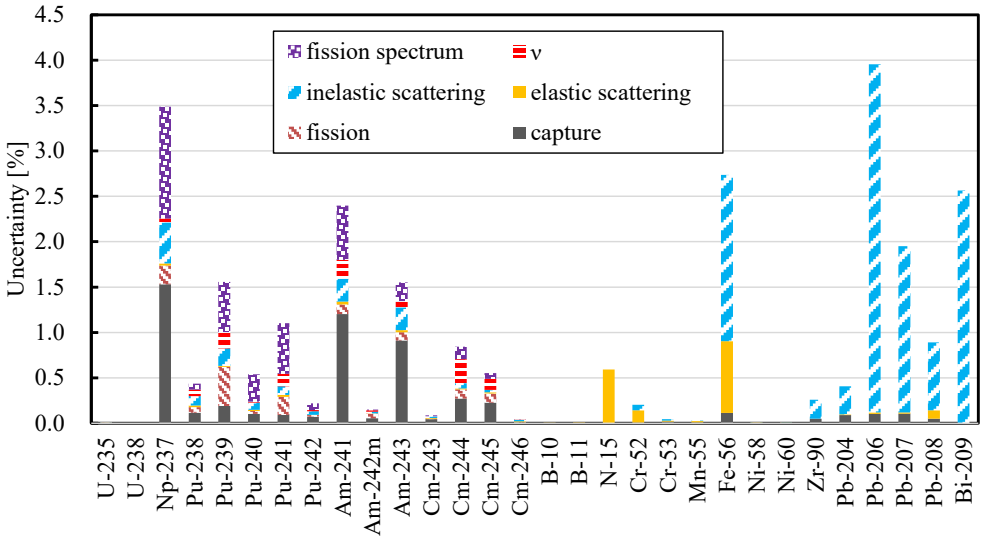

(a) Prior (without DA)

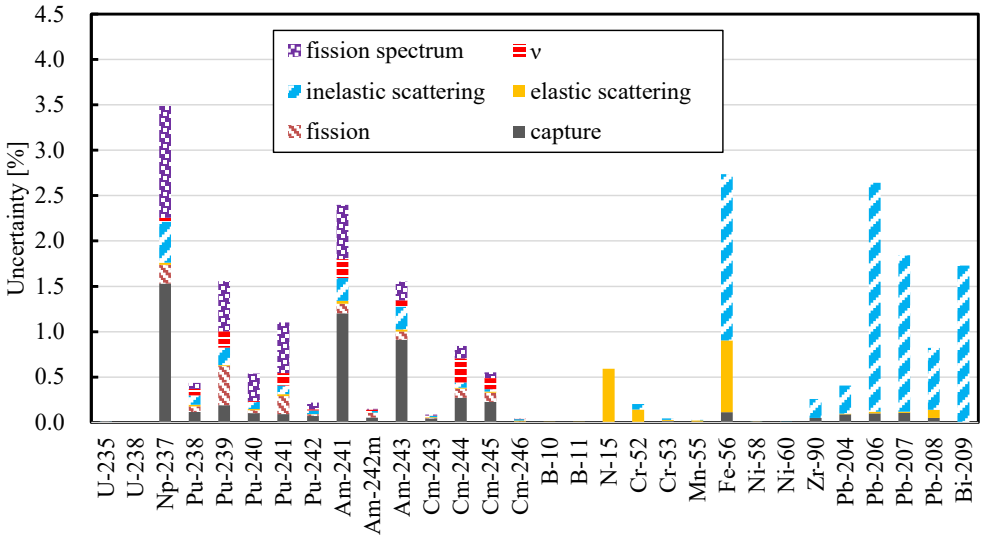

(b) Posterior (with DA using KUCA data)

Figure 4.6 Uncertainty breakdown of coolant void reactivity of ADS.

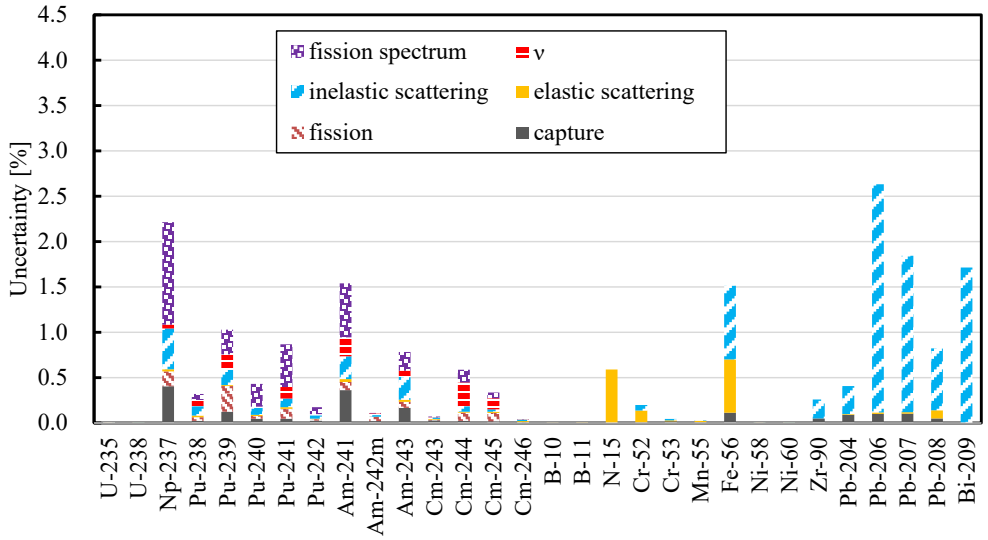

(c) Posterior (with DA using KUCA and ADJ2017)

Figure 4.6 (continued) Uncertainty breakdown of coolant void reactivity of ADS.

It should be stressed that, owing to the sensitivity coefficients, the breakdown of the uncertainty sources was evaluated, and then the importance of reduction of the uncertainty contributions from MA nuclides and ^{56}Fe is clarified. Also, further reduction of the uncertainty was successfully achieved using the available sensitivity database for ADJ2017 without the detailed information and the re-analyses of the integral experiments.

In light of the absence of ^{27}Al covariance data, the effectiveness of the KUCA data in this chapter was an ideal situation, and additional efforts are required to further reduce the contributions from Pb and Bi nuclides. Although it is important to evaluate the ^{27}Al covariance data and expand integral experiment data to evaluate the more practical effectiveness of the KUCA data, and to validate the alterations observed in the inelastic-scattering cross sections of the Pb and Bi nuclides, the major sources of the uncertainty of the coolant void reactivity in the ADS have already been efficiently reduced by the currently available ADJ2017 data.

4.5. Conclusions

DA analysis using sample reactivity experiments conducted in the HEU and LEU cores at KUCA was performed with the combined use of Pb and Bi plates. The sample reactivities were expected to be highly sensitive to the cross sections of Pb and Bi, which are major contributors to uncertainty in the ADS. Section 4.2 described the experimental and calculation covariance matrices of sample reactivities for the control rod position, the control rod worth, and the mass of sample materials, as well as cross section-induced uncertainties by MCNP-6.2 and JENDL-4.0. The DA results demonstrated some reduction in the uncertainty of the LBE coolant void reactivity of the ADS, achieving the target criterion for the uncertainty in this chapter (i.e., 5%). With the application of the KUCA data, the major sources of uncertainty changed from Pb and Bi to ^{237}Np and ^{56}Fe. It is indicated that the aid of ADJ2017 efficiently reduced the contributions from these nuclides, resulting in 3.6% of the cross section-induced uncertainty. In conclusion, the applicability of the forward-based SA, UQ, and DA analysis to the ADS using the sensitivity coefficients and the experimental data has been successfully demonstrated.

There are still open issues related to Chapter 4 that should be tackled in the future. First, the DA analysis for the other properties should be performed. In this chapter, the DA analysis was done only for the coolant void reactivity of the ADS at the BOC, which is relatively easy to calculate using PT, though SA for several neutronics parameters after burnup was performed in Chapter 3. Second, the covariance data of ^{27}Al were not provided in JENDL-4.0 (even JENDL-5), although a previous study [9] revealed that the sample reactivities obtained in the KUCA A-core were as sensitive to the inelastic-scattering cross section of ^{27}Al as to those of Pb and Bi. Hence, the evaluation and verification of ^{27}Al covariance data in the future would help evaluate the more practical effectiveness of the KUCA experimental data. Finally, validation of the cross section alterations obtained in this chapter by the expansion of the integral experimental data (e.g.,

void reactivity measurements in a fast system [21]) will be addressed in the future.

4.6. References for Chapter 4

[1] H. IWAMOTO et al., "Sensitivity and Uncertainty Analysis for a Minor-actinide Transmuter with JENDL-4.0," *Nuclear Data Sheets*, **118**, 519 (2014); https://doi.org/10.1016/j.nds.2014.04.123.

[2] M. SALVATORES, R. JACQMIN, "Uncertainty and Target Accuracy Assessment for Innovative Systems using Recent Covariance Data Evaluations," ISBN 978-92-64-99053-1, NEA/WPEC-26 (2008).

[3] "WPEC/SG46 Zoom Target Accuracy Requirements (TAR) Meeting," online, Apr. 14, 2021.

[4] T. SUGAWARA, R. KATANO, and K. TSUJIMOTO, "Impact of Impurity in Transmutation Cycle on Neutronics Design of Revised Accelerator-Driven System," *Ann. Nucl. Energy,* **111**, 449 (2018); https://doi.org/10.1016/j.anucene.2017.09.017.

[5] G. ALIBERTI et al., "Nuclear Data Sensitivity, Uncertainty and Target Accuracy Assessment for Future Nuclear Systems," *Ann. Nucl. Energy,* **33**, *8*, 700 (2006); https://doi.org/10.1016/j.anucene.2006.02.003.

[6] "International Handbook of Evaluated Criticality Safety Benchmark Experiments," NEA/NSC/DOC(95)03, T. IVANOVA et al., Eds., Organization for Economic Cooperation and Development, Nuclear Energy Agency (July 2019).

[7] "International Reactor Physics Experiment Evaluation (IRPhE) Project," Organisation for Economic Co-operation and Development, Nuclear Energy Agency, Nuclear Science Committee, https://www.oecd-nea.org/science/wprs/irphe/ (current as Jan. 27, 2023).

[8] C. H. PYEON, Ed., Accelerator-Driven System at Kyoto University Critical Assembly, Springer Singapore, Singapore (2021); https://doi.org/10.1007/978-981-16-0344-0.

[9] C. H. PYEON et al., “Void Reactivity in Lead and Bismuth Sample Reactivity Experiments at Kyoto University Critical Assembly,” *Nucl. Sci. Eng.,* published online on Mar. 13 (2023); https://doi.org/10.1080/00295639.2023.2172311.

[10] C. J. WERNER, J. S. BULL, C. J. SOLOMON, et al., “MCNP6.2 Release Notes,” LA-UR-18-20808, Los Alamos National Laboratory, New Mexico (2018).

[11] K. SHIBATA, O. IWAMOTO, T. NAKAGAWA, et al., “JENDL-4.0: A New Library for Nuclear Science and Engineering,” *J. Nucl. Sci. Technol*., 48, 1 (2011); https://doi.org/10.1080/18811248.2011.9711675

[12] K. YOKOYAMA et al., “Development of Comprehensive and Versatile Framework for Reactor Analysis, MARBLE,” *Ann. Nucl. Energy*, 66, 51 (2014); https://doi.org/10.1016/j.anucene.2013.11.047.

[13] K. YOKOYAMA et al., “Development of the Unified Cross section Set ADJ2017,” JAEA-Research 2018-011, Japan Atomic Energy Agency (Mar. 2019) (in Japanese); https://doi.org/10.11484/jaea-research-2018-011.

[14] J. A. FAVORITE et al., “Adjoint-Based Sensitivity and Uncertainty Analysis for Density and Composition: A User’s Guide,” *Nucl. Sci. Eng.,* 185 3, 384 (2017); https://doi.org/10.1080/00295639.2016.1272990.

[15] B. T. REARDEN and M. A. JESSEE, “SCALE Code System,” ORNL/TM-2005/39, Version 6.2.1, Oak Ridge National Laboratory (2016).

[16] R. E. MacFARLANE and D. W. MUIR, “NJOY99.0 Code System for Producing Pointwise and Multigroup Neutron and Photon Cross Sections from ENDF/B Data,” PSR-480/NJOY99.0, Los Alamos National Laboratory (2000).

[17] D. G. CACUCI and M. IONESCU-BUJOR, “Sensitivity and Uncertainty Analysis, Data Assimilation, and Predictive Best-Estimate Model Calibration,” in Handbook of Nuclear

Engineering, D. G. Cacuci, Ed., pp. 1913–2051, Springer US, Boston, MA (2010); https://doi.org/10.1007/978-0-387-98149-9_17.

[18] K. YOKOYAMA and T. KITADA, “Generalized Formulation of Extended Cross section Adjustment Method Based on Minimum Variance Unbiased Linear Estimation,” *J. Nucl. Sci. Technol.,* 56 1, 87 (2019); https://doi.org/10.1080/00223131.2018.1531078.

[19] K. SUGINO et al., “Preparation of Fast Reactor Group Constant Sets UFLIB.J40 and JFS-3-J4.0 Based on the JENDL-4.0 Data,” JAEA-Data/Code 2011-017, Japan Atomic Energy Agency (Jan. 2012) (in Japanese); https://doi.org/10.11484/jaea-data-code-2011-017.

[20] O. IWAMOTO et al., “Japanese Evaluated Nuclear Data Library Version 5: JENDL-5,” *J. Nucl. Sci. Technol.*, 60 1, 1 (2023); https://doi.org/10.1080/00223131.2022.2141903.

[21] M. FUKUSHIMA et al., “Systematic Measurements and Analyses for Lead Void Reactivity Worth in a Plutonium Core and Two Uranium Cores with Different Enrichment,” *Nucl. Sci. Eng.,* 194, 2, 138 (2020); https://doi.org/10.1080/00295639.2019.1663089.

5. Conclusion

5.1 Summary

The evaluation of the sensitivity coefficients to the nuclear data is crucial to quantify and reduce the nuclear-data-induced uncertainty and to establish the credibility of the core analyses. The sensitivity coefficients benefit performing UQ and DA when analysts prefer to update the covariance data and/or make comparisons between different nuclear data libraries without detailed knowledge and reevaluations of benchmarks. Due to the difficulty in its formulations and complicated treatment, the adjoint-based method requires expensive costs and/or is impractical to implement. Furthermore, the adjoint-based method suffers from a large number of outputs, such as time-dependent spatial distribution in burnup calculations. Therefore, there is a strong motivation to develop innovative SA methods that use no adjoint calculations.

To address this challenge, this thesis focuses on the advantages of forward calculations. The main objective of this thesis is to develop an efficient method for the SA using only forward calculations and to demonstrate UQ and DA using the sensitivity coefficients obtained along with the work in this thesis. For this purpose, two methods using the random sampling have been newly proposed: the adaptive smooth lasso and the ROM-Lasso method. In addition, DA using the sensitivity coefficients obtained in this thesis is performed with the primary aim of examining the uncertainty reduction of the void reactivity of the LBE coolant in the ADS as an example of DA for a future system using the sensitivity coefficients.

The adaptive smooth lasso is a lasso-type linear regression whose penalty term is designed to capture the features of the sensitivity coefficients to the nuclear data. In Chapter 2, through the estimation of the sensitivity coefficients of k_{eff} of the ADS at the BOC, it is demonstrated that the number of samples required in the proposed method can be reduced compared to the conventional regression methods and can achieve one-tenth of the calculation

cost of the direct method (i.e., about 1000 calculations for about 10000 cross sections).

However, the adaptive smooth lasso still requires a large number of forward calculations. Then, the ROM-Lasso method has been newly proposed in Chapter 3. The ROM-Lasso method expands the sensitivity coefficients by the AS bases to reduce the effective dimensionality of the nuclear data and estimates the expansion coefficients using the conventional lasso regression. Based on the idea of the M_LROM, the approximated AS is constructed using the sensitivity matrix obtained in the lower-fidelity model whose calculation cost is much smaller than that of the higher-fidelity model for which SA is performed. Through the one-cycle AS core analysis, it is demonstrated that the number of forward calculations in the higher-fidelity model can be dramatically reduced by a couple of orders of magnitude of the direct method (i.e., from about 1000 to 30 in the verification in this thesis) for several neutronics parameters.

In Chapter 4, the DA aiming at the reduction of the nuclear-data-induced uncertainty of the design property of the ADS is investigated as a practice of the application of the SA. In this study, the lead-bismuth sample reactivity measurements conducted at the KUCA are employed with the primary aim of examining the uncertainty reduction of the void reactivity of the coolant in the ADS. Through the analysis, the uncertainty is successfully reduced to 3.6%, achieving the provisional target accuracy (i.e., 5%) in this thesis. In conclusion, the applicability of the forward-based SA, UQ, and DA analysis to the ADS using the sensitivity coefficients and the experimental data has been successfully demonstrated.

As summarized in this chapter, the present study has established the methodology of SA without the adjoint calculations (i.e., ROM-Lasso) that can resolve the primary issue of SA and promote the application of SA to the various types of neutronics parameters. Furthermore, the present study has demonstrated the forward-based UQ and DA making use of the sensitivity coefficients for a design property of an innovative system. Therefore, it can be concluded that the

main objectives of this thesis have been accomplished.

5.2. Recommendations for future works

Although this thesis established new efficient methods using only the forward calculations for SA and demonstrated the DA reducing the nuclear data-induced uncertainty of a design property, several technical issues are still open. The recommended future tasks would be summarized as follows:

(1) Efficient construction of the AS bases (related to Chapter 3)

As demonstrated in Chapter 3, by expanding the sensitivity coefficients with the AS bases, the number of forward calculations in the higher-fidelity model is dramatically reduced by a couple of orders of magnitude compared to the direct method. However, in this thesis, the AS bases are constructed uszxting the sensitivity matrix of the lower-fidelity model obtained by the direct method. The duration of a single forward calculation of the lower-fidelity model (i.e., the 2-D cylindrical model) is about one-tenth of that of the higher-fidelity model (i.e., the 3-D Cartesian model) in this thesis, which impedes the reduction of the total calculation cost including the construction of the AS bases. The reduction of the calculation cost to construct the AS bases and the choice of a lower-fidelity model should be tacked in the future to enhance the applicability of the ROM-Lasso method. A possible remedy to address this challenge could be the employment of a model with coarser mesh and/or looser convergence tolerances.

(2) Finding an optimal lower-fidelity model for ROM-Lasso (related to Chapter 3)

In this thesis, the feasibility of the ROM-Lasso method for the highly symmetrical system is demonstrated where the 2-D cylindrical model may adequately reproduce the 3-D

Cartesian model. However, more general systems do not necessarily have geometric symmetry, and it is not obvious how to construct the lower-fidelity model. Therefore, the choice of an appropriate lower-fidelity model should be addressed in the future.

A possible option to tackle this issue is the following. If a neutronics parameter of the lower-fidelity model had a particularly strong correlation factor with a neutronics parameter of the higher-fidelity model for which one evaluates the sensitivity coefficients, such a parameter of the lower-fidelity model would have the sensitivity vector that is proportional to that of the neutronics parameter the higher-fidelity model. In such a case, using the sensitivity vector of the lower-fidelity model as an AS basis, only one dimension and one sample would be enough to completely reproduce the sensitivity vector of the higher-fidelity model. Thus, this issue could be resolved by finding neutronics parameters of the lower-fidelity model that are strongly correlated with the neutronics parameter of the higher-fidelity model during the random sampling process and then using them for AS construction.

(3) Estimation of error bounds of the orthogonal components to AS (related to Chapter 3)

In this thesis, the reproducibility of the sensitivity coefficients by the ROM-Lasso was confirmed by directly comparing the estimated values and the reference values obtained by the direct method. However, in more general cases, it is important to estimate the error bounds by the orthogonal components to the AS without the direct method to check whether the sensitivity vector of the higher-fidelity model is well included in a subspace spanned by the sensitivity vectors of the lower-fidelity model. Estimation of such an error bound is a challenging future topic.

(4) Application of continuous energy Monte Carlo method (related to Chapter 3)

In the verification of Chapter 3, transport calculations on both the lower- and higher-fidelity models were based on the deterministic method. For more accurate SA, application of the continuous energy Monte Carlo calculations would be a future topic of interest. In terms of improvement of the relative calculation cost of the AS construction, it should be addressed in the future.

(5) DA analysis for various neutronics parameters of ADS (related to Chapter 4)

In Chapter 4, the DA analysis was done only for the coolant void reactivity of the ADS at the BOC, which is relatively easy to calculate using PT, though SA for several neutronics parameters after burnup was performed in Chapter 3. To demonstrate the more practical applicability of the forward-based methodology established in this thesis, the DA analyses for the other properties should be performed in the future.

(6) Expansion of the integral experimental data (related to Chapter 4)

Although the ultimate goal of the DA analysis is to improve the accuracy of the core analysis for designed systems, Chapter 4 only aimed at the reduction of the nuclear-data-induced uncertainty, and it is not yet confirmed whether the adjustment of the nuclear data can improve the predictions made for the ADS. The possible remedy is to expand the integral experimental data so that the design region is confidently covered. To validate the DA analysis in this thesis for the application to the ADS, the evaluation of the integral experimental data related to Pb and Bi cross sections should be addressed in the future.

(7) Completeness of the covariance data (related to Chapter 4)

To quantify the uncertainty propagation from the nuclear data to the core analysis, the

covariance data of the nuclear data must be given. In this thesis, the DA analysis with the sample reactivities obtained at the KUCA was performed to reduce the uncertainty of the coolant void reactivity of the ADS derived from the lead and bismuth inelastic scattering cross sections. However, as pointed out in Chapter 4, the covariance data of ^{27}Al is not given in JENDL-4.0 and JENDL-5 though the inelastic scattering cross section of ^{27}Al potentially has as significant impact on the measurement results as the lead and bismuth. The DA analysis performed in this thesis is an ideal case in which zero covariance data is assumed for ^{27}Al. Then, the evaluation and verification of ^{27}Al covariance data in the future would help evaluate the more practical effectiveness of the KUCA experimental data.

(8) SA to the infinite diluted cross sections (related to Chapters 2 and 3)

In Chapters 2 and 3, the evaluated sensitivity coefficients were those to the effective self-shielded microscopic cross sections. As briefly mentioned in Section 3.3.2, the impact of the self-shielding effect will not be significant on UQ for fast systems. However, for systems and neutronics parameters where giant resonances play an important role (e.g., thermal reactors), appropriate corrections are necessary to evaluate sensitivity coefficients for infinite dilution cross sections. The use of correction methods would be a future topic.

(9) Range of the perturbation (related to Chapters 2 and 3)

Both proposed methods consider only the first-order Taylor expansion to formulate the SA as linear equations that can be easily handled. However, it is well known that the excessive range of the perturbation degrades the accuracy of the sensitivity coefficients due to the higher order effect while the insufficient range causes the numerical round-off errors, indicating the existence of the optimal range of the perturbation that minimizes the sum of these errors. Then,

finding such an optimal range could be a future work. This would be a more crucial problem when the proposed methods are applied to Monte Carlo codes because the small range of the perturbation will suffer from the statistical errors (i.e., too small perturbations are indistinguishable from statistical errors).

In Chapters 2 and 3, ±5% range of the uniform sampling was applied to all nuclear data. In such a case, most of the deviation of a neutronics parameter is contributed from the perturbations of nuclear data with large sensitivity coefficients, and nuclear data with small sensitivity coefficients would not be considered properly in the regression, leading to the degradation of reproducibility of the small sensitivity coefficients. This would be a problem for UQ and DA when there were nuclear data with small sensitivity coefficients but quite large uncertainties. From this viewpoint in addition to the above-mentioned point, the range of the perturbation should be tackled in the future.

Acknowledgment

My thanks go first of all to my supervisor Associate Professor Tomohiro Endo of Nagoya University whose insightful and kind guidance has been essential to organizing this thesis. Under the difficult situation due to the COVID-19 pandemic, he continued to devote much of his time to the management of this PhD work.

I am deeply indebted to Professor Akio Yamamoto of Nagoya University for his invaluable advice and support.

Chapter 4 of this thesis benefited greatly from the experiments conducted at the KUCA under the direction of Associate Professor Cheol Ho Pyeon of Kyoto University. I would like to express my deep gratitude for his generous cooperation and advice.

I would like to be grateful to all the staff at the KUCA for their assistance during the experiments.

I am thankful to Professor Sachiko Yoshihashi, Associate Professor Atsushi Okamoto, and Associate Professor Hideki Tomita of Nagoya University and Professor Go Chiba of Hokkaido University for reviewing and commenting on this thesis.

I also would like to express my appreciation to the Japan Atomic Energy Agency (JAEA) and the staff in the Research Group for Nuclear Transmutation System of JAEA for their support in the doctoral course at Nagoya University.

Finally, I would like to give special thanks to my wife and my son for understanding me to be a Ph.D. student at Nagoya University and keeping a place to go back.

Appendix

A. Sensitivity profile of ADS

Figure A.1 (1/4). Sensitivity coefficients of beam current at EOC estimated by the ROM-Lasso method.

(Top 20 largest absolute value)

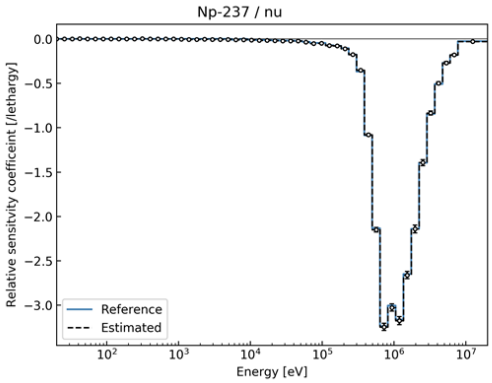

(**^{237}Np, $\bar{\nu}$**)

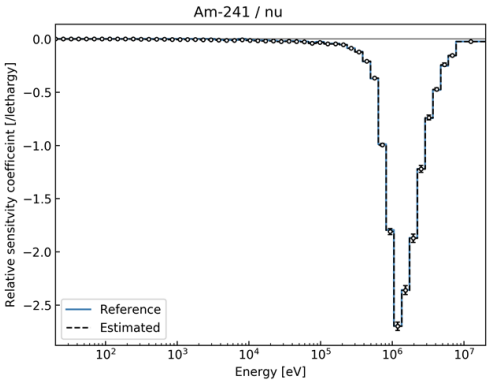

(**^{241}Am, $\bar{\nu}$**)

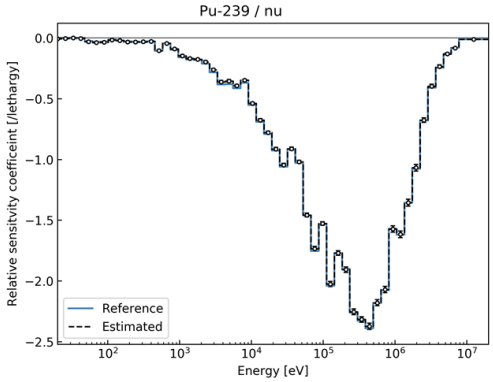

(**^{239}Pu, $\bar{\nu}$**)

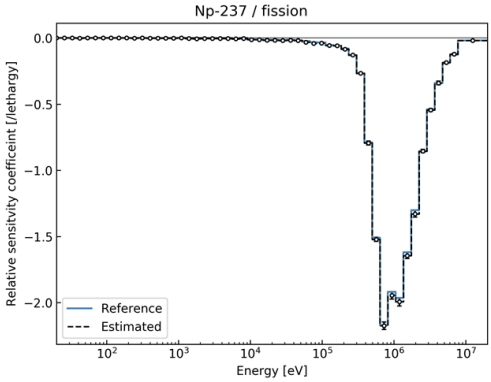

(**^{237}Np, fission**)

Figure A.1 (2/4). Sensitivity coefficients of beam current at EOC estimated by the ROM-Lasso method.

(Top 20 largest absolute value)

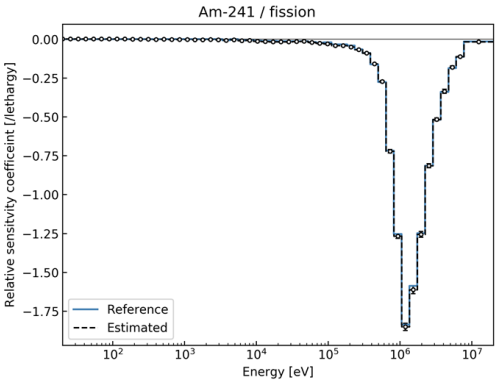

(**^{241}Am, fission**)

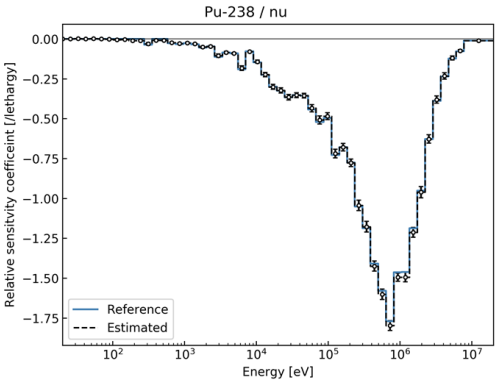

(**^{238}Pu, $\bar{\nu}$**)

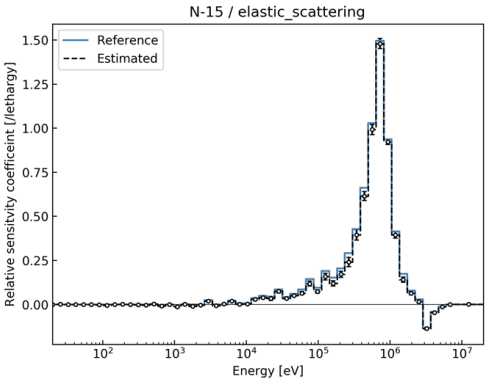

(**^{15}N, elastic scattering**)

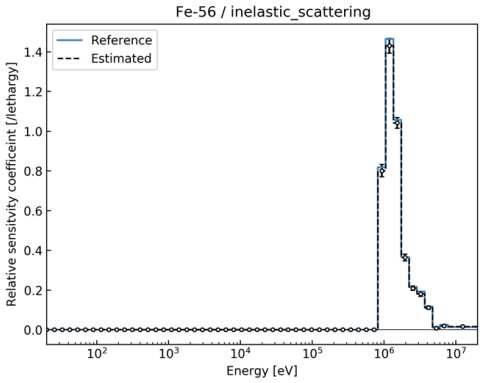

(**^{56}Fe, inelastic scattering**)

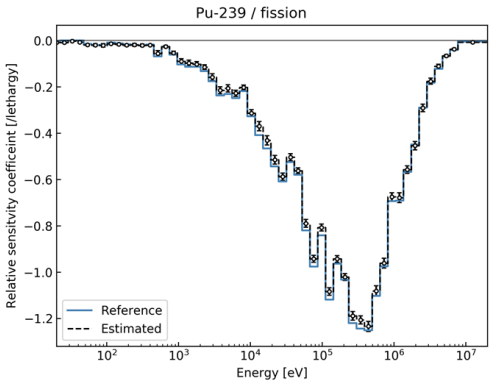

(**^{239}Pu, fission**)

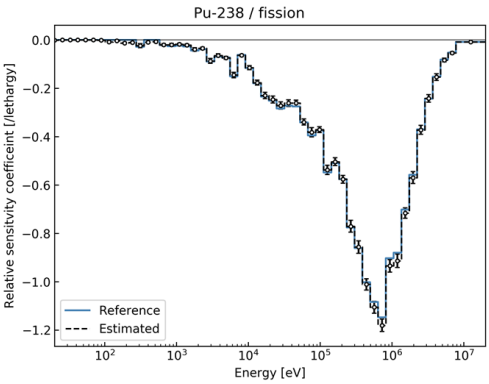

(**^{238}Pu, fission**)

Figure A.1 (3/4). Sensitivity coefficients of beam current at EOC estimated by the ROM-Lasso method.

(Top 20 largest absolute value)

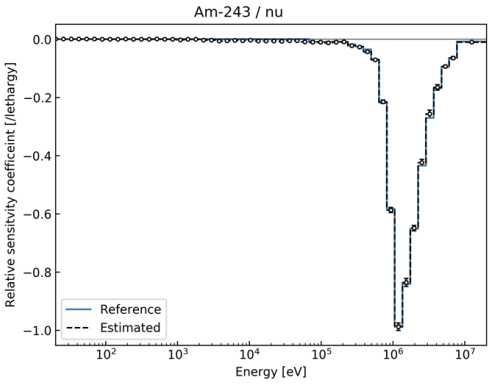

(^{243}Am, $\bar{\nu}$)

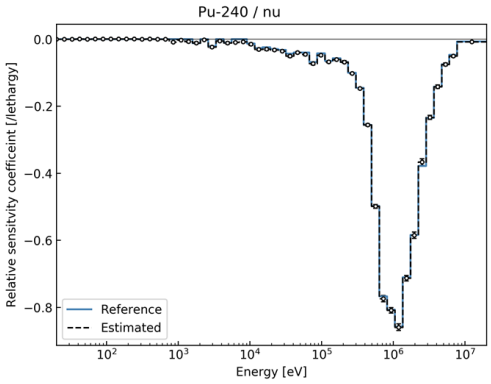

(^{240}Pu, $\bar{\nu}$)

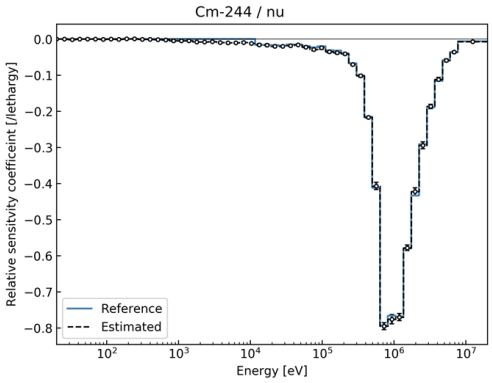

(^{244}Cm, $\bar{\nu}$)

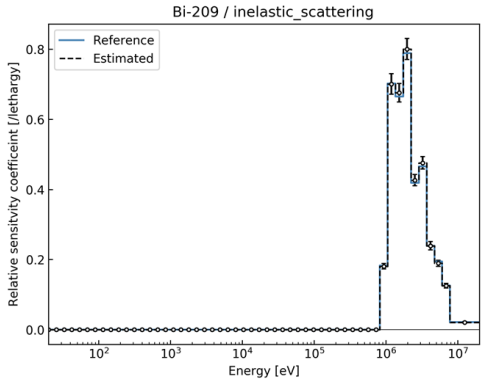

(^{209}Bi, inelastic scattering)

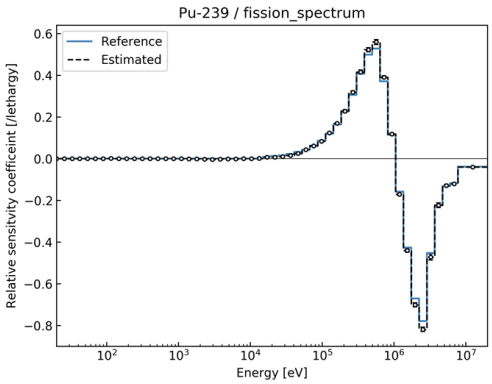

(^{239}Pu, fission spectrum)

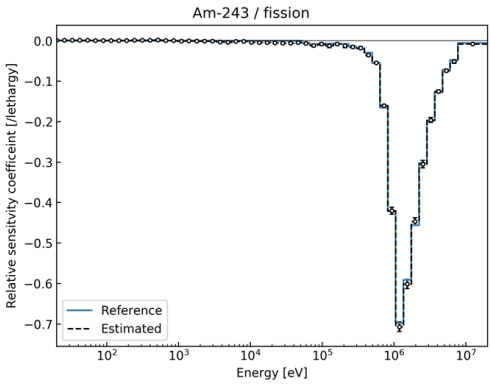

(^{243}Am, fission)

Figure A.1 (4/4). Sensitivity coefficients of beam current at EOC estimated by the ROM-Lasso method.

(Top 20 largest absolute value)

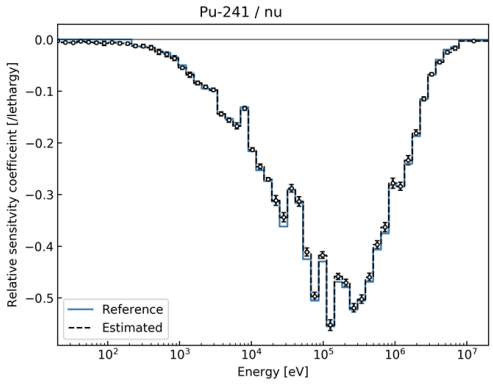

(**^{241}Pu, $\bar{\nu}$**)

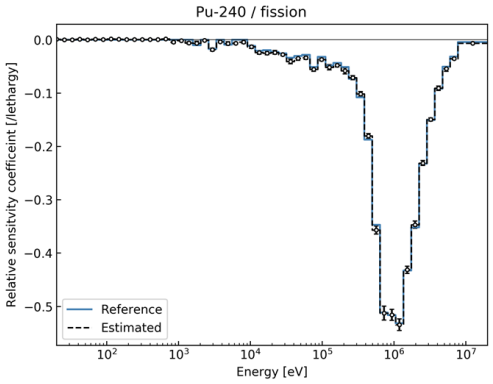

(**^{240}Pu, fission**)

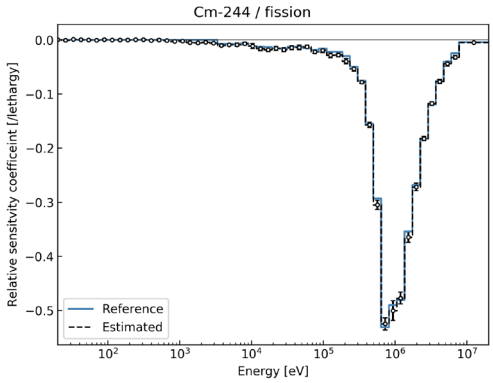

(**^{244}Cm, fission**)

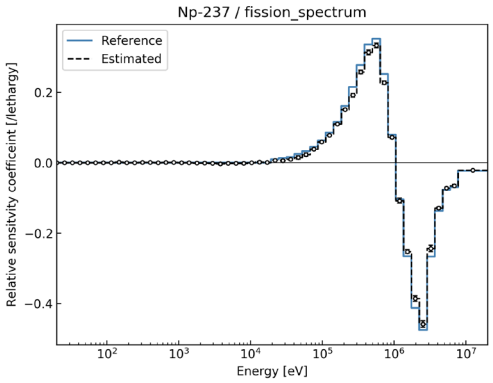

(**^{237}Np, fission spectrum**)

Figure A.2 (1/4). Sensitivity coefficients of beam current at EOC estimated by the lasso method with 30 and 300 samples.

(Top 20 largest absolute value)

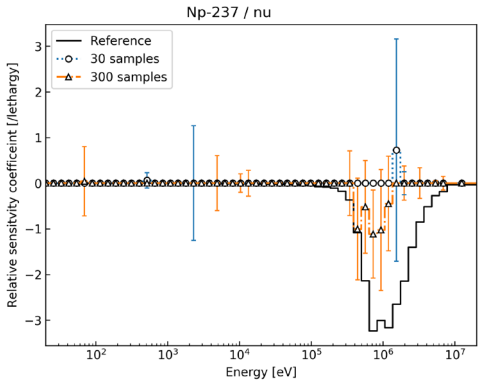

(^{237}Np, $\bar{\nu}$)

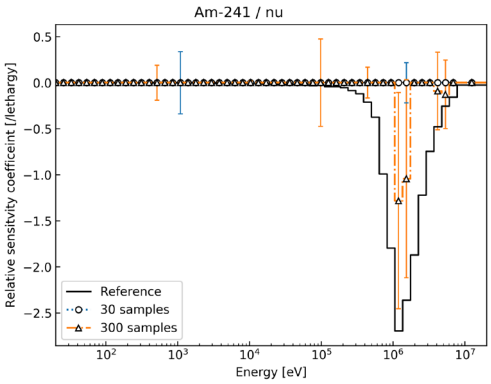

(^{241}Am, $\bar{\nu}$)

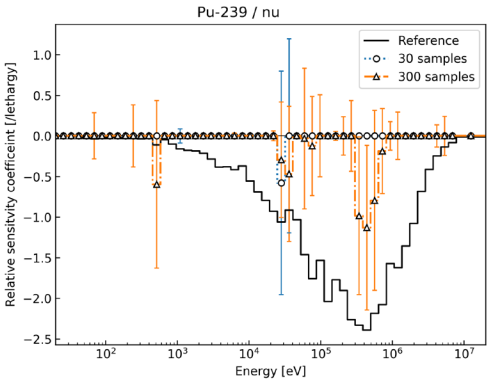

(^{239}Pu, $\bar{\nu}$)

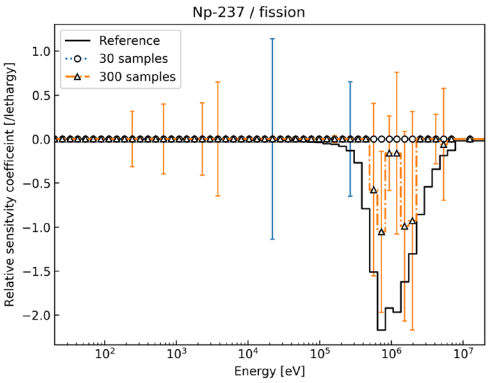

(^{237}Np, fission)

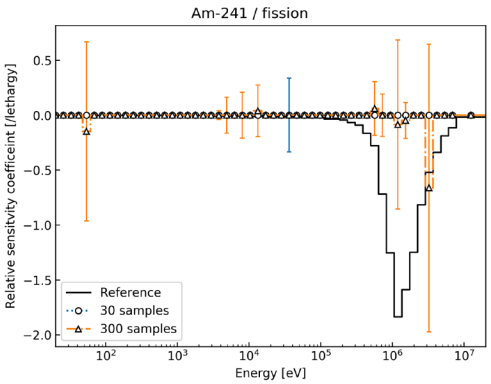

(^{241}Am, fission)

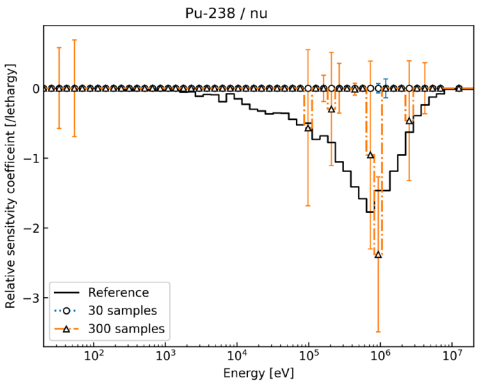

(^{238}Pu, $\bar{\nu}$)

Figure A.2 (2/4). Sensitivity coefficients of beam current at EOC estimated by the lasso method with 30 and 300 samples.

(Top 20 largest absolute value)

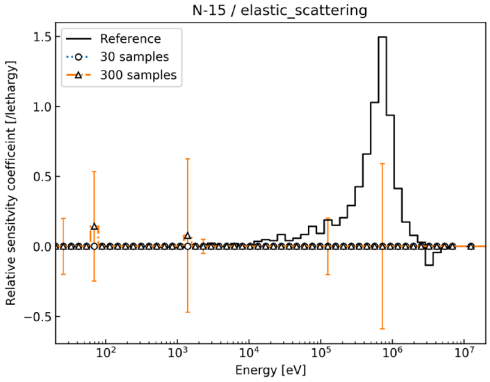

(**^{15}N, elastic scattering**)

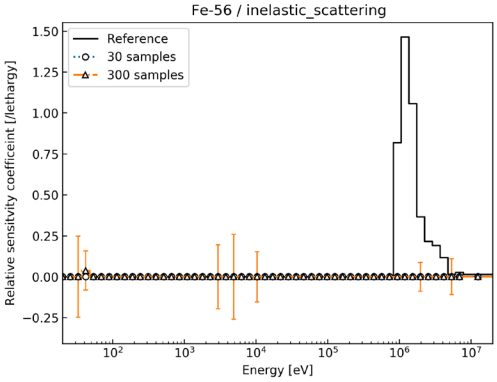

(**^{56}Fe, inelastic scattering**)

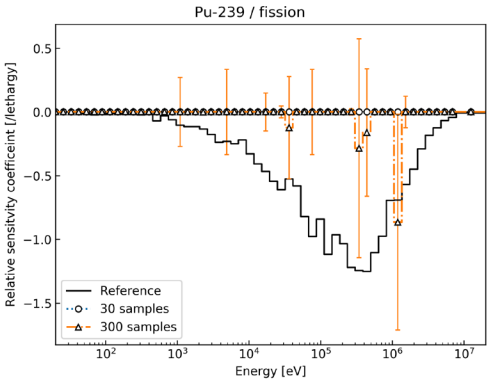

(**^{239}Pu, fission**)

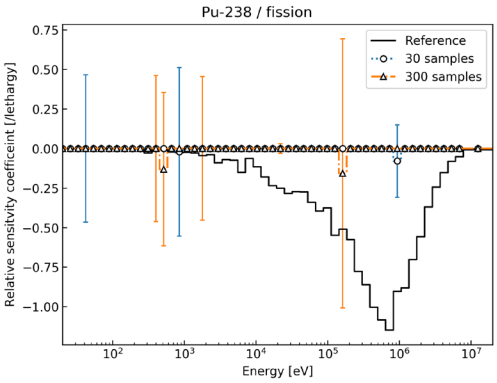

(**^{238}Pu, fission**)

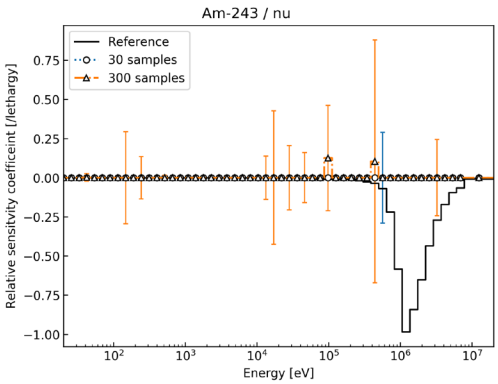

(**^{243}Am, $\bar{\nu}$**)

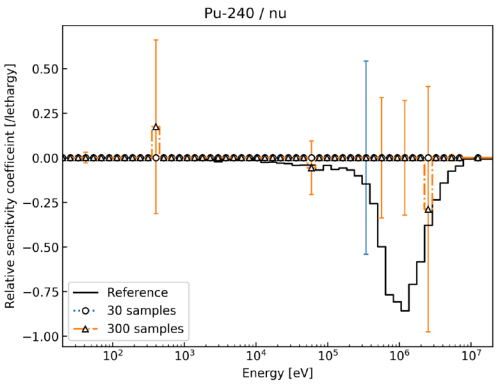

(**^{240}Pu, $\bar{\nu}$**)

Figure A.2 (3/4). Sensitivity coefficients of beam current at EOC estimated by the lasso method with 30 and 300 samples.

(Top 20 largest absolute value)

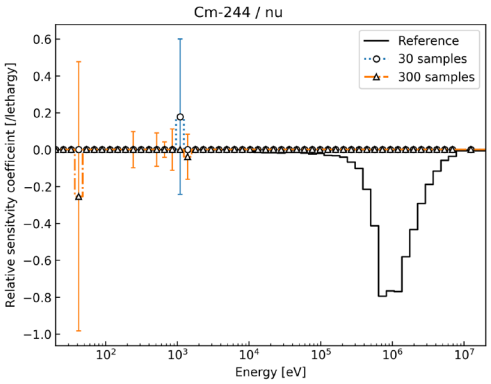

(^{244}Cm, $\bar{\nu}$)

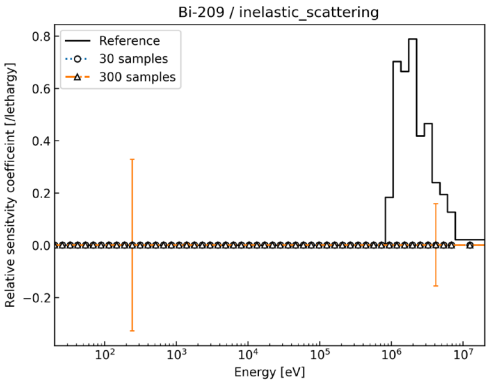

(^{209}Bi, inelastic scattering)

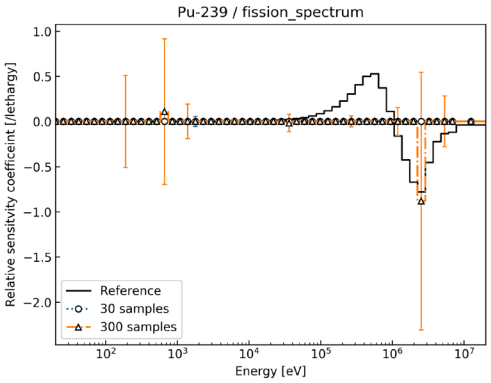

(^{239}Pu, fission spectrum)

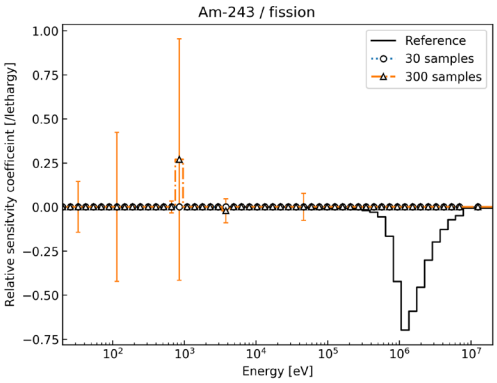

(^{243}Am, fission)

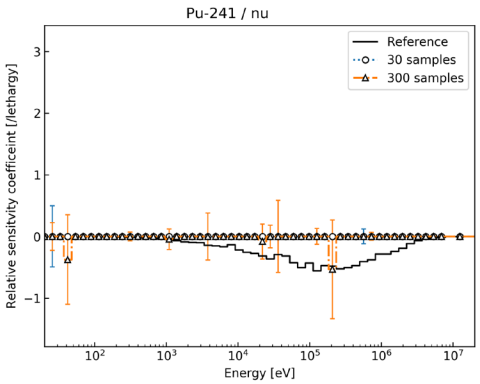

(^{241}Pu, $\bar{\nu}$)

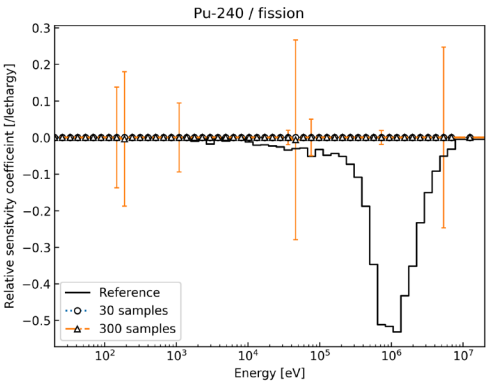

(^{240}Pu, fission)

Figure A.2 (4/4). Sensitivity coefficients of beam current at EOC estimated by the lasso method with 30 and 300 samples.

(Top 20 largest absolute value)

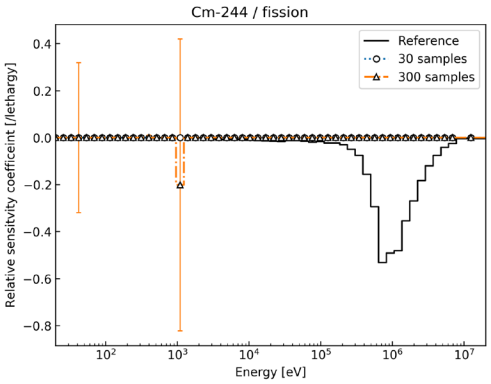

(^{244}Cm, fission)

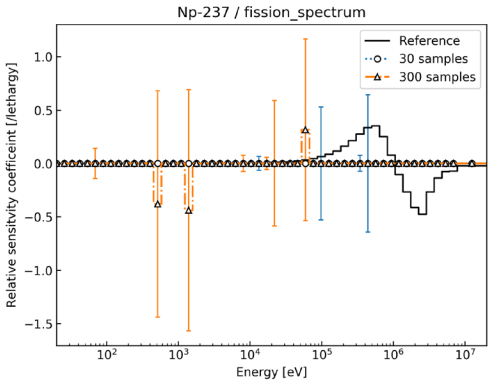

(^{237}Np, fission spectrum)

Figure A.3 (1/4). Sensitivity coefficients of beam current at EOC estimated by the adaptive smooth lasso method with 30 and 300 samples.

(Top 20 largest absolute value)

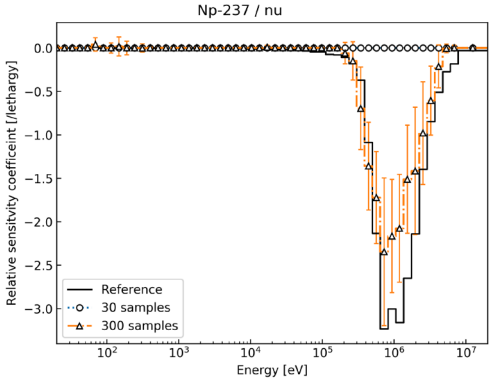

(**^{237}Np, $\bar{\nu}$**)

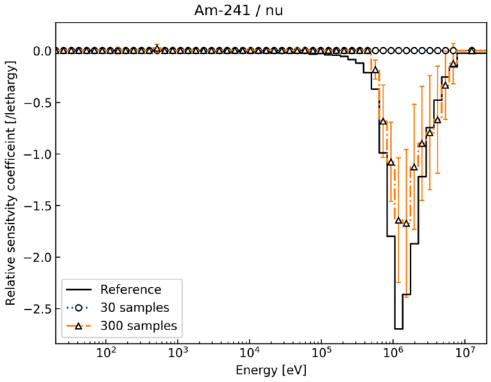

(**^{241}Am, $\bar{\nu}$**)

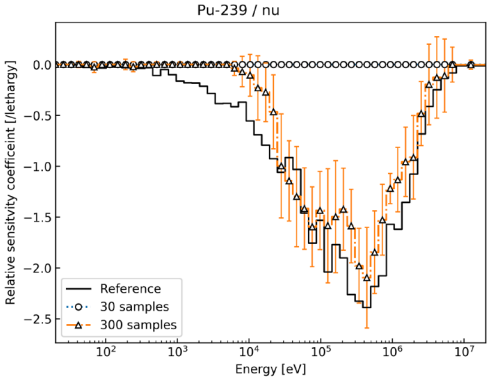

(**^{239}Pu, $\bar{\nu}$**)

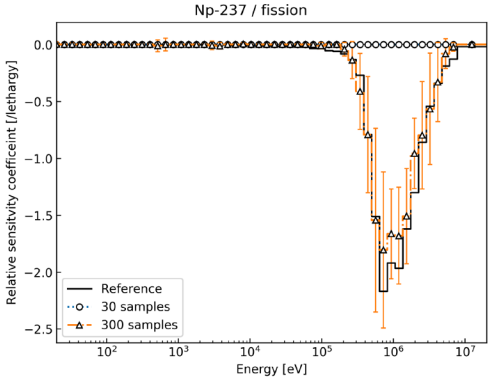

(**^{237}Np, fission**)

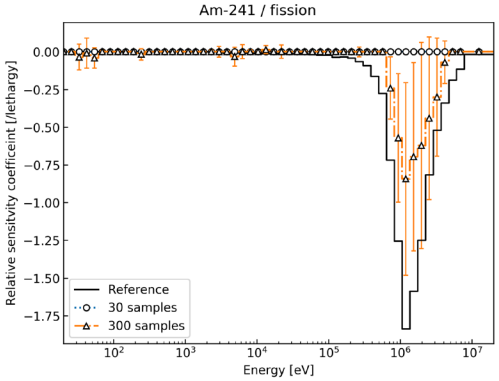

(**^{241}Am, fission**)

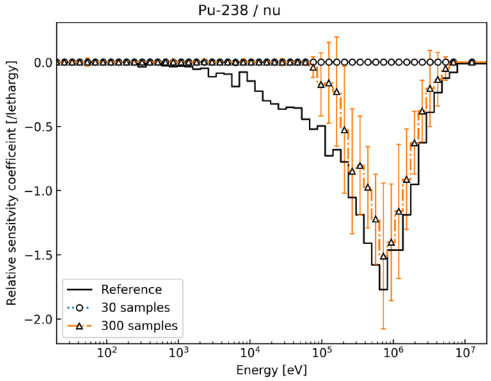

(**^{238}Pu, $\bar{\nu}$**)

Figure A.3 (2/4). Sensitivity coefficients of beam current at EOC estimated by the adaptive smooth lasso method with 30 and 300 samples.

(Top 20 largest absolute value)

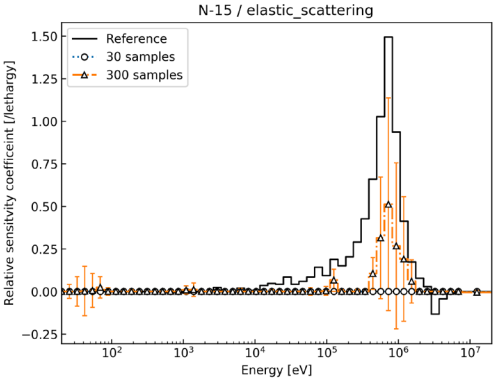

(**^{15}N, elastic scattering**)

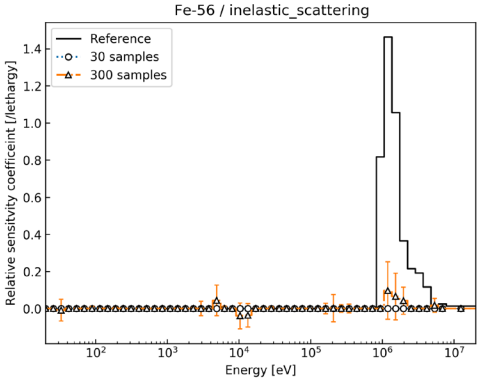

(**^{56}Fe, inelastic scattering**)

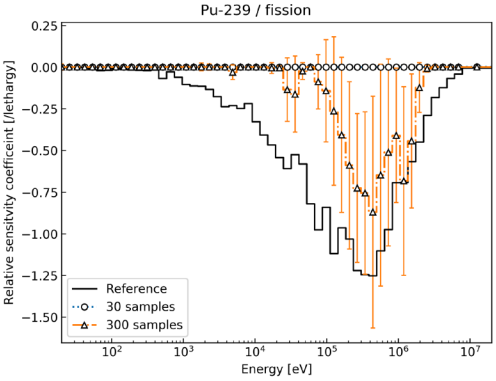

(**^{239}Pu, fission**)

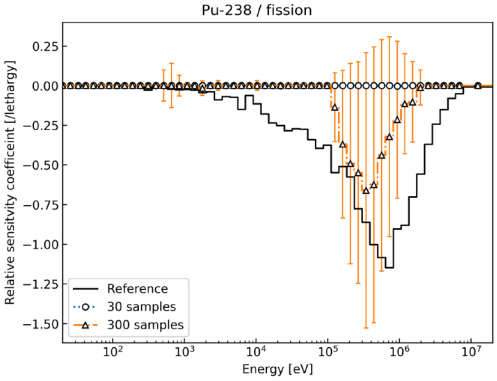

(**^{238}Pu, fission**)

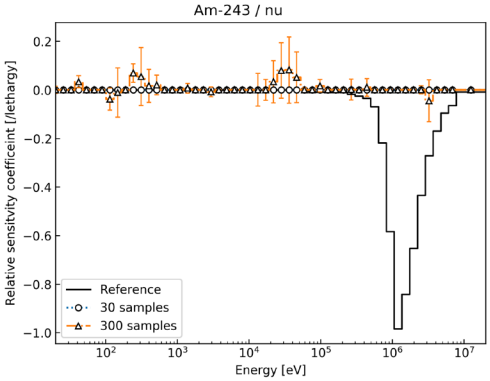

(**^{243}Am, $\bar{\nu}$**)

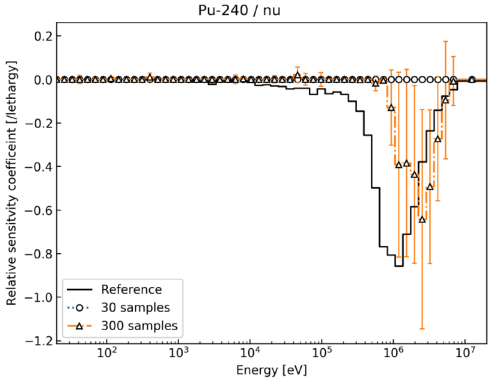

(**^{240}Pu, $\bar{\nu}$**)

Figure A.3 (3/4). Sensitivity coefficients of beam current at EOC estimated by the adaptive smooth lasso method with 30 and 300 samples.

(Top 20 largest absolute value)

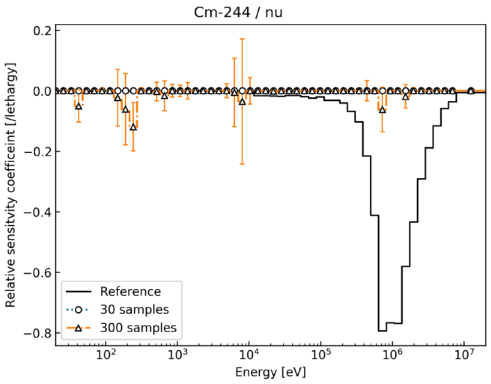

(**^{244}Cm, $\bar{\nu}$**)

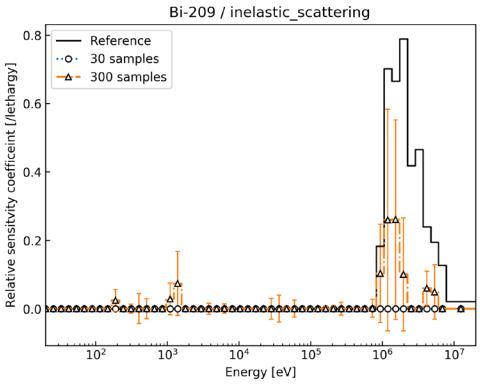

(**^{209}Bi, inelastic scattering**)

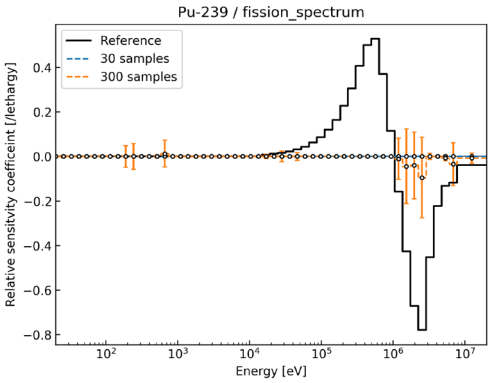

(**^{239}Pu, fission spectrum**)

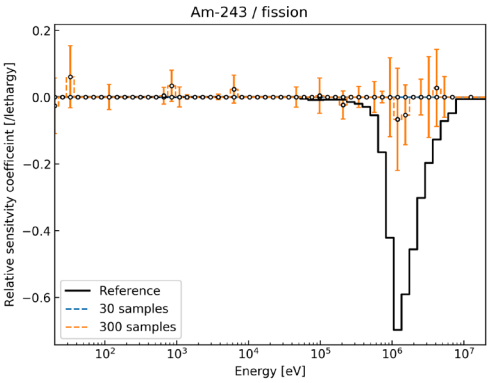

(**^{243}Am, fission**)

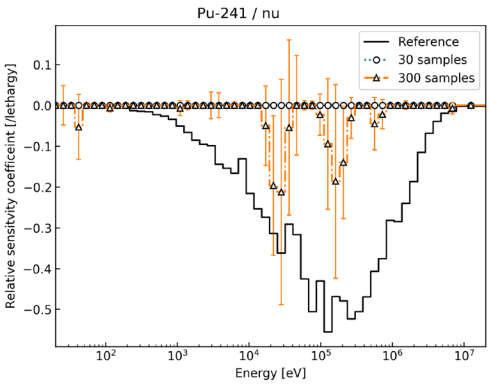

(**^{241}Pu, $\bar{\nu}$**)

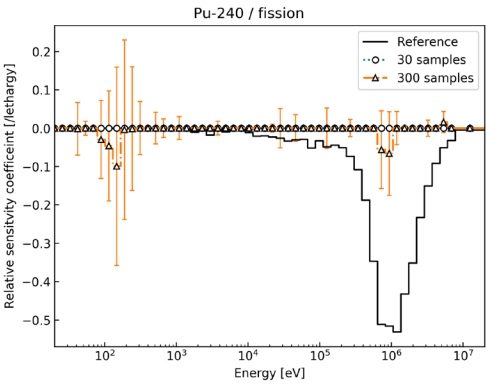

(**^{240}Pu, fission**))

Figure A.3 (4/4). Sensitivity coefficients of beam current at EOC estimated by the adaptive smooth lasso method with 30 and 300 samples.

(Top 20 largest absolute value)

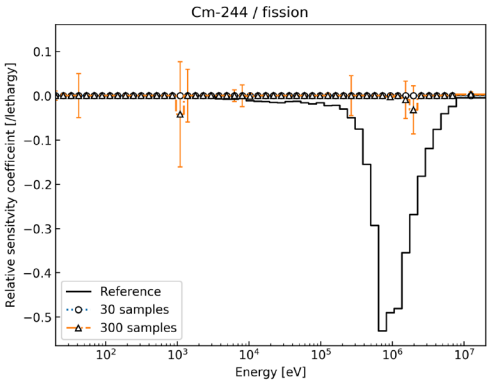

(^{244}Cm, fission)

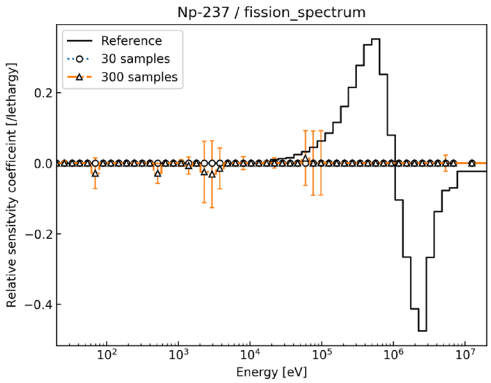

(^{237}Np, fission spectrum)

Figure A.4 (1/4). Sensitivity coefficients of mass of ^{241}Am at EOC estimated by the ROM-Lasso method.

(Top 20 largest absolute value)

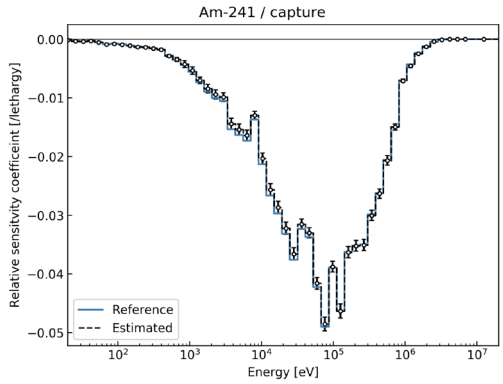

(^{241}Am, capture)

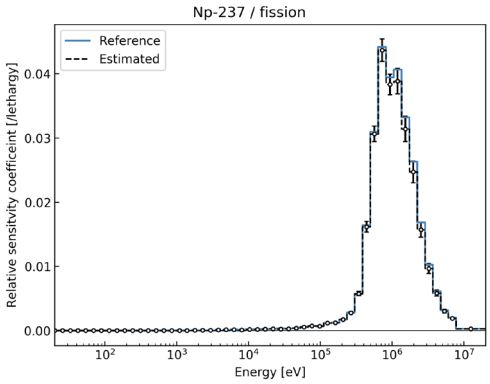

(^{237}Np, fission)

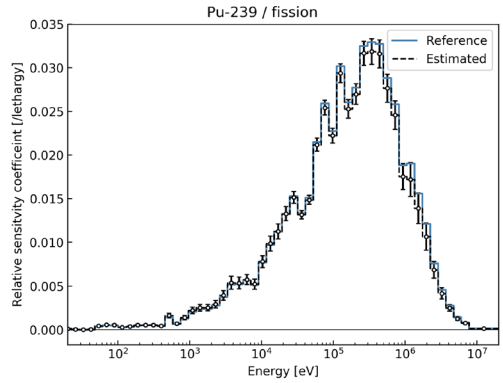

(^{239}Pu, fission)

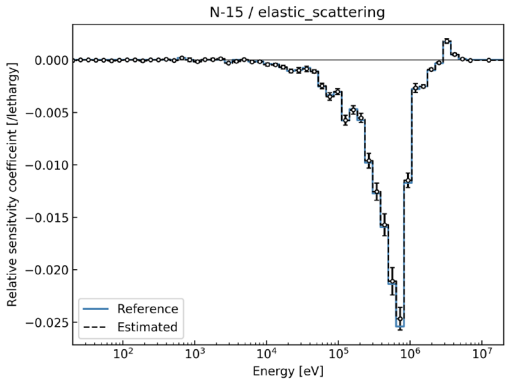

(^{15}N, elastic scattering)

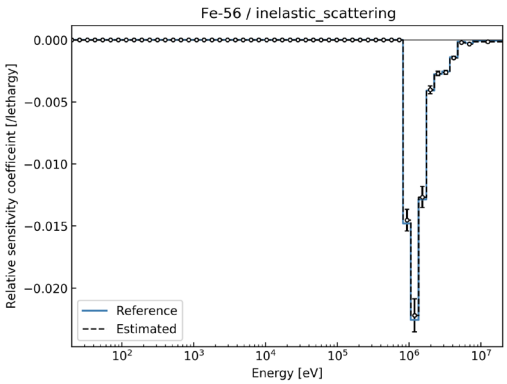

(^{56}Fe, inelastic scattering)

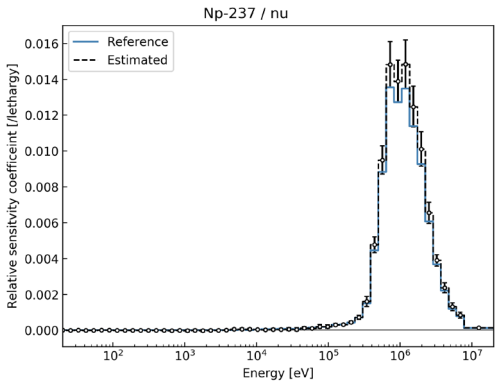

(^{237}Np, $\bar{\nu}$)

Figure A.4 (2/4). Sensitivity coefficients of mass of ^{241}Am at EOC estimated by the ROM-Lasso method.

(Top 20 largest absolute value)

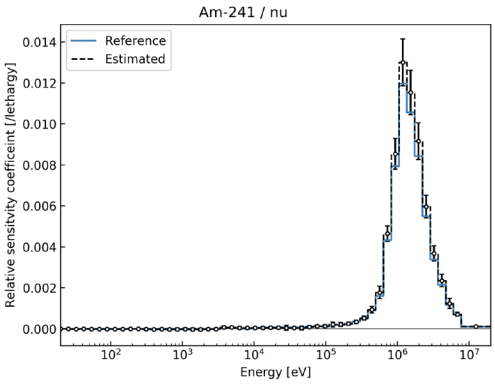

(^{241}Am, $\bar{\nu}$)

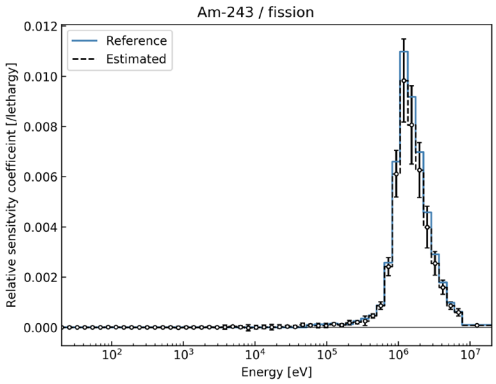

(^{243}Am, fission)

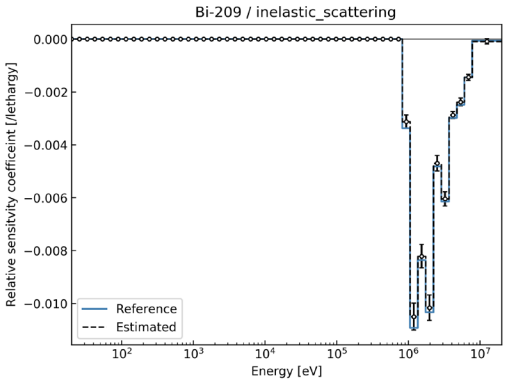

(^{209}Bi, inelastic scattering)

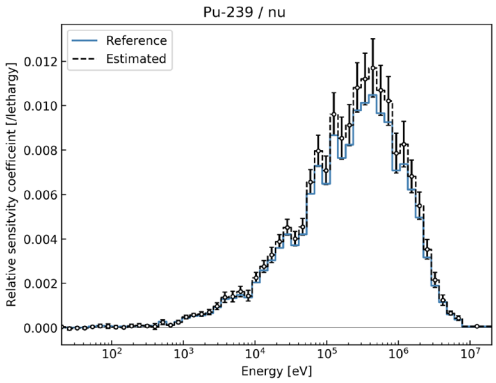

(^{239}Pu, $\bar{\nu}$)

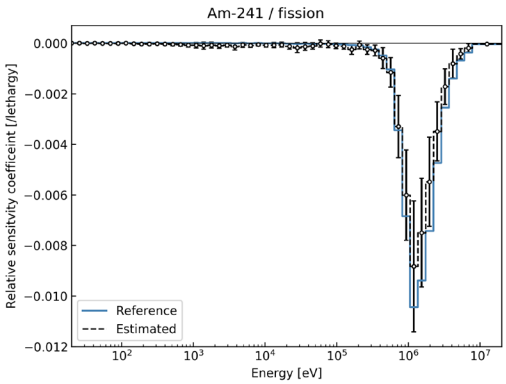

(^{241}Am, fission)

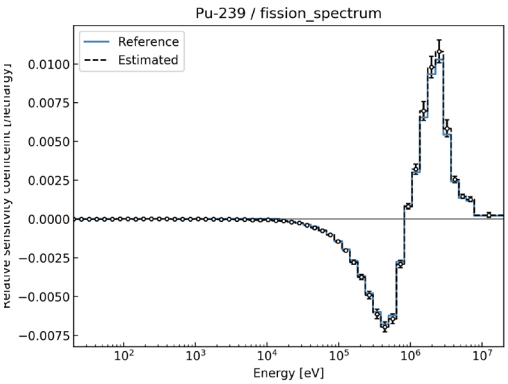

(^{239}Pu, fission spectrum)

Figure A.4 (3/4). Sensitivity coefficients of mass of ^{241}Am at EOC estimated by the ROM-Lasso method.

(Top 20 largest absolute value)

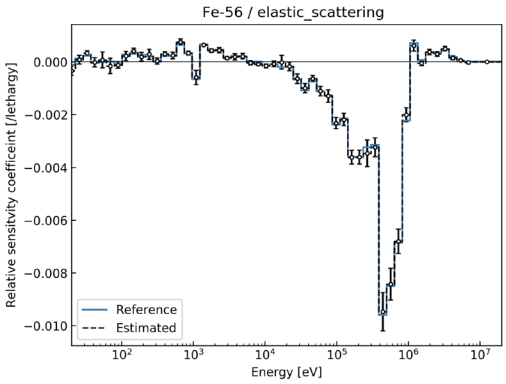

(^{56}Fe, elastic scattering)

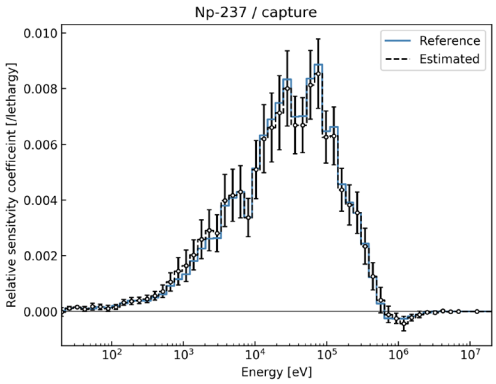

(^{237}Np, capture)

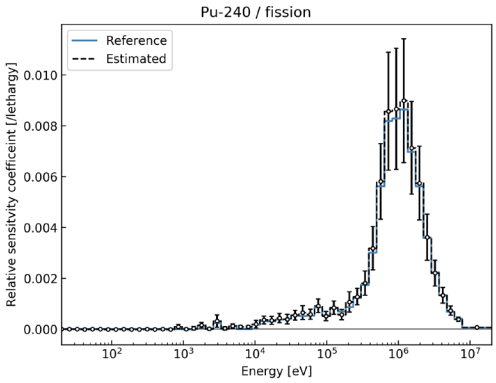

(^{240}Pu, fission)

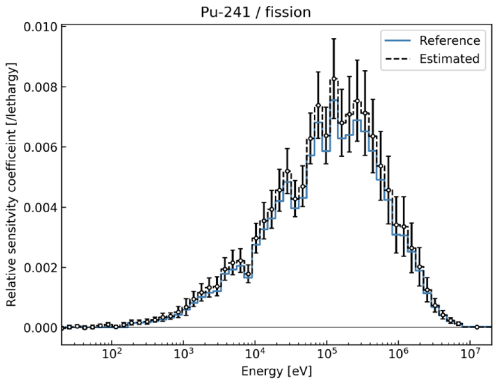

(^{241}Pu, fission)

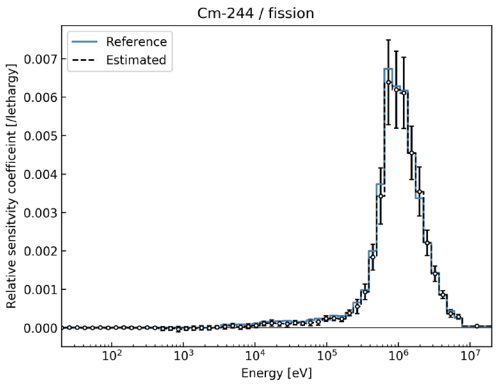

(^{244}Cm, fission)

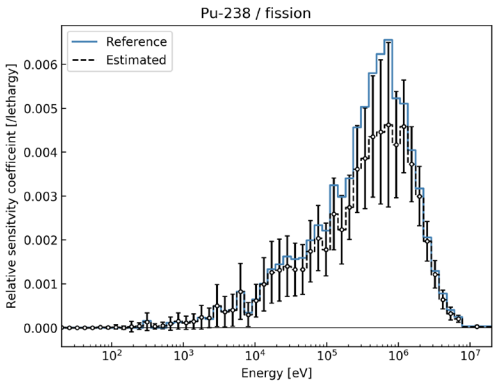

(^{238}Pu, fission)

Figure A.4 (4/4). Sensitivity coefficients of mass of ^{241}Am at EOC estimated by the ROM-Lasso method.

(Top 20 largest absolute value)

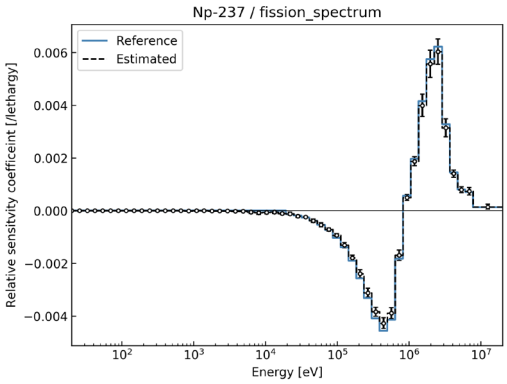

(^{237}Np, fission spectrum)

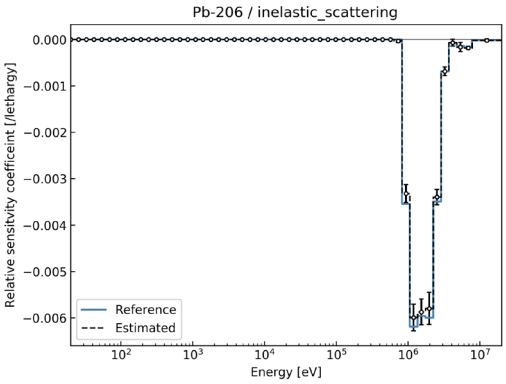

(^{206}Pb, inelastic scattering)

Figure A.5 (1/4). Sensitivity coefficients of mass of La element at EOC estimated by the ROM-Lasso method.

(Top 20 largest absolute value)

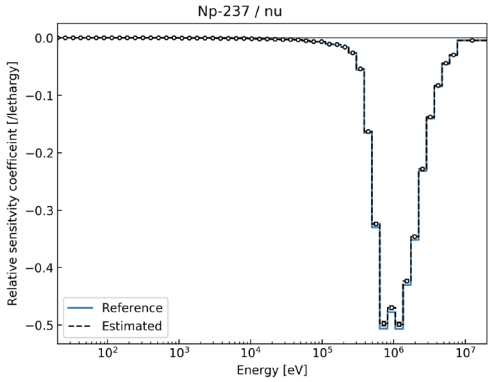

(^{237}Np, $\bar{\nu}$)

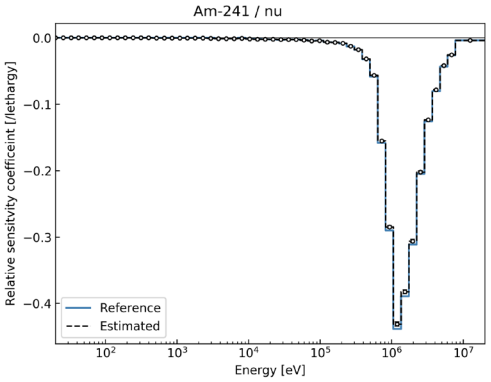

(^{241}Am, $\bar{\nu}$)

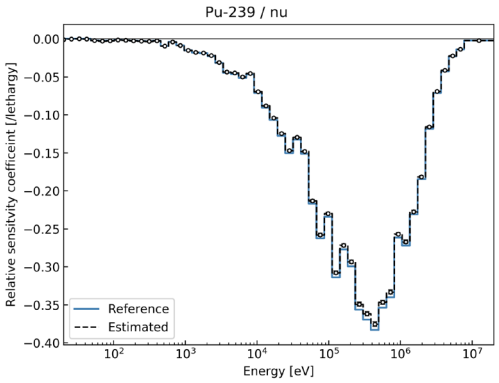

(^{239}Pu, $\bar{\nu}$)

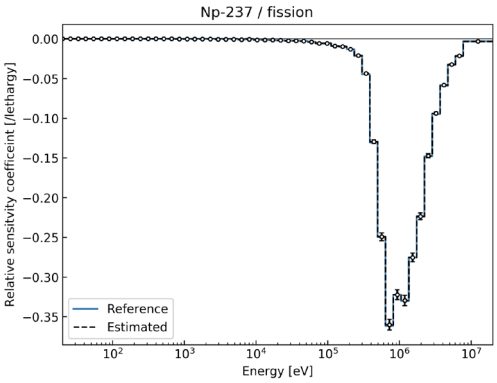

(^{237}Np, fission)

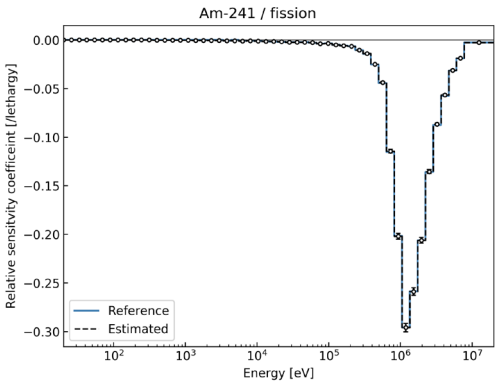

(^{241}Am, fission)

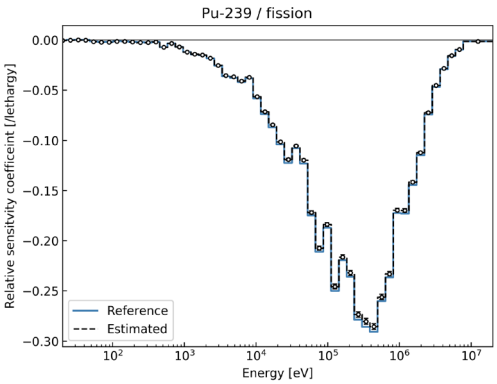

(^{239}Pu, fission)

Figure A.5 (2/4). Sensitivity coefficients of mass of La element at EOC estimated by the ROM-Lasso method.

(Top 20 largest absolute value)

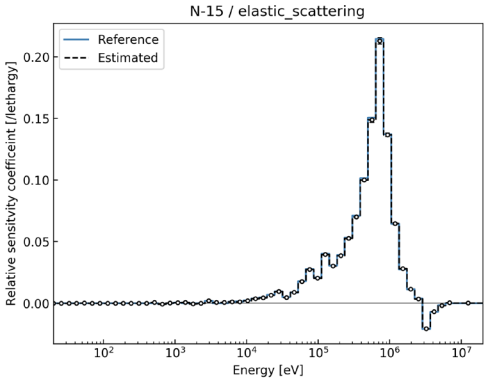

(**^{15}N, elastic scattering**)

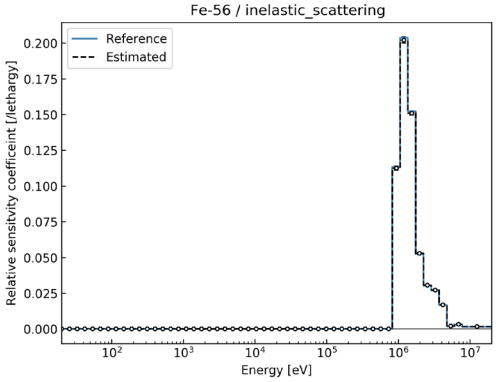

(**^{56}Fe, inelastic scattering**)

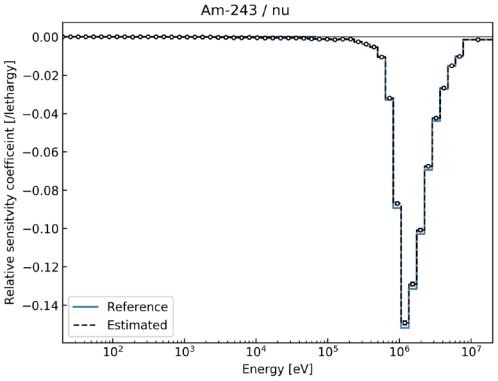

(**^{243}Am, $\bar{\nu}$**)

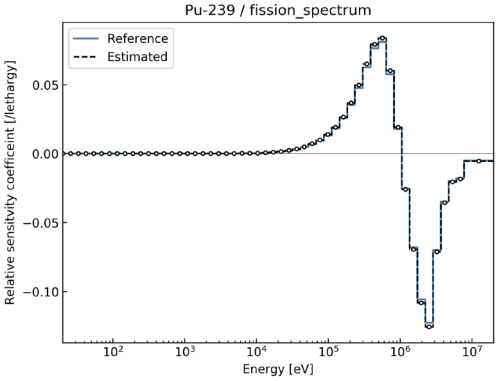

(**^{239}Pu, fission spectrum**)

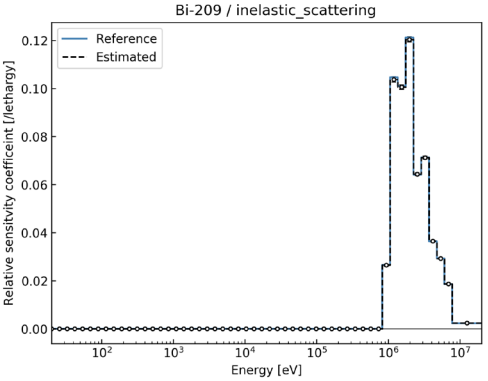

(**^{209}Bi, inelastic scattering**)

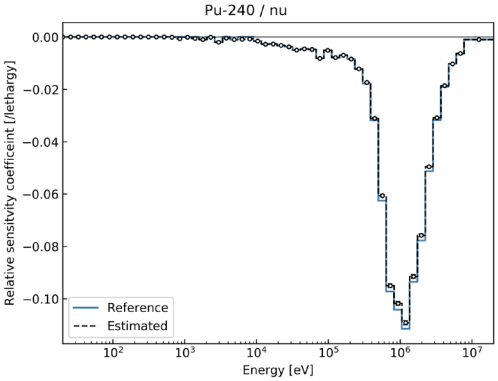

(**^{240}Pu, $\bar{\nu}$**)

Figure A.5 (3/4). Sensitivity coefficients of mass of La element at EOC estimated by the ROM-Lasso method.

(Top 20 largest absolute value)

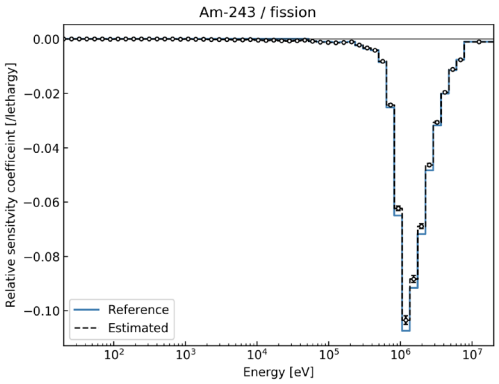

(**^{243}Am, fission**)

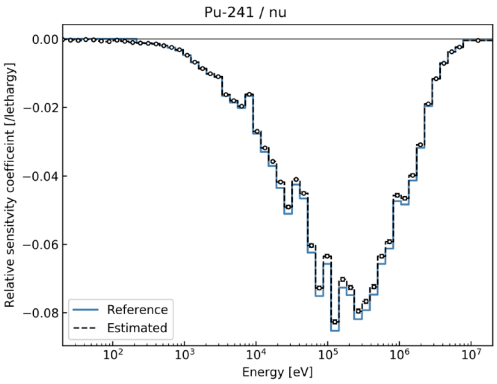

(**^{241}Pu, $\bar{\nu}$**)

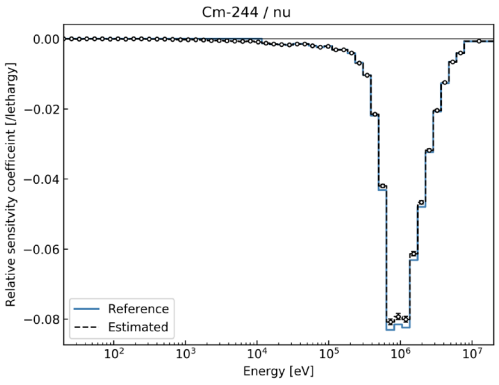

(**^{244}Cm, $\bar{\nu}$**)

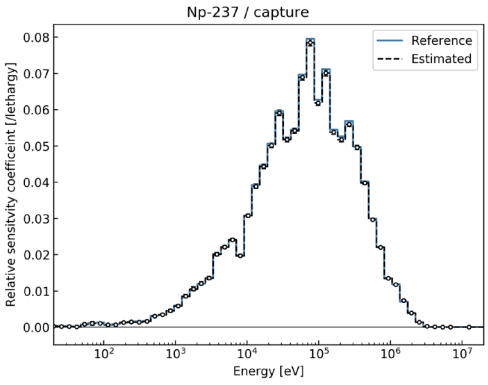

(**^{237}Np, capture**)

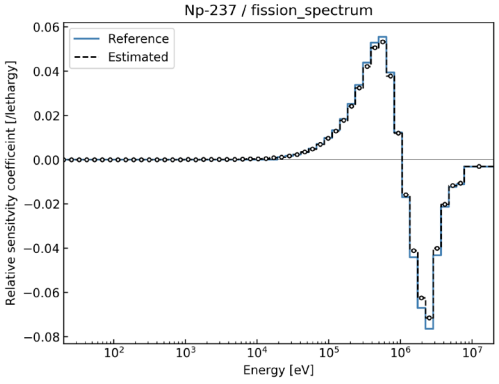

(**^{237}Np, fission spectrum**)

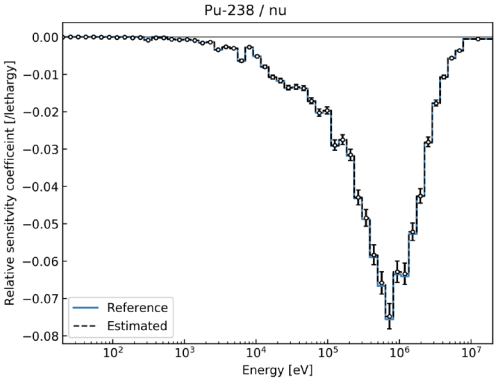

(**^{238}Pu, $\bar{\nu}$**)

Figure A.5 (4/4). Sensitivity coefficients of mass of La element at EOC estimated by the ROM-Lasso method.

(Top 20 largest absolute value)

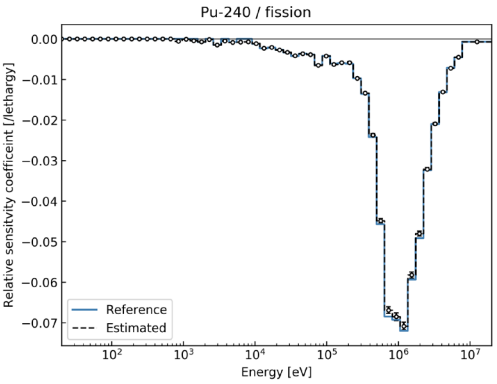

(^{240}Pu, fission)

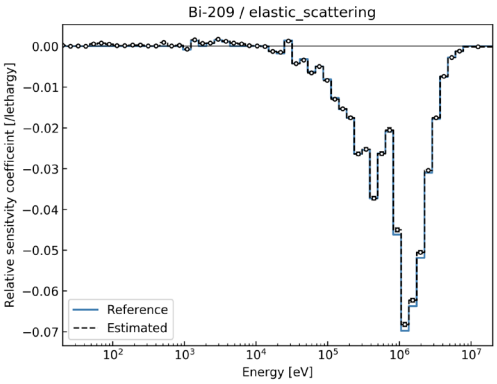

(^{209}Bi, elastic scattering)

Figure A.6 (1/4). Sensitivity coefficients of maximum relative power at EOC estimated by the ROM-Lasso method.

(Top 20 largest absolute value)

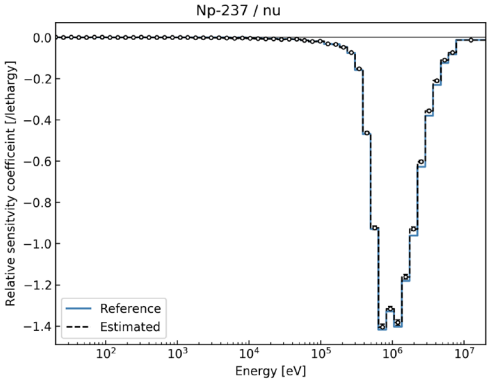

(**^{237}Np, $\bar{\nu}$**)

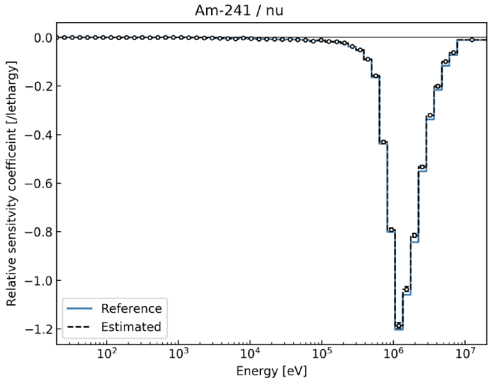

(**^{241}Am, $\bar{\nu}$**)

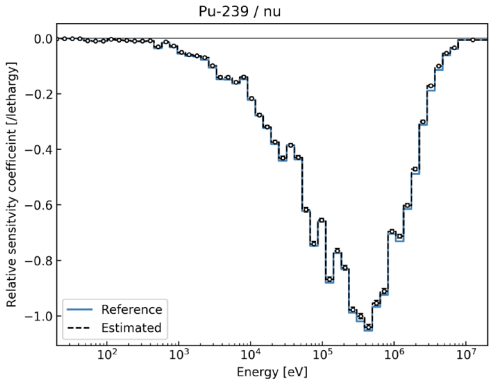

(**^{239}Pu, $\bar{\nu}$**)

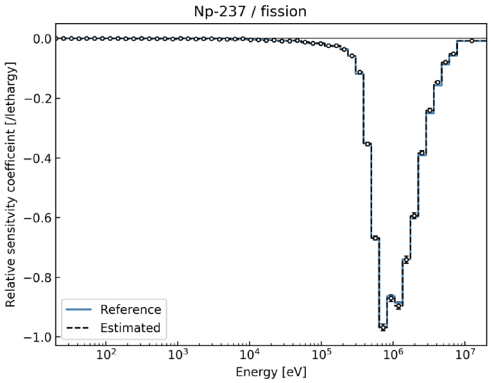

(**^{237}Np, fission**)

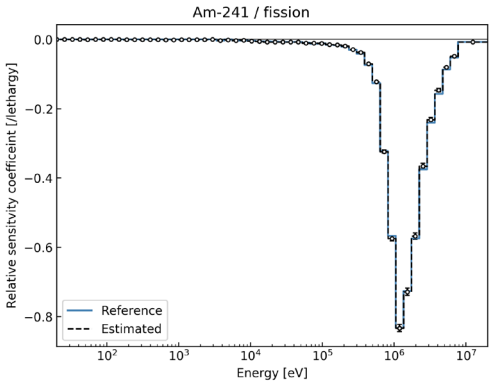

(**^{241}Am, fission**)

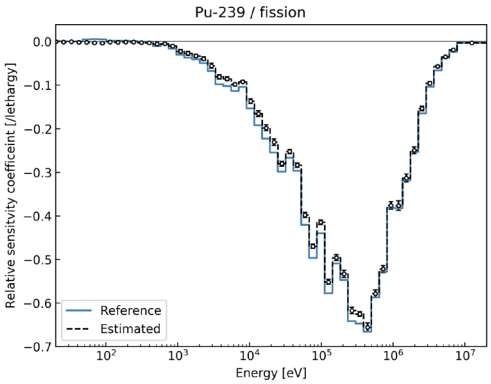

(**^{239}Pu, fission**)

Figure A.6 (2/4). Sensitivity coefficients of maximum relative power at EOC estimated by the ROM-Lasso method.

(Top 20 largest absolute value)

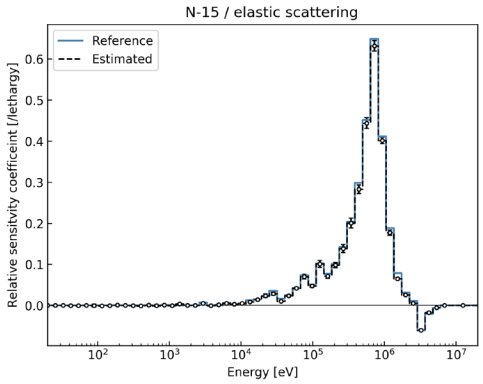

(**^{15}N, elastic scattering**)

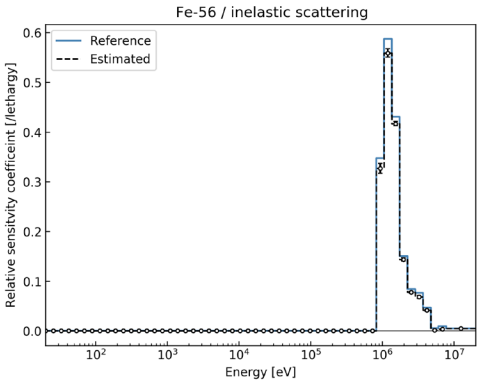

(**^{56}Fe, inelastic scattering**)

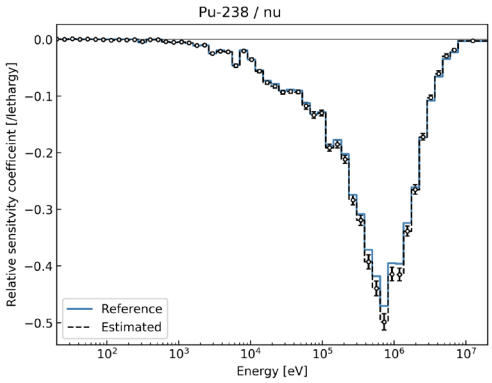

(**^{238}Pu, $\bar{\nu}$**)

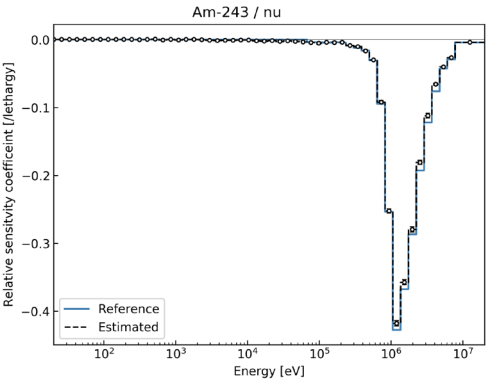

(**^{243}Am, $\bar{\nu}$**)

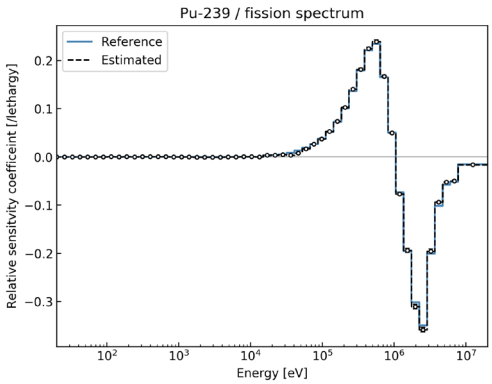

(**^{239}Pu, fission spectrum**)

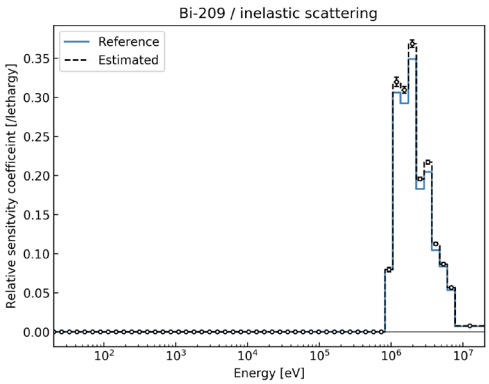

(**^{209}Bi, inelastic scattering**)

Figure A.6 (3/4). Sensitivity coefficients of maximum relative power at EOC estimated by the ROM-Lasso method.

(Top 20 largest absolute value)

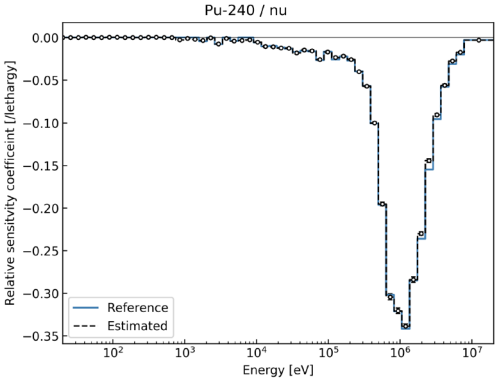

(**^{240}Pu, $\bar{\nu}$**)

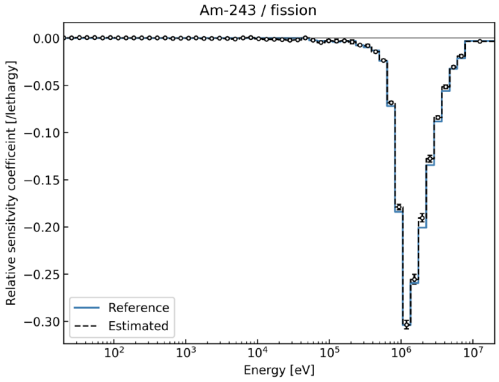

(**^{243}Am, fission**)

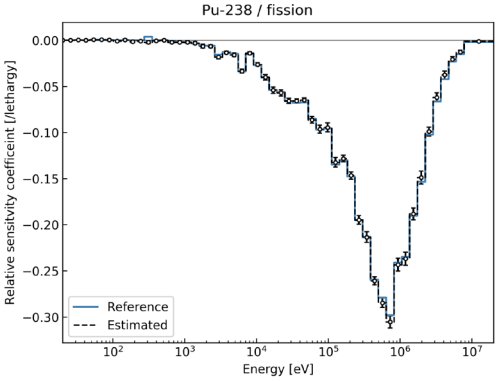

(**^{238}Pu, fission**)

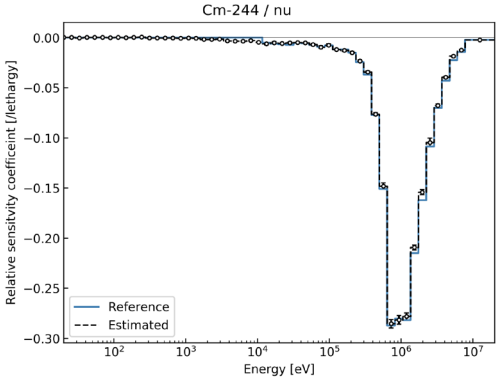

(**^{244}Cm, $\bar{\nu}$**)

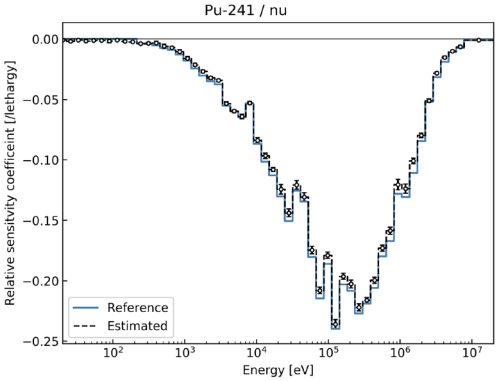

(**^{241}Pu, $\bar{\nu}$**)

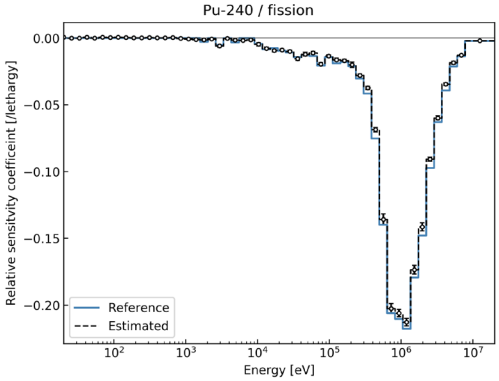

(**^{240}Pu, fission**)

Figure A.6 (4/4). Sensitivity coefficients of maximum relative power at EOC estimated by the ROM-Lasso method.

(Top 20 largest absolute value)

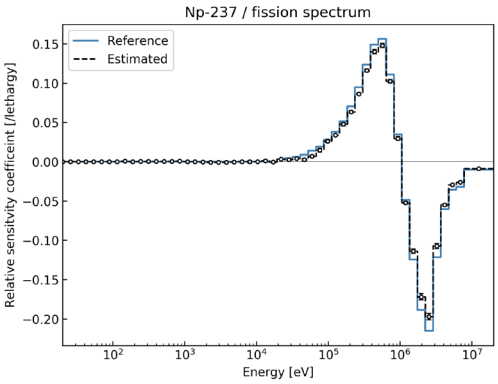

(^{237}Np, fission spectrum)

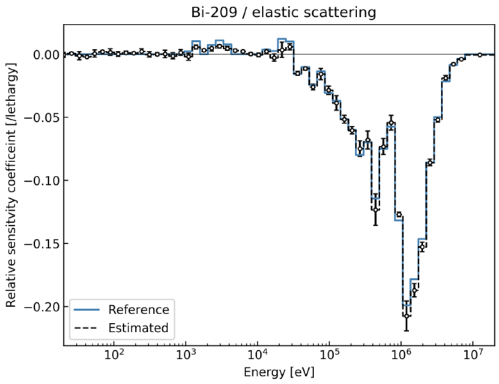

(^{209}Bi, elastic scattering)

Figure A.7 (1/4). Sensitivity coefficients of coolant void reactivity at BOC estimated by the ROM-Lasso method.

(Top 20 largest absolute value)

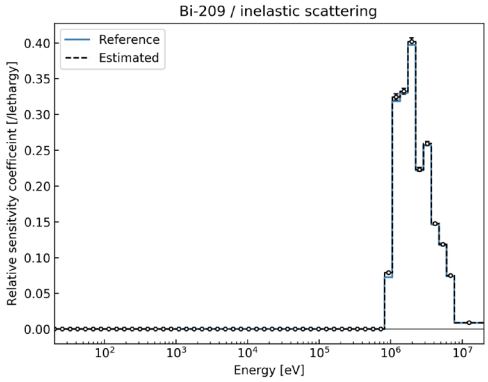

(**^{209}Bi, inelastic scattering**)

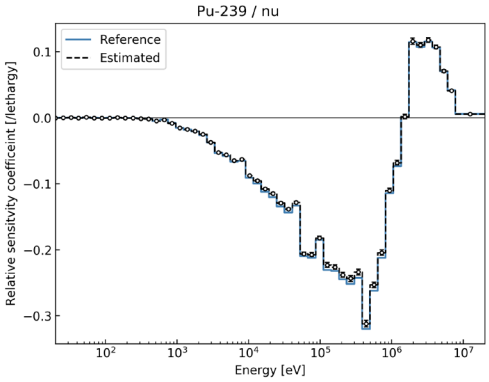

(**^{239}Pu, $\bar{\nu}$**)

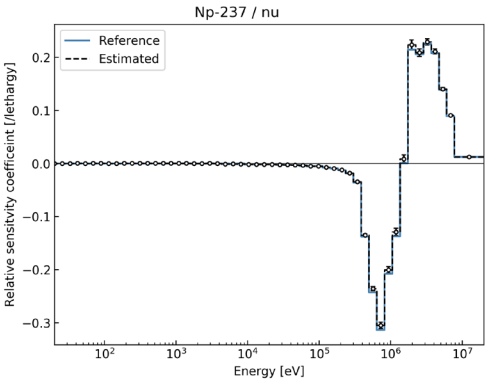

(**^{237}Np, $\bar{\nu}$**)

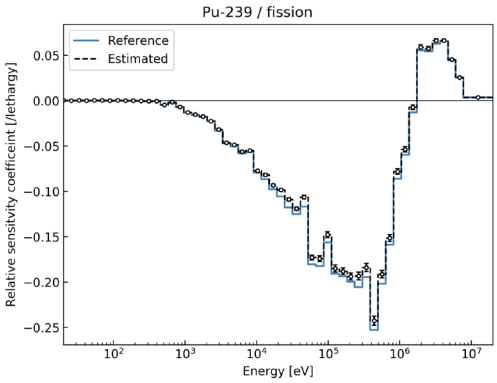

(**^{239}Pu, fission**)

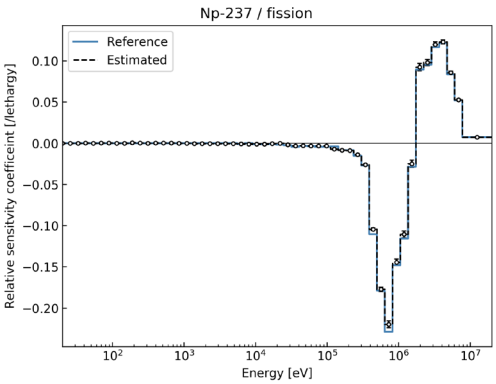

(**^{237}Np, fission**)

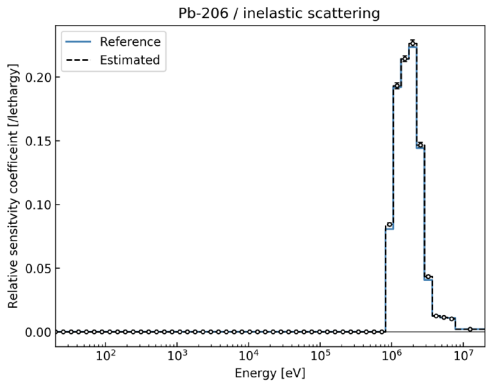

(**^{206}Pb, inelastic scattering**)

Figure A.7 (2/4). Sensitivity coefficients of coolant void reactivity at BOC estimated by the ROM-Lasso method.

(Top 20 largest absolute value)

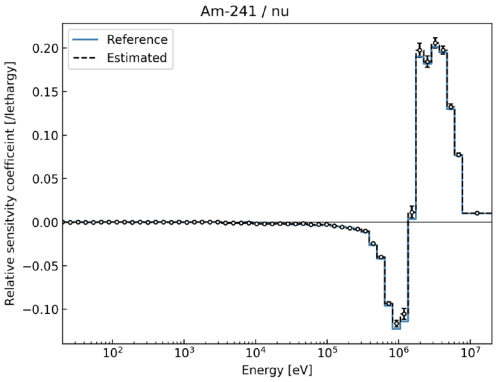

(^{241}Am, $\bar{\nu}$)

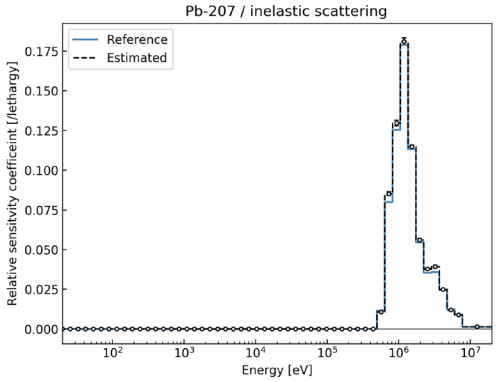

(^{207}Pb, inelastic scattering)

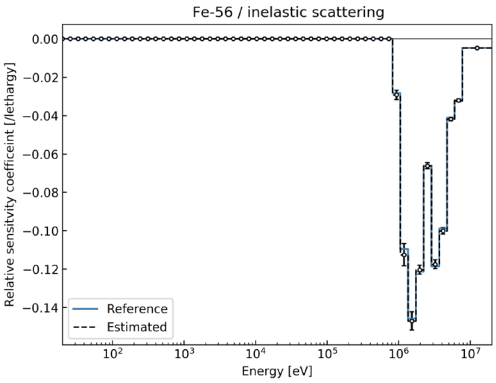

(^{56}Fe, inelastic scattering)

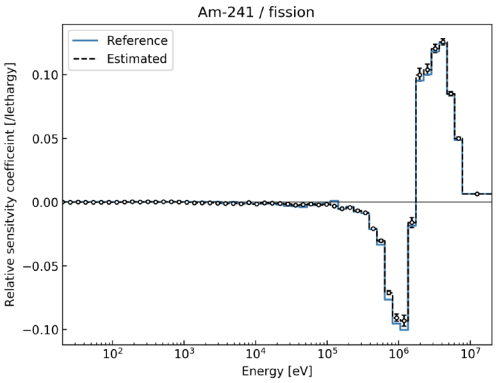

(^{241}Am, fission)

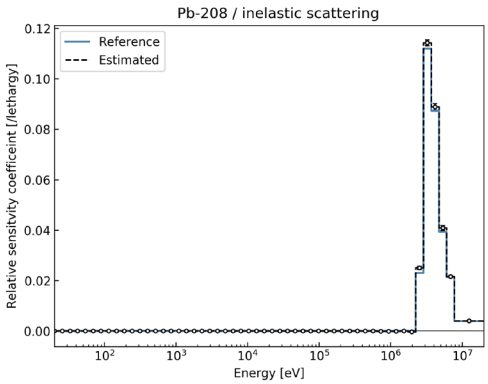

(^{208}Pb, inelastic scattering)

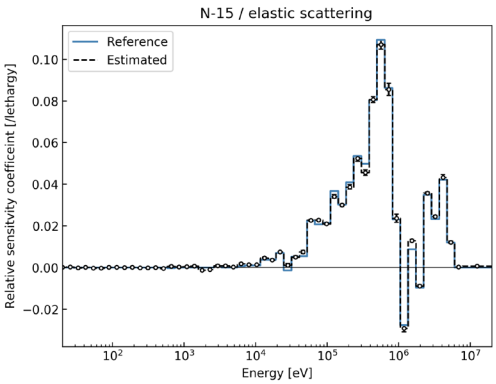

(^{15}N, elastic scattering)

Figure A.7 (3/4). Sensitivity coefficients of coolant void reactivity at BOC estimated by the ROM-Lasso method.

(Top 20 largest absolute value)

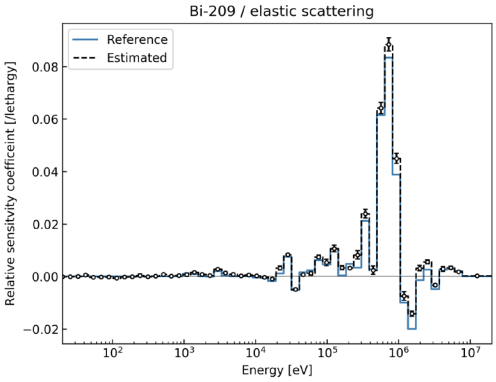

(**^{209}Bi, elastic scattering**)

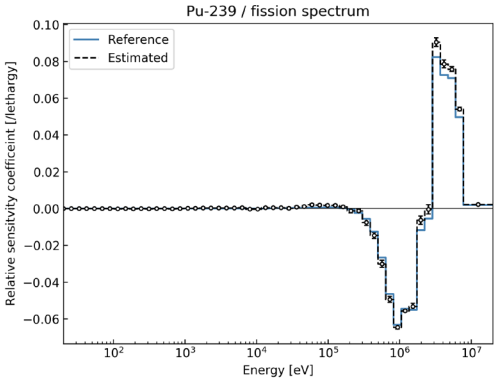

(**^{239}Pu, fission spectrum**)

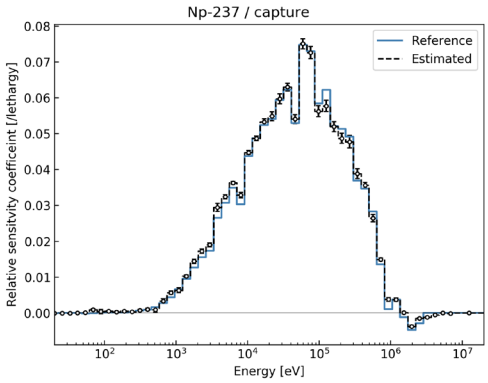

(**^{237}Np, capture**)

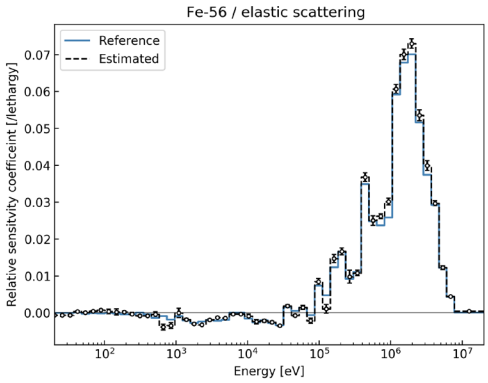

(**^{56}Fe, elastic scattering**)

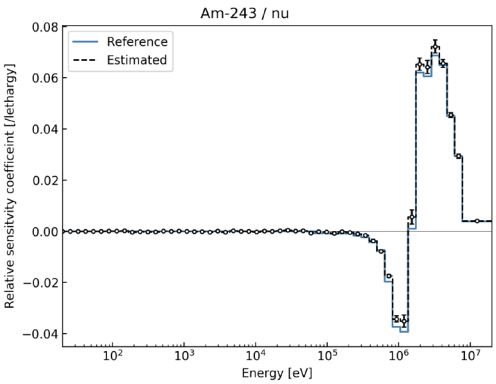

(**^{243}Am, $\bar{\nu}$**)

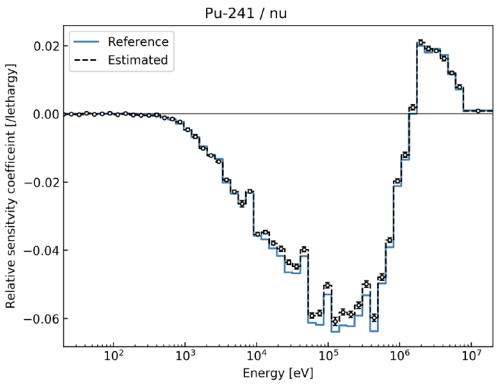

(**^{241}Pu, $\bar{\nu}$**)

Figure A.7 (4/4). Sensitivity coefficients of coolant void reactivity at BOC estimated by the ROM-Lasso method.

(Top 20 largest absolute value)

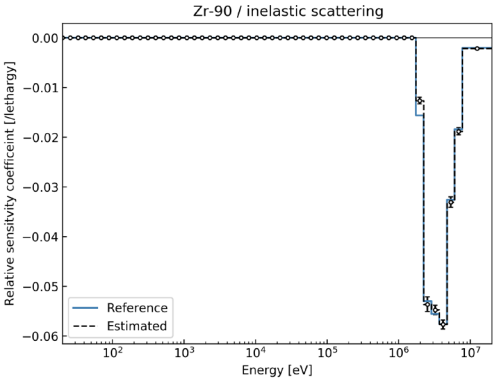

(**^{90}Zr, inelastic scattering**)

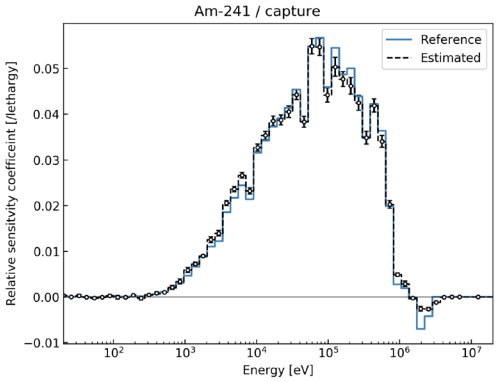

(**^{241}Am, capture**)

B. Re-evaluation of experimental uncertainty of excess reactivity

As mentioned in Section 4.2.3.1, the deviation of the excess reactivities is modeled as deviations in the control rod positions around a normal distribution, whose mean is taken to be zero. First, the excess reactivity was measured using the control rod worth and calibration curve as:

$$\rho_{\mathrm{ex}} = Rf(c), \tag{B.1}$$

where ρ_{ex} is the measured excess reactivity, R is the control rod worth, and $f(c)$ is a calibration curve function for control rod position c.

R was measured by the rod drop method before the experiment. Assuming an axial cosine distribution, $f(c)$ can be given as:

$$\begin{gathered} f(c) = 1 - (t - \frac{1}{2\pi}\sin(2\pi t)), \\ t = \frac{c-a}{b}. \end{gathered} \tag{B.2}$$

The parameters a and b are the lower edges of the active core and the active core height, respectively, and were calibrated by the period method. Then, the error propagation from the control rod position to the excess reactivity is given as:

$$\Delta\rho_{\mathrm{ex}} = R\frac{df}{dc}\Big|_{c=c_{\mathrm{cri}}} \Delta c, \tag{B.3}$$

where, c_{cri} is the critical control rod position. During measurements, the critical control

positions were judged by visually checking that the flux level was maintained at a constant value. Then, some uncertainty was expected in the critical control positions. It was assumed that the uncertainty was independent of the loading pattern and modeled the probability of the control rod position based on a normal distribution. **Table B.1** lists the measured control rod positions for each loading pattern for each measurement in units of mm. Then, these positions were centered by subtracting the average positions for each loading pattern, as shown in **Table B.2**. By assuming that the values in Table B.2 are realizations of a normal distribution, the standard deviation of the control rod position was estimated as Δc = 3.3 mm and the values in Table 4.5 were evaluated by Equation (B.3).

Table B.1. Measured control rod positions for each loading pattern.

The hyphenation indicates that no measurement was performed.

No.	Position [mm]									
	HEU					LEU				
	Al/Al/Al	Pb/Pb/Pb	Pb/Vd/Pb	Bi/Bi/Bi	Bi/Vd/Bi	Al/Al/Al	Pb/Pb/Pb	Pb/Vd/Pb	Bi/Bi/Bi	Bi/Vd/Bi
1	716.91	567.07	753.03	633.14	0.00[a]	692.44	596.91	707.96	630.54	743.49
2	715.36	563.85	759.91	632.92	0.00[a]	682.64	598.66	707.72	631	741.62
3	-	-	-	-	-	682.64	596.54	710.67	630.87	742.45
4	-	-	-	-	-	682.64	597.56	710.48	631.65	741.94
5	-	-	-	-	-	682.64	597.71	-	630.83	-
6	-	-	-	-	-	678.99	593.81	-	629.68	-
7	-	-	-	-	-	681.93	592.75	-	629.93	-
8	-	-	-	-	-	682.25	606.23	-	640.22	-
9	-	-	-	-	-	-	604.86	-	640.53	-
Average	716.14	565.46	756.47	633.03	0	683.27	598.34	709.21	632.81	742.38

[a] Critical with full withdrawal.

Table B.2. Centered control rod positions.

The hyphenation indicates that no measurement was performed.

No.	Position [mm]									
	HEU					LEU				
	Al/Al/Al	Pb/Pb/Pb	Pb/Vd/Pb	Bi/Bi/Bi	Bi/Vd/Bi	Al/Al/Al	Pb/Pb/Pb	Pb/Vd/Pb	Bi/Bi/Bi	Bi/Vd/Bi
1	0.77	1.61	−3.44	0.11	0.00	9.17	−1.43	−1.25	−2.27	1.11
2	−0.77	−1.61	3.44	−0.11	0.00	−0.63	0.32	−1.49	−1.81	−0.76
3	-	-	-	-	-	−0.63	−1.80	1.46	−1.94	0.07
4	-	-	-	-	-	−0.63	−0.78	1.27	−1.16	−0.44
5	-	-	-	-	-	−0.63	−0.63	-	−1.98	-
6	-	-	-	-	-	−4.28	−4.53	-	−3.13	-
7	-	-	-	-	-	−1.34	−5.59	-	−2.88	-
8	-	-	-	-	-	−1.02	7.89	-	7.41	-
9	-	-	-	-	-	-	6.52	-	7.72	-

C. Dataset of sample reactivity measurement at KUCA for data assimilation

In Appendix C, the dataset of the sample reactivity measurement at KUCA used for the data assimilation analysis in Chapter 4 is provided in the YAML format readable by the MARBLE system. The experimental uncertainties and the corresponding correlations are given in Appendix C.1. The calculation uncertainty and the corresponding correlations are given in Appendix C.2. Due to the large data size, the sensitivity coefficients of the sample reactivity experiments are given as the supplemental material on the webpage of the related article (see "List of publications" in this thesis).

C.1. Experimental uncertainties and corresponding correlations

```
ExperimentalParameterSet:
  data:
    - corename: 'kuca'
      charname: 'Al_Al_Al_HEU'  # k-eff of "Al/Al/Al" of the HEU core.
      value: 1.00000000e+00
      error: 5.00000000e-05
    - corename: 'kuca'
      charname: 'Al_to_Bi_HEU'
      value: 1.00000000e+00
      error: 8.46679000e-02
    - corename: 'kuca'
      charname: 'Al_to_Bi_LEU'
      value: 1.00000000e+00
      error: 1.39217000e-01
    - corename: 'kuca'
      charname: 'Al_to_Pb_HEU'
      value: 1.00000000e+00
      error: 4.46143000e-02
    - corename: 'kuca'
      charname: 'Al_to_Pb_LEU'
      value: 1.00000000e+00
      error: 8.11038000e-02
    - corename: 'kuca'
      charname: 'Bi_sample_HEU'
      value: 1.00000000e+00
      error: 3.90464000e-02
    - corename: 'kuca'
      charname: 'Bi_sample_LEU'
      value: 1.00000000e+00
      error: 6.25353000e-02
    - corename: 'kuca'
      charname: 'Pb_sample_HEU'
```

```
    value: 1.00000000e+00
    error: 3.37954000e-02
  - corename: 'kuca'
    charname: 'Pb_sample_LEU'
    value: 1.00000000e+00
    error: 6.07587000e-02
correlation:
  - corename1: 'kuca'
    charname1: 'Al_Al_Al_HEU'
    corename2: 'kuca'
    charname2: 'Al_Al_Al_HEU'
    value: 1.00000000e+00
  - corename1: 'kuca'
    charname1: 'Al_Al_Al_HEU'
    corename2: 'kuca'
    charname2: 'Al_to_Bi_HEU'
    value: -5.83522000e-01
  - corename1: 'kuca'
    charname1: 'Al_Al_Al_HEU'
    corename2: 'kuca'
    charname2: 'Al_to_Bi_LEU'
    value: 0.00000000e+00
  - corename1: 'kuca'
    charname1: 'Al_Al_Al_HEU'
    corename2: 'kuca'
    charname2: 'Al_to_Pb_HEU'
    value: -6.01776000e-01
  - corename1: 'kuca'
    charname1: 'Al_Al_Al_HEU'
    corename2: 'kuca'
    charname2: 'Al_to_Pb_LEU'
    value: 0.00000000e+00
  - corename1: 'kuca'
    charname1: 'Al_Al_Al_HEU'
    corename2: 'kuca'
    charname2: 'Bi_sample_HEU'
    value: 3.75336000e-02
  - corename1: 'kuca'
    charname1: 'Al_Al_Al_HEU'
    corename2: 'kuca'
    charname2: 'Bi_sample_LEU'
    value: 0.00000000e+00
  - corename1: 'kuca'
    charname1: 'Al_Al_Al_HEU'
    corename2: 'kuca'
    charname2: 'Pb_sample_HEU'
    value: 4.33653000e-02
  - corename1: 'kuca'
    charname1: 'Al_Al_Al_HEU'
    corename2: 'kuca'
    charname2: 'Pb_sample_LEU'
    value: 0.00000000e+00
  - corename1: 'kuca'
    charname1: 'Al_to_Bi_HEU'
    corename2: 'kuca'
    charname2: 'Al_to_Bi_HEU'
    value: 1.00000000e+00
  - corename1: 'kuca'
    charname1: 'Al_to_Bi_HEU'
```

```
  corename2: 'kuca'
  charname2: 'Al_to_Bi_LEU'
  value: 0.00000000e+00
- corename1: 'kuca'
  charname1: 'Al_to_Bi_HEU'
  corename2: 'kuca'
  charname2: 'Al_to_Pb_HEU'
  value: 4.16145000e-01
- corename1: 'kuca'
  charname1: 'Al_to_Bi_HEU'
  corename2: 'kuca'
  charname2: 'Al_to_Pb_LEU'
  value: 0.00000000e+00
- corename1: 'kuca'
  charname1: 'Al_to_Bi_HEU'
  corename2: 'kuca'
  charname2: 'Bi_sample_HEU'
  value: 7.89522000e-01
- corename1: 'kuca'
  charname1: 'Al_to_Bi_HEU'
  corename2: 'kuca'
  charname2: 'Bi_sample_LEU'
  value: 0.00000000e+00
- corename1: 'kuca'
  charname1: 'Al_to_Bi_HEU'
  corename2: 'kuca'
  charname2: 'Pb_sample_HEU'
  value: 3.49481000e-02
- corename1: 'kuca'
  charname1: 'Al_to_Bi_HEU'
  corename2: 'kuca'
  charname2: 'Pb_sample_LEU'
  value: 0.00000000e+00
- corename1: 'kuca'
  charname1: 'Al_to_Bi_LEU'
  corename2: 'kuca'
  charname2: 'Al_to_Bi_LEU'
  value: 1.00000000e+00
- corename1: 'kuca'
  charname1: 'Al_to_Bi_LEU'
  corename2: 'kuca'
  charname2: 'Al_to_Pb_HEU'
  value: 0.00000000e+00
- corename1: 'kuca'
  charname1: 'Al_to_Bi_LEU'
  corename2: 'kuca'
  charname2: 'Al_to_Pb_LEU'
  value: 4.93632000e-01
- corename1: 'kuca'
  charname1: 'Al_to_Bi_LEU'
  corename2: 'kuca'
  charname2: 'Bi_sample_HEU'
  value: 0.00000000e+00
- corename1: 'kuca'
  charname1: 'Al_to_Bi_LEU'
  corename2: 'kuca'
  charname2: 'Bi_sample_LEU'
  value: 5.90924000e-01
- corename1: 'kuca'
```

```
  charname1: 'Al_to_Bi_LEU'
  corename2: 'kuca'
  charname2: 'Pb_sample_HEU'
  value: 0.00000000e+00
- corename1: 'kuca'
  charname1: 'Al_to_Bi_LEU'
  corename2: 'kuca'
  charname2: 'Pb_sample_LEU'
  value: 1.18222000e-02
- corename1: 'kuca'
  charname1: 'Al_to_Pb_HEU'
  corename2: 'kuca'
  charname2: 'Al_to_Pb_HEU'
  value: 1.00000000e+00
- corename1: 'kuca'
  charname1: 'Al_to_Pb_HEU'
  corename2: 'kuca'
  charname2: 'Al_to_Pb_LEU'
  value: 0.00000000e+00
- corename1: 'kuca'
  charname1: 'Al_to_Pb_HEU'
  corename2: 'kuca'
  charname2: 'Bi_sample_HEU'
  value: 5.74043000e-02
- corename1: 'kuca'
  charname1: 'Al_to_Pb_HEU'
  corename2: 'kuca'
  charname2: 'Bi_sample_LEU'
  value: 0.00000000e+00
- corename1: 'kuca'
  charname1: 'Al_to_Pb_HEU'
  corename2: 'kuca'
  charname2: 'Pb_sample_HEU'
  value: 6.56399000e-01
- corename1: 'kuca'
  charname1: 'Al_to_Pb_HEU'
  corename2: 'kuca'
  charname2: 'Pb_sample_LEU'
  value: 0.00000000e+00
- corename1: 'kuca'
  charname1: 'Al_to_Pb_LEU'
  corename2: 'kuca'
  charname2: 'Al_to_Pb_LEU'
  value: 1.00000000e+00
- corename1: 'kuca'
  charname1: 'Al_to_Pb_LEU'
  corename2: 'kuca'
  charname2: 'Bi_sample_HEU'
  value: 0.00000000e+00
- corename1: 'kuca'
  charname1: 'Al_to_Pb_LEU'
  corename2: 'kuca'
  charname2: 'Bi_sample_LEU'
  value: 1.97167000e-02
- corename1: 'kuca'
  charname1: 'Al_to_Pb_LEU'
  corename2: 'kuca'
  charname2: 'Pb_sample_HEU'
  value: 0.00000000e+00
```

```
- corename1: 'kuca'
  charname1: 'Al_to_Pb_LEU'
  corename2: 'kuca'
  charname2: 'Pb_sample_LEU'
  value: 5.25928000e-01
- corename1: 'kuca'
  charname1: 'Bi_sample_HEU'
  corename2: 'kuca'
  charname2: 'Bi_sample_HEU'
  value: 1.00000000e+00
- corename1: 'kuca'
  charname1: 'Bi_sample_HEU'
  corename2: 'kuca'
  charname2: 'Bi_sample_LEU'
  value: 0.00000000e+00
- corename1: 'kuca'
  charname1: 'Bi_sample_HEU'
  corename2: 'kuca'
  charname2: 'Pb_sample_HEU'
  value: 7.57812000e-02
- corename1: 'kuca'
  charname1: 'Bi_sample_HEU'
  corename2: 'kuca'
  charname2: 'Pb_sample_LEU'
  value: 0.00000000e+00
- corename1: 'kuca'
  charname1: 'Bi_sample_LEU'
  corename2: 'kuca'
  charname2: 'Bi_sample_LEU'
  value: 1.00000000e+00
- corename1: 'kuca'
  charname1: 'Bi_sample_LEU'
  corename2: 'kuca'
  charname2: 'Pb_sample_HEU'
  value: 0.00000000e+00
- corename1: 'kuca'
  charname1: 'Bi_sample_LEU'
  corename2: 'kuca'
  charname2: 'Pb_sample_LEU'
  value: 2.63188000e-02
- corename1: 'kuca'
  charname1: 'Pb_sample_HEU'
  corename2: 'kuca'
  charname2: 'Pb_sample_HEU'
  value: 1.00000000e+00
- corename1: 'kuca'
  charname1: 'Pb_sample_HEU'
  corename2: 'kuca'
  charname2: 'Pb_sample_LEU'
  value: 0.00000000e+00
- corename1: 'kuca'
  charname1: 'Pb_sample_LEU'
  corename2: 'kuca'
  charname2: 'Pb_sample_LEU'
  value: 1.00000000e+00
```

C.2. Calculation uncertainties and corresponding correlations

```
CalculationalParameterSet:
  data:
    - corename: 'kuca'
      charname: 'Al_Al_Al_HEU'  # k-eff of "Al/Al/Al" of the HEU core.
      value: 1.00040500e+00
      error: 1.00000000e-03     # 100 pcm, empirically determined.
    - corename: 'kuca'
      charname: 'Al_to_Bi_HEU'
      value: 1.15450000e+00
      error: 1.39008000e-02
    - corename: 'kuca'
      charname: 'Al_to_Bi_LEU'
      value: 9.54188000e-01
      error: 2.08035000e-02
    - corename: 'kuca'
      charname: 'Al_to_Pb_HEU'
      value: 1.00883000e+00
      error: 8.85333000e-03
    - corename: 'kuca'
      charname: 'Al_to_Pb_LEU'
      value: 9.98436000e-01
      error: 1.18761000e-02
    - corename: 'kuca'
      charname: 'Bi_sample_HEU'
      value: 1.15916000e+00
      error: 7.85790000e-03
    - corename: 'kuca'
      charname: 'Bi_sample_LEU'
      value: 1.00392000e+00
      error: 9.86069000e-03
    - corename: 'kuca'
      charname: 'Pb_sample_HEU'
      value: 1.09596000e+00
      error: 6.80995000e-03
    - corename: 'kuca'
      charname: 'Pb_sample_LEU'
      value: 1.11206000e+00
      error: 8.30545000e-03
  correlation:
    - corename1: 'kuca'
      charname1: 'Al_Al_Al_HEU'
      corename2: 'kuca'
      charname2: 'Al_Al_Al_HEU'
      value: 1.00000000e+00
    - corename1: 'kuca'
      charname1: 'Al_Al_Al_HEU'
      corename2: 'kuca'
      charname2: 'Al_to_Bi_HEU'
      value:-6.74602000e-03
    - corename1: 'kuca'
      charname1: 'Al_Al_Al_HEU'
      corename2: 'kuca'
      charname2: 'Al_to_Bi_LEU'
      value: 0.00000000e+00
    - corename1: 'kuca'
      charname1: 'Al_Al_Al_HEU'
      corename2: 'kuca'
```

```
  charname2: 'Al_to_Pb_HEU'
  value:-6.74603000e-03
- corename1: 'kuca'
  charname1: 'Al_Al_Al_HEU'
  corename2: 'kuca'
  charname2: 'Al_to_Pb_LEU'
  value: 0.00000000e+00
- corename1: 'kuca'
  charname1: 'Al_Al_Al_HEU'
  corename2: 'kuca'
  charname2: 'Bi_sample_HEU'
  value: 0.00000000e+00
- corename1: 'kuca'
  charname1: 'Al_Al_Al_HEU'
  corename2: 'kuca'
  charname2: 'Bi_sample_LEU'
  value: 0.00000000e+00
- corename1: 'kuca'
  charname1: 'Al_Al_Al_HEU'
  corename2: 'kuca'
  charname2: 'Pb_sample_HEU'
  value: 0.00000000e+00
- corename1: 'kuca'
  charname1: 'Al_Al_Al_HEU'
  corename2: 'kuca'
  charname2: 'Pb_sample_LEU'
  value: 0.00000000e+00
- corename1: 'kuca'
  charname1: 'Al_to_Bi_HEU'
  corename2: 'kuca'
  charname2: 'Al_to_Bi_HEU'
  value: 1.00000000e+00
- corename1: 'kuca'
  charname1: 'Al_to_Bi_HEU'
  corename2: 'kuca'
  charname2: 'Al_to_Bi_LEU'
  value: 0.00000000e+00
- corename1: 'kuca'
  charname1: 'Al_to_Bi_HEU'
  corename2: 'kuca'
  charname2: 'Al_to_Pb_HEU'
  value: 5.00000000e-01
- corename1: 'kuca'
  charname1: 'Al_to_Bi_HEU'
  corename2: 'kuca'
  charname2: 'Al_to_Pb_LEU'
  value: 0.00000000e+00
- corename1: 'kuca'
  charname1: 'Al_to_Bi_HEU'
  corename2: 'kuca'
  charname2: 'Bi_sample_HEU'
  value: 5.00000000e-01
- corename1: 'kuca'
  charname1: 'Al_to_Bi_HEU'
  corename2: 'kuca'
  charname2: 'Bi_sample_LEU'
  value: 0.00000000e+00
- corename1: 'kuca'
  charname1: 'Al_to_Bi_HEU'
```

```
  corename2: 'kuca'
  charname2: 'Pb_sample_HEU'
  value: 0.00000000e+00
- corename1: 'kuca'
  charname1: 'Al_to_Bi_HEU'
  corename2: 'kuca'
  charname2: 'Pb_sample_LEU'
  value: 0.00000000e+00
- corename1: 'kuca'
  charname1: 'Al_to_Bi_LEU'
  corename2: 'kuca'
  charname2: 'Al_to_Bi_LEU'
  value: 1.00000000e+00
- corename1: 'kuca'
  charname1: 'Al_to_Bi_LEU'
  corename2: 'kuca'
  charname2: 'Al_to_Pb_HEU'
  value: 0.00000000e+00
- corename1: 'kuca'
  charname1: 'Al_to_Bi_LEU'
  corename2: 'kuca'
  charname2: 'Al_to_Pb_LEU'
  value: 5.00000000e-01
- corename1: 'kuca'
  charname1: 'Al_to_Bi_LEU'
  corename2: 'kuca'
  charname2: 'Bi_sample_HEU'
  value: 0.00000000e+00
- corename1: 'kuca'
  charname1: 'Al_to_Bi_LEU'
  corename2: 'kuca'
  charname2: 'Bi_sample_LEU'
  value: 4.99997000e-01
- corename1: 'kuca'
  charname1: 'Al_to_Bi_LEU'
  corename2: 'kuca'
  charname2: 'Pb_sample_HEU'
  value: 0.00000000e+00
- corename1: 'kuca'
  charname1: 'Al_to_Bi_LEU'
  corename2: 'kuca'
  charname2: 'Pb_sample_LEU'
  value: 0.00000000e+00
- corename1: 'kuca'
  charname1: 'Al_to_Pb_HEU'
  corename2: 'kuca'
  charname2: 'Al_to_Pb_HEU'
  value: 1.00000000e+00
- corename1: 'kuca'
  charname1: 'Al_to_Pb_HEU'
  corename2: 'kuca'
  charname2: 'Al_to_Pb_LEU'
  value: 0.00000000e+00
- corename1: 'kuca'
  charname1: 'Al_to_Pb_HEU'
  corename2: 'kuca'
  charname2: 'Bi_sample_HEU'
  value: 0.00000000e+00
- corename1: 'kuca'
```

```
  charname1: 'Al_to_Pb_HEU'
  corename2: 'kuca'
  charname2: 'Bi_sample_LEU'
  value: 0.00000000e+00
- corename1: 'kuca'
  charname1: 'Al_to_Pb_HEU'
  corename2: 'kuca'
  charname2: 'Pb_sample_HEU'
  value: 4.99999000e-01
- corename1: 'kuca'
  charname1: 'Al_to_Pb_HEU'
  corename2: 'kuca'
  charname2: 'Pb_sample_LEU'
  value: 0.00000000e+00
- corename1: 'kuca'
  charname1: 'Al_to_Pb_LEU'
  corename2: 'kuca'
  charname2: 'Al_to_Pb_LEU'
  value: 1.00000000e+00
- corename1: 'kuca'
  charname1: 'Al_to_Pb_LEU'
  corename2: 'kuca'
  charname2: 'Bi_sample_HEU'
  value: 0.00000000e+00
- corename1: 'kuca'
  charname1: 'Al_to_Pb_LEU'
  corename2: 'kuca'
  charname2: 'Bi_sample_LEU'
  value: 0.00000000e+00
- corename1: 'kuca'
  charname1: 'Al_to_Pb_LEU'
  corename2: 'kuca'
  charname2: 'Pb_sample_HEU'
  value: 0.00000000e+00
- corename1: 'kuca'
  charname1: 'Al_to_Pb_LEU'
  corename2: 'kuca'
  charname2: 'Pb_sample_LEU'
  value: 5.00001000e-01
- corename1: 'kuca'
  charname1: 'Bi_sample_HEU'
  corename2: 'kuca'
  charname2: 'Bi_sample_HEU'
  value: 1.00000000e+00
- corename1: 'kuca'
  charname1: 'Bi_sample_HEU'
  corename2: 'kuca'
  charname2: 'Bi_sample_LEU'
  value: 0.00000000e+00
- corename1: 'kuca'
  charname1: 'Bi_sample_HEU'
  corename2: 'kuca'
  charname2: 'Pb_sample_HEU'
  value: 0.00000000e+00
- corename1: 'kuca'
  charname1: 'Bi_sample_HEU'
  corename2: 'kuca'
  charname2: 'Pb_sample_LEU'
  value: 0.00000000e+00
```

```
- corename1: 'kuca'
  charname1: 'Bi_sample_LEU'
  corename2: 'kuca'
  charname2: 'Bi_sample_LEU'
  value: 1.00000000e+00
- corename1: 'kuca'
  charname1: 'Bi_sample_LEU'
  corename2: 'kuca'
  charname2: 'Pb_sample_HEU'
  value: 0.00000000e+00
- corename1: 'kuca'
  charname1: 'Bi_sample_LEU'
  corename2: 'kuca'
  charname2: 'Pb_sample_LEU'
  value: 0.00000000e+00
- corename1: 'kuca'
  charname1: 'Pb_sample_HEU'
  corename2: 'kuca'
  charname2: 'Pb_sample_HEU'
  value: 1.00000000e+00
- corename1: 'kuca'
  charname1: 'Pb_sample_HEU'
  corename2: 'kuca'
  charname2: 'Pb_sample_LEU'
  value: 0.00000000e+00
- corename1: 'kuca'
  charname1: 'Pb_sample_LEU'
  corename2: 'kuca'
  charname2: 'Pb_sample_LEU'
  value: 1.00000000e+00
```

List of publications

Publication in journals

(1) R. KATANO, T. ENDO, A. YAMAMOTO, and K. TSUJIMOTO, "Estimation of Sensitivity Coefficient Based on Lasso-Type Penalized Linear Regression," *J. Nucl. Sci. Technol.*, **55**, *10*, 1099 (2018); https://doi.org/10.1080/00223131.2018.1479988.

(2) R. KATANO, A. YAMAMOTO, and T. ENDO, "Sensitivity Coefficient Evaluation of an Accelerator-Driven System Using ROM-Lasso Method," *Nucl. Sci. Eng.*, **196**, *10*, 1194 (2022); https://doi.org/10.1080/00295639.2022.2067447.

(3) R. KATANO, A. OIZUMI, M. FUKUSHIMA, C. H. PYEON, A. YAMAMOTO, and T. ENDO, "Impact of Uncertainty Reduction on Lead-Bismuth Coolant in Accelerator Driven System Using Sample Reactivity Experiments," *Nucl. Sci. Eng.*, published online on Oct. 4, (2023); https://doi.org/10.1080/00295639.2023.2246779.

Publication in international conferences

(1) R. KATANO, A. YAMAMOTO, and T. ENDO, "Proposal and Application of ROM-Lasso Method for Sensitivity Coefficient Evaluation," *Proc. PHYSOR 2022*, Pittsburgh, PA, (2022).